Robert Hussein

Noise–induced quantum transport

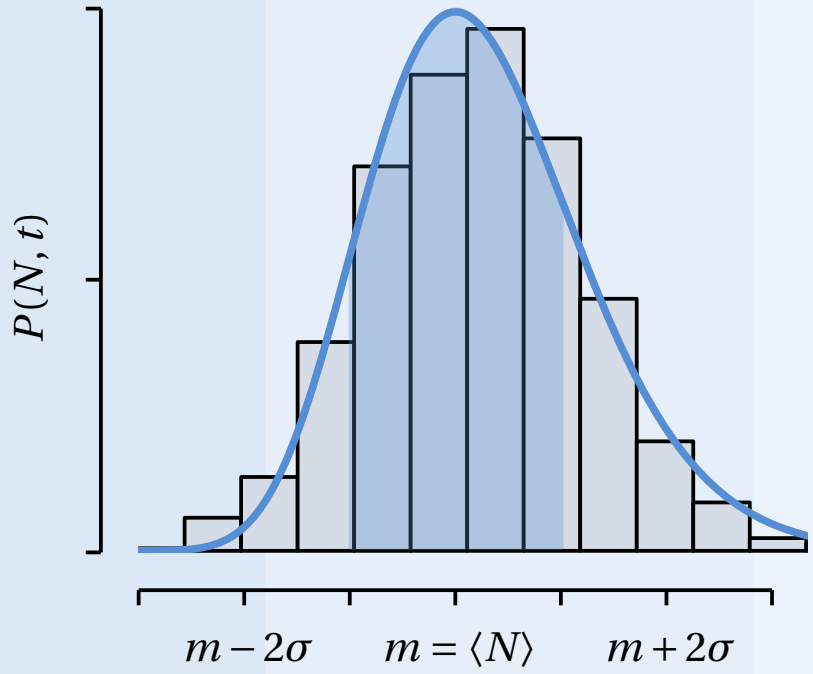

Noise–induced quantum transport

presentado por

Robert Hussein

para optar al grado de Doctor en Ciencias Físicas

en la

Universidad Autónoma de Madrid

Facultad de Ciencias

Departamento de Física Teórica de la Materia Condensada

Madrid, noviembre 2014

Director: Dr. Sigmund Kohler

Tutor: Prof. Juan-Carlos Cuevas

No hay placer más complejo que el pensamiento y a él nos entregábamos.

There is no pleasure more complex than that of thought and we surrendered ourselves to it.

(Jorge Luis Borges, El Aleph)

Resumen

Los puntos cuánticos laterales son heteroestructuras semiconductoras de unos pocos micrómetros de tamaño, los cuales forman un gas bidimensional de electrones a unos nanómetros por de bajo de la superficie. Se definen por puertas metálicas superpuestas que forman barreras de potencial debido a la carga negativa. Los puntos cuánticos son pozos de potencial caracterizados por niveles electrónicos discretos formando circuitos eléctricos cuando se acoplan mediante túnel a contactos. Aplicando diferencias de potencial se logra la realización de experimentos de transporte en puntos cuánticos por los cuales dos sistemas electrónicos aislados próximos pueden interaccionar capacitivamente.

En esta tesis, consideramos transporte cuántico en este tipo de circuitos acoplados capacitivamente. Estudiamos teóricamente la influencia entre subsistemas interactuantes en sus propiedades de transporte así como la monitorización del transporte electrónico. Se analizan las corrientes estacionarias y las correlaciones corriente-corriente en términos de *full-counting statistics* obtenidas mediante la correspondiente ecuación maestra de Bloch-Redfield la cual la usamos también para calcular las correlaciones dependientes de la frecuencia.

En concreto, estudiamos un trinquete cuántico formado por un doble punto cuántico sin *bias* pero con sus niveles fuera de resonancia, el cual está acoplado capacitivamente a otro doble punto cuántico con un *bias* grande. Este circuito causa una fuerza forzada efectiva mediada por las oscilaciones de túnel en el punto cuántico anterior recordando al efecto de un campo c.a. Esto induce una corriente continua en la ausencia de cualquier *bias* y clasifica el sistema como un trinquete cuántico.

El estudio con *full-counting statistics* revela que cuando la corriente del trinquete es grande, también aparecen efectos de procesos poissonianos. La eliminación del circuito forzado nos permite obtener una ecuación maestra reducida que proporciona resultados analíticos.

En otro sistema, estudiamos un contacto túnel que está acoplado capacitivamente a un doble punto cuántico el cual lo empleamos para monitorizar la carga del doble punto cuántico. Consideramos tanto el régimen cuántico como el límite clásico caracterizado por la ausencia de coherencia cuántica. Generalizando la ya mencionada aproximación de Bloch-Redfield aplicada al contacto de punto cuántico, obtenemos medidas de correlación produciendo enunciados cuantitativos sobre el régimen de parámetros en los cuales el sistema de detección funciona correctamente. Por otra parte, demostramos que no solamente las ocupaciones del doble punto cuántico pueden mostrar fuertes correlaciones con la corriente del detector, sino que también con su propia corriente. La solución mecánica cuántica muestra que la *backaction* de la medición tiende a localizar los electrones en el doble punto cuántico y por lo

tanto, reducir significativamente la corriente; suministrando los parámetros efectivos del tratamiento clásico. Se ve que la descripción clásica por si misma es suficiente para describir la mayoría de los regímenes operacionales.

Finalmente, abordamos la pregunta de en qué medida una descripción de la ecuación maestra de Bloch-Redfield en este tipo de transporte cuántico es consistente con las relaciones exactas de simetría, conocidas como los teoremas de fluctuación. Identificamos una categoría de ecuaciones maestras que satisfacen estas relaciones. Mas allá de esta categoría, encontramos desarrollos que muestran leyes características de escala en función de los parámetros de túnel y la temperatura. Estos desarrollos mas allá de la aproximación de onda rotante están acompañados por un aumento de las fluctuaciones de energía en los contactos inherentes en la ecuación de Bloch-Redfield. Mostramos nuestros resultados con datos numéricos para un doble y un cuádruple punto cuántico acoplados a cuatro contactos.

Abstract

Lateral quantum dots are semiconductor heterostructures of a few micrometers in size providing a two dimensional electron gas below the surface. They are defined by superimposed metallic gates which upon negative charging form potential barriers. Quantum dots are potential wells characterized by discrete electron levels forming electric circuits when tunnel coupled to leads. Application of bias voltages enable transport experiments on such quantum dots whereby two electrically isolated nearby circuits may interact capacitively.

In this thesis, we consider quantum transport in such capacitively coupled quantum circuits to theoretically study the influence between interacting subsystems on their transport properties as well as the monitoring of electron transport. Stationary currents and current–current correlations are analyzed in terms of full-counting statistics obtained from a corresponding Bloch-Redfield master equation which we also use to compute frequency-dependent correlations.

In particular, we study a quantum ratchet formed by an unbiased but detuned double quantum dot that capacitively couples to a further strongly biased double quantum dot. The latter circuit entails an effective driving force mediated by tunnel oscillations on the former double quantum dot reminiscent to an applied ac field. This induces a dc current in the absence of any bias voltage and qualifies the setup as quantum ratchet. Full-counting statistics reveals that whenever the ratchet current is large, it also exhibits some features of a Poissonian process. Elimination of the drive circuit permits us to obtain a reduced master equation which provides analytical results.

As further system, we study a tunnel contact that is capacitively coupled to a double quantum dot and employed as charge monitor for the latter. We consider both the quantum regime and the classical limit characterized by the absence of quantum coherence. Generalizing the aforementioned Bloch-Redfield approach to be applicable to the quantum point contact, we derive measurement correlations yielding quantitative statements about the parameter regime in which the detection scheme works well. Moreover, we demonstrate that not only the occupations of the double quantum dot may exhibit strong correlations with the detector current but also the corresponding current. The quantum mechanical solution shows that the backaction of the measurement tends to localize the electrons on the double quantum dot and, thus, significantly reduces the corresponding current. Furthermore, it provides the effective parameters of the classical treatment. It turns out that already the classical description is adequate for most operating regimes.

Finally, we address the question to which extent a Bloch-Redfield master equation description of this kind of quantum transport is consistent with exact symmetry

relations known as exchange fluctuation theorems. We identify a class of master equations that satisfy these relations. Beyond this class, we find deviations which exhibit characteristic scaling laws as functions of the dot-lead tunneling, the inter-dot tunneling, and the temperature. These deviations are accompanied by an increase of lead energy fluctuations inherent in the Bloch-Redfield equation beyond rotating-wave approximation. We illustrate our results with numerical data for a double and a quadruple quantum dot attached to four leads.

Contents

1 Introduction

The ongoing miniaturization of integrated circuits, predicted and propelled by Gorden E. Moore,[1] has reached scales where quantum effects become important. Most prominent thereof is electron tunneling, the ability of electrons to penetrate a potential barrier, leading to current leakage, power dissipation and heat generation.[2] Furthermore, delocalization of electron states can occur. To face these engineering defiances in the continuing trend of down-scaling, a good understanding of electron transport on the mesoscopic length scale becomes inevitable.

Quantum dots: An ideal testbed of quantum transport[3–5] are semiconductor heterostructures[6–8] such as GaAs/AlGaAs which are only of a few micrometers in size. The peculiarity of these electronic circuits is that the heterostructure interface provides a two dimensional electron gas of a low density in which electrons move freely. This low electron concentration offers a large mean-free path and a large Fermi wavelength of about 40 nm.[4,9,10] Electrostatic potentials are defined by attached metallic contacts to confine a few electrons in all three spatial dimensions. This confinement to zero dimensions, termed "quantum dots" by Mark A. Reed[11] in 1988, allows electrons to only occupy discrete energy levels. In this respect, the level structure of an isolated quantum dot or coupled quantum dots are reminiscent of the atomic[12–14] and molecular spectra.[15,16] Here, we focus on lateral gated quantum dots as described above due to their flexible design and their high tunability. Albeit lateral quantum dots where already studied relatively early[11] in this branch of condensed matter physics, they gained new interest when Ciorga et al.[6] managed to reach the few electron limit and controllably emptied them of electrons. Up until then, this was reserved to vertical quantum dots.[13,14]

The realization of double or triple quantum dots in a linear arrangement[17–20] or in a ring configuration[21,22] enables transport experiments in which electrons flow through delocalized orbitals. Here, the strength of the inter-dot couplings determines the grade of delocalization and therewith whether tunneling is sequential, and can be described by standard rate equations, or coherent.[10,23,24] The measurement of the differential conductance in dependence on applied gate voltages gives information about the equilibrium charge configuration. Moreover, this stability analysis reveals delocalization which manifests itself in modified quadruple points.[17–20,25] Modulation of the electron occupations by applying, for instance, a microwave field[16,26] is used to probe charge transitions and therewith to measure the electronic spectrum and inter-dot couplings. Otherwise, resonant tunneling experiments[5,27] allow one to infer the lifetime of electronic states from the width of Lorentzian resonance peaks.

Quantum computation: Two-level systems formed by charge[8,28,29] or spin[30,31] states of electrons in quantum dots or based on[32–35] superconducting Josephson junctions[36] are of particular interest, since they realize quantum bits (qubits)—the basic unit for quantum computation.[37–41] While localized two-level systems represent a classical bit with two possible states, coherence leads to a superposition of these states and, thus, forms a two dimensional state space equivalent to the surface of a Bloch sphere. Albeit, the measurement of qubits realize concrete states, operations can be performed on whole state spaces. Therein lies the major advantage[42] to conventional computation, since coherence allows parallel processing of a collection of states.

The main concerns of quantum computation are the preparation of qubit states, their manipulation involving interactions with other qubits and the environment, and their readout. Especially, the readout is one guiding theme of this work. Together with the requirement that they are well defined and satisfy low decoherence, these five criteria[37,43] of Loss and DiVincenzo are essential to implement a scalable quantum computer. Although strong measurement is suggested in which observables[44] are projectively and instantaneously measured causing the collapse of probed quantum states into eigenstates, weak measurement schemes[45–48] are considered as well allowing partial recycling[49] of the measured states. This recovery of measured states in combination with feedback techniques[50–52] may enhance the accuracy of measurements. Nevertheless, the loss of coherence caused by relaxation and dephasing as well as scalability are the main issues of realizing a practical quantum computer. Although its realization is a long-term objective, it is, and has been, an important promoter of innovation in various fields such as condensed matter physics, quantum optics, quantum information, quantum computation and quantum error correction.[39,53,54] Beside academic aspects, short term goals are the improvement of accuracies of sensors as charge detectors and interferometers, and the development of novel ultrasensitive detectors. A further perspective is that single-charge-counting with quantum-dot pumps becomes so accurate that it would allow refining the standard of the ampere.[55]

The readout of qubits and the associated problem of monitoring electron charges and currents are of utmost significance and form a central question in our investigation. Although, spin qubits seem to be a promising future candidate for performing quantum operations, charge qubits[56–59] are equally relevant. Sooner or later, spin qubits need to be read out, e.g. by spin echo,[30,31,60,61] which eventually involves spin-to-charge conversion.[30,39] The task of measuring a qubit with an adequate detector is intriguing since the detector needs to be of the same length scale as the qubit. In quantum transport, the detector circuit and the system that is supposed to be measured are not independent but rather interact with each other and establish correlations. This interaction influences mutually the detector and the measurement and leads to backaction[62,63] of the detector on the measured circuit. Often, this adulteration of the measurement introduces noise and reduces the measurement signal, but it may also be used to enhance[59] the signal-to-noise ratio.

Monitoring electron transport: Candidates for current and charge detection are, for instance, other quantum dots or quantum point contacts[64–67] that couple e.g. to the qubit which is ought to be measured. The coupling may be capacitive as recently achieved for two interacting double quantum dots[7,8,28] (DQD) and allow on-chip detection. This system is of special interest since it represents two interacting qubits when each double dot is occupied by one electron. Moreover, by opening both double dots it enables the study of two interacting mesoscopic currents.

Quantum point contacts (QPC) serve as sensitive charge detectors[68] and are used to monitor single-electron tunneling through a quantum dot.[69–73] Similar to zero dimensional quantum dots, a point contact is a narrow constriction of the two dimensional electron gas in quasi one dimension. In contrast to the former, electrons can move in one direction and form a conductor. Since its length is below the mean free path, the electron transport is no longer diffusive and dominated by scattering but rather ballistic. So, electron movement is only defined by the geometry of the point contact, such as the trajectories of billiard balls are only determined by the boundary of their table when scattering can be neglected. However, if the point contact is of the order of the Fermi wavelength, or below, the wave character of the electrons becomes evident and one terms it a *quantum* point contact. This quantum point contact acts, at low temperatures about a few milli Kelvin, as a waveguide, through which an integer number of transverse modes[67] propagates. In consequence, the current becomes quantized.[64,65,74] The charge quantization of quantum point contacts manifests in a step-like current-voltage characteristic with a step size of $2e^2/h$ only depending on the elementary charge e and Planck's constant h. For a sensitive response to a nearby electron, thus, one operates the QPC at a working point between to steps. In contrast to diffusive transport, conductance or its inverse, the resistance, are no longer a result of scattering events on impurities but rather a result of transmission as discovered by Rolf Landauer and extended by Markus Büttiker[4,9] to multiple transmission channels.

Main objective and organization of this thesis: The investigation of electron transport in capacitively coupled quantum dots is one of the main issues of this work. Stationary transport properties are analyzed in terms of full-counting statistics[75–77] in the formalism of Bloch-Redfield master equations.[78,79]

Chapters 2 and 3 provide the theoretical framework of this thesis. Chapter 2 is subjected to capacitively coupled quantum dots and an orthodox theory of master equations. Chapter 3 contains our generalizations and developments concerning heat transport, equilibrium fluctuation relations, and frequency dependent transport.

After developing the theoretical framework, we treat in the subsequent chapters three particular problems concerning quantum transport. In chapter 4, we consider a coherent quantum ratchet setup[80] formed by two coupled double quantum dots, where one of the double quantum dots serves as unbiased ratchet circuit and the other as driving source, see Ref. 81. Tunnel oscillations induce phenomena known from ac-driven transport. In absence of any driving no electron current flows in the ratchet. However, application of an external force with zero net bias, may induce

local fluctuations causing a dc current. Hence, the ratchet circuit may be either used as current rectifier or as noise detector.[21,82,83] Counting statistics of the ratchet circuit and its influence on the drive are studied. In chapter 5, we address the question of monitoring electron transport of a double quantum dot with a nearby quantum point contact. We study its suitability as charge and current detector, see Ref. 63. Amongst others, we consider the backaction of the monitor on the coherence of the measured circuit, which is a main issue of quantum measurement. Finally, we investigate in chapter 6 formal properties of Bloch-Redfield master equations, see Ref. 84. At equilibrium, exact relations between transport coefficients such as conductance and noise are known. We study to which extent the Bloch-Redfield description complies with these exact exchange fluctuation relations.

2 Capacitive coupled quantum dots and master equations

Gated quantum dots represent a mesoscopic conductor and consist of a central system of discrete electron levels that are in contact with a few leads. These leads form, on the contrary, fermionic baths of quasi-continuous states and serve as electron donators and acceptors. They enable tunneling events between the system–bath interfaces which are commonly characterized by full-counting statistics of transported electrons.[85–87] The basic idea is that the tunneling events change the charge occupations on the leads such that a description of the charge moments also captures the electron transport. So, the moment generating function is the central quantity of full-counting statistics.

In this chapter, we first regard two transport experiments on lateral quantum dots. Then, we turn towards the theoretical foundation and introduce the moment and cumulant generating function. Briefly, we show how they can be expressed in terms of a master equation, and how stationary quantities, such as the average current and current–current correlations,[88] can be calculated recursively.[76,89] In addition, we generalize the moment generating function to describe the energy exchange at the leads, and remark on exchange fluctuation theorems in transport.[90–93] Finally, we illustrate some of these concepts by applying them to a double quantum dot.

2.1. Experiments on lateral quantum dots

We discuss two experiments on capacitively coupled quantum dots to motivate our theoretical studies. First, we consider a current measurement of a driven quantum ratchet performed by Khrapai et al., Ref. 7. Afterwards, we describe an experiment on nonequilibrium fluctuation relations conducted by Nakamura et al., Ref. 94.

Quantum ratchet: Figure 2.1(a) shows a semiconductor heterostructure sample providing a two dimensional electron gas with metallic gates. Application of external gate voltages are used to raise potential barriers and electrostatically define quantum dots. In particular, by charging the central gate C sufficiently negative two separated circuits are obtained where tunneling of electrons between these circuits is forbidden. A double quantum dot circuit is defined by the gates 1–5 while the gates 7–9 are used to form a quantum point contact.

The double quantum dot, unbiased but possessing detuned energy levels, may act as quantum ratchet. Weakly inter-dot tunneling localizes an electron on one of the dots and, thus, prohibits elastic tunneling between them. However, nonequilibrium

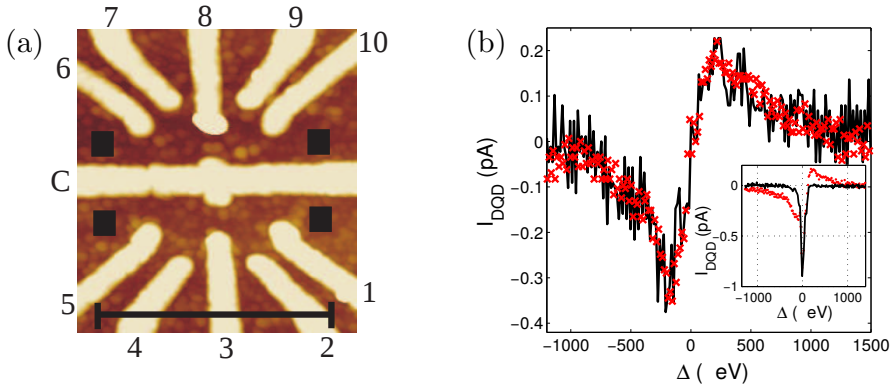

Fig. 2.1.: (a) Micrograph of a GaAs/AlGaAs heterostructure, where the light colored regions show superimposed metallic contacts. Black squares mark source and drain, and the black bar displays the length scale of 1 μm. (b) Inelastic DQD current as function of the detuning for various values of the QPC bias voltage, V_{QPC}. Values are $V_{\mathrm{QPC}} = -1.55$ mV (symbols) and $V_{\mathrm{QPC}} = -1.15$ mV (solid line, scaled by 3.3). Other parameters are DQD tunnel rates about 40 μeV and inter-dot tunneling of about 0.1 μeV. The inset shows the raw data of the DQD current for $V_{\mathrm{QPC}} = 0$ (solid line) and $V_{\mathrm{QPC}} = -1.45$ mV (symbols) containing elastic and inelastic tunnel contributions. A small bias voltage on the double quantum dot, $V_{\mathrm{DQD}} = -20$ μV, is applied. The figures are taken from Ref. 7.

fluctuations can mediate inelastic tunneling of the charge which then may leave the dot through the adjacent contact, followed by a recharging of the former dot. Nonequilibrium fluctuations induce, thus, a directed net current. Here, the quantum point contact serves as source of such nonequilibrium fluctuations when strongly biased. Then, electrons traverse the QPC and interact capacitively with the localized charge on the DQD. The resulting ratchet current is shown in Fig. 2.1(b) as a function of the detuning and for two QPC bias voltages. It possesses a generic shape and assumes finite values close to its reversal point at zero detuning. For large detuning the current vanishes since resonant driving is no longer possible. Such transport experiments are typically performed in a dilution refrigerator to achieve operating temperatures of a few hundred milli Kelvin.

Notice that for clarity the elastic contribution characterized by a resonance peak at zero detuning has been subtracted. The inset in panel (b), however, shows the raw data for finite and zero QPC bias voltage, where the latter only is affected by elastic tunneling.

In chapter 4, we theoretically investigate a similar setup. In contrast to this experiment, we consider in our model a strongly biased double quantum dot as source of nonequlibrium fluctuations. This enables us to control the distance of the resonance peaks by means of its inter-dot tunneling.

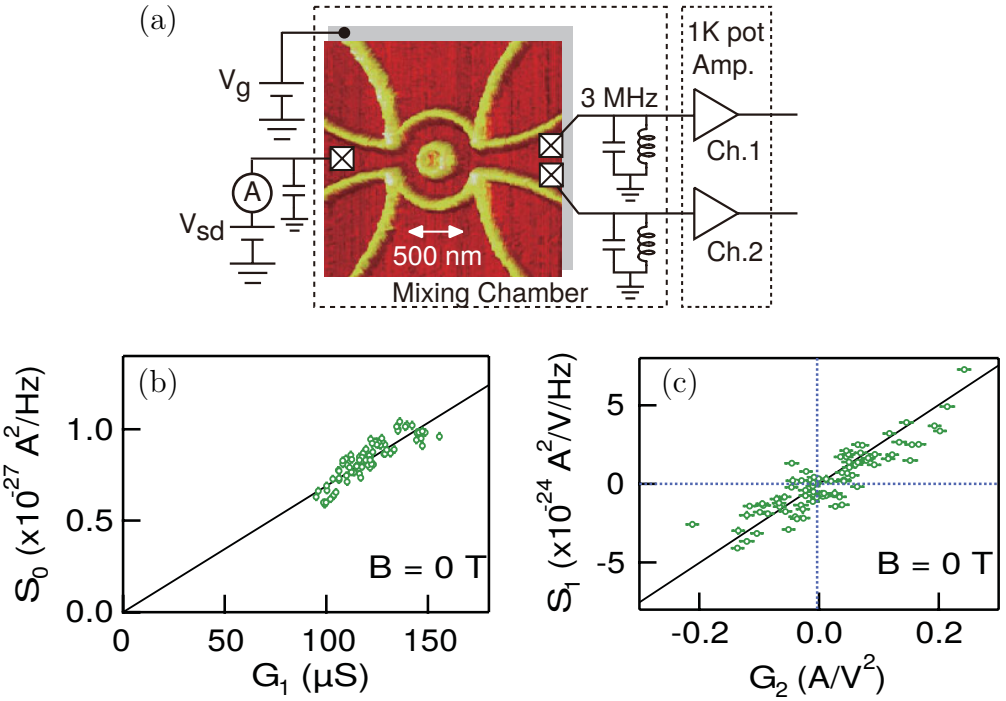

Fig. 2.2.: (a) Micrograph of a coherent conductor. Panels (b) and (c) show dependences between the Taylor coefficients of the current and its variance, see Eqs. (2.1) and (2.2), respectively. Solid lines serve as guiding lines. (b) S_0 as function of the conductance G_1. (c) S_1 as function of the nonlinear conductance G_2. The figures are taken from Ref. 94.

Exchange fluctuations: The experiment by Nakamura et al.[94] is devoted to study a coherent quantum conductor with respect to nonequilibrium fluctuation relations. Figure 2.2(a) shows an Aharonov-Bohm ring serving as coherent quantum conductor on which such relations have been probed at zero magnetic field, B. The sample is a GaAs/AlGaAs heterostructure allowing transport experiments where a back-gate is used to alter the conductance with a bias voltage V_g.

The question is to relate the Taylor coefficients of the conductor current with respect to the source drain bias voltage V,

$$I = G_1 V + \frac{1}{2!} G_2 V^2 + \frac{1}{3!} G_3 V^3 + \cdots, \tag{2.1}$$

to those of its variance or zero-frequency noise,

$$S = S_0 + S_1 V + \frac{1}{2!} S_2 V^2 + \cdots. \tag{2.2}$$

From linear response theory it is known that the conductance is proportional to the lowest order coefficient of the zero-frequency noise power, S_0. They obey the relation $S_0 = 4k_B T G_1$ with Boltzmann factor k_B and temperature T. One can also derive similar relations of higher order such as $S_1 = 4k_B T G_2$, see Sec. 2.3 and Appendix E. These proportionalities are shown in figures 2.2(b) and 2.2(c) for the experimental

setup. In practice, current and noise have been measured as function of the bias voltage V_g from which the Taylor coefficients have been extracted and mapped.

In chapter 6, we study exchange fluctuations in the context of the master equation description which we introduce in the following section. Notice that our definition of the power spectrum, used later on, differs by a factor 2 originating from a different convention of the Fourier transform.

2.2. Moments, cumulants, and the master equation

Low-frequency properties of transport can be characterized by the distribution of the number of transported electrons through the leads at large times. The central quantity is the moment generating function $M(\boldsymbol{\chi}, t) = \langle e^{i\boldsymbol{\chi}\cdot(\boldsymbol{N}-\boldsymbol{N}_0)}\rangle_t$ which assigns to each lead α a counting variable χ_α such that derivation with respect to these counting variables yields moments in the lead occupations, N_α. Here, we introduced the counting field $\boldsymbol{\chi} = (\chi_1, \chi_2, \ldots)$ and the vector $\boldsymbol{N} = (N_1, N_2, \ldots)$ of electron numbers that reside on each lead after a period t. To quantify the change of electrons, the initial electron numbers, $\boldsymbol{N}_0$, are subtracted. The occupation cumulants are the Taylor coefficients of $\ln M(\boldsymbol{\chi}, t)$ which, for long times, eventually grow linearly in time.[86] Thus, division by the time period yields stationary quantities describing particle currents. This motivates the definition of the generating function of current cumulants

$$Z(\boldsymbol{\chi}) = \lim_{t\to\infty} \frac{\partial \ln M(\boldsymbol{\chi}, t)}{\partial t}. \tag{2.3}$$

A series expansion[95–98] of both generating functions in the counting field establishes a relation between $\boldsymbol{n}$th current cumulants $\kappa^{\boldsymbol{n}}$ and $\boldsymbol{n}$th occupation moments $m^{\boldsymbol{n}}$,

$$\sum_{\boldsymbol{n}\neq\boldsymbol{0}} \frac{(i\boldsymbol{\chi})^{\boldsymbol{n}}}{\boldsymbol{n}!}\kappa^{\boldsymbol{n}} = \lim_{t\to\infty} \frac{\partial}{\partial t} \ln\Big[1 + \sum_{\boldsymbol{n}\neq\boldsymbol{0}} \frac{(i\boldsymbol{\chi})^{\boldsymbol{n}}}{\boldsymbol{n}!} m^{\boldsymbol{n}}(t)\Big], \tag{2.4}$$

where the factorial of the multi-index is defined as $\boldsymbol{n}! = n_1! n_2! \cdots$ and the polynomial in the counting field is evaluated by $(i\boldsymbol{\chi})^{\boldsymbol{n}} = (i\chi_1)^{n_1}(i\chi_2)^{n_2}\cdots$.

In the following, we use superscripts to express the multiplicity of derivations with respect to a counting variable and subscripts to define their ordering such that, for instance,

$$\kappa_{\alpha\beta}^{n_\alpha n_\beta} = \frac{\partial^{n_\alpha+n_\beta}}{(\partial i\chi_\alpha)^{n_\alpha}(\partial i\chi_\beta)^{n_\beta}} Z\Big|_{\boldsymbol{\chi}=\boldsymbol{0}}. \tag{2.5}$$

Omission of the superscripts indicates that only simple derivatives are involved while subscripts are omitted when an ordering is agreed as above, Eq. (2.4), by the position of the vector elements. Of particular interest are first-order and second-order cumulants. The former corresponds to the current $I_\alpha = \kappa_\alpha$ that is passing a lead α, while the latter relates to the zero-frequency limit, $S_{\alpha\beta} = \kappa_{\alpha\beta}$, of the current–current correlation function[88] $\langle I_\alpha, I_\beta\rangle_{\omega\to 0}$. Their noise-to-signal ratio $F_\alpha = S_{\alpha\alpha}/|I_\alpha|$

indicates whether transport is sub or super Poissonian.[4] A Fano factor of $F_\alpha = 1$ suggests a Poissonian process where tunneling events occur statistically independent, although a more faithful criterion is the $g^{(2)}$ function.[99] Since the noise contains information about the transport process, it can be considered as signal[100,101] and the first few orders such as the variance are meaningful. However, beyond a certain order, cumulants exhibit universal features,[102,103] as we also encounter in chapter 4.

Master equation: To evaluate the moment generating function, we assume that the total Hamiltonian that governs the time-evolution of the total density matrix, $\sigma(t)$, can be decomposed into three contributions: A system and a bath part which commute with the electron numbers on each dot and a system–bath tunneling term that weakly couples the system to the environment. This allows treating the tunneling term perturbatively. As starting point serves the augmented density matrix, $\rho(\boldsymbol{\chi}, t) = \mathrm{tr}_{\mathrm{leads}}\, e^{i\boldsymbol{\chi}\cdot(\boldsymbol{N}-\boldsymbol{N}_0)}\sigma(t)$, which yields the moment generating function when traced out over the system degrees of freedom. Notice that for vanishing counting field, $\rho(\boldsymbol{\chi}, t)$ yields the common reduced density matrix of the system. To determine the augmented density matrix, one establishes therefore an equation of motion that follows the usual Bloch-Redfield or Born-Markov master equation approach.[78,79,104,105] The only peculiarity in the derivation is that the interaction picture of the total density matrix is now extended by a counting field which leads to a non-Hermitian time-evolution, $\tilde{\sigma}(\boldsymbol{\chi}, t) \equiv \tilde{U}(\boldsymbol{\chi}, t)\sigma(0)\tilde{U}(-\boldsymbol{\chi}, -t)$, with $\tilde{U}(\boldsymbol{\chi}, t) = e^{i\boldsymbol{\chi}\cdot\boldsymbol{N}/2}\tilde{U}(t)e^{-i\boldsymbol{\chi}\cdot\boldsymbol{N}/2}$. The tilde indicates the usual interaction picture and $U(t)$ denotes the total time-evolution operator. Thus, derivation in time transfers the counting field in the tunneling Hamiltonian,[87,106] H_V, and in consequence the Liouville-von-Neumann equation and its interaction picture no longer can be expressed as commutator. So, the generalized master equation becomes,

$$\dot{\rho} = -i[H_S,\ \rho] - \int_0^\infty dt\ \mathrm{tr}_{\mathrm{leads}}[\![H_V(p\boldsymbol{\chi}),\ [\![\tilde{H}_V(q\boldsymbol{\chi}, -t),\ \rho \otimes \rho_{\boldsymbol{\mu}}^{\mathrm{leads}}]\!]_{q=+}^{-}]\!]_{p=+}^{-}, \tag{2.6}$$

with the abbreviation

$$[\![A(p),\ B(p)]\!]_{p=\alpha}^{\beta} = A(\alpha)B(\alpha) - B(\beta)A(\beta), \tag{2.7}$$

where $\rho_{\boldsymbol{\mu}}^{\mathrm{leads}} \propto \exp[-\beta\sum_\alpha(H_\alpha - \mu_\alpha N_\alpha)]$ refers to the grand canonical ensemble of each lead at the respective chemical potential, μ_α. The H_α are the lead Hamiltonians while β denotes the inverse temperature $\beta = 1/k_BT$. Alternatively, one may start with a number-resolved master equation and attribute a virtual detector,[107] or consider the common Bloch-Redfield equation and multiply therein the full density operator by a counting phase $e^{i\boldsymbol{\chi}\cdot\boldsymbol{N}}$ before tracing out the leads.[108]

In order to solve the master equation (2.6), one can cast it into the matrix form

$$\dot{\rho}(\boldsymbol{\chi}, t) = \mathcal{L}(\boldsymbol{\chi})\rho(\boldsymbol{\chi}, t) \equiv \Big[\mathcal{L}(\mathbf{0}) + \mathcal{W}(\boldsymbol{\chi})\Big]\rho(\boldsymbol{\chi}, t), \tag{2.8}$$

where $\mathcal{L}_{\mathbf{0}} \equiv \mathcal{L}(\mathbf{0})$ is the Liouville operator that determines the stationary solution ρ_{st} via $\mathcal{L}_{\mathbf{0}}\rho_{\mathrm{st}} = \mathbf{0}$, while the long-time solution is captured by the smallest eigenvalue

of $\mathcal{L}(\boldsymbol{\chi})$. This representation allows reducing the computation of current cumulants to an eigenvalue problem, $\mathcal{L}(\boldsymbol{\chi})\phi(\boldsymbol{\chi}) = \lambda(\boldsymbol{\chi})\phi(\boldsymbol{\chi})$, since the cumulant generating function is given by the eigenvalue with the smallest real value.[86] This eigenvalue $\lambda(\boldsymbol{\chi}) = \sum_{\boldsymbol{n}}(i\boldsymbol{\chi})^{\boldsymbol{n}}\lambda^{\boldsymbol{n}}/\boldsymbol{n}!$ can be expanded in the counting field by Rayleigh-Schrödinger perturbation theory[109] and computed iteratively.[76] Thus, $\lambda^{\boldsymbol{n}}$ follow from the recursion

$$\lambda^{\boldsymbol{n}} = \sum_{\boldsymbol{m}\neq\boldsymbol{0}} \binom{\boldsymbol{n}}{\boldsymbol{m}} \operatorname{tr}(\mathcal{W}^{\boldsymbol{m}}\phi^{\boldsymbol{n}-\boldsymbol{m}}), \tag{2.9}$$

$$\phi^{\boldsymbol{n}} = \mathcal{R}_0 \sum_{\boldsymbol{m}\neq\boldsymbol{0}} \binom{\boldsymbol{n}}{\boldsymbol{m}} \big(\mathcal{W}^{\boldsymbol{m}} - \lambda^{\boldsymbol{m}}\big)\phi^{\boldsymbol{n}-\boldsymbol{m}}, \tag{2.10}$$

with the initial condition $\lambda^{\boldsymbol{0}} = 0$ and $\phi^{\boldsymbol{0}} = \rho_{\mathrm{st}}$. The $\mathcal{W}^{\boldsymbol{m}}$ refer to the Taylor coefficients of $\mathcal{W}(\boldsymbol{\chi})$, and $\mathcal{R}(z) = \mathcal{Q}(z - \mathcal{L}_{\boldsymbol{0}})^{-1}\mathcal{Q}$ defines the pseudoresolvent of the Liouvillian $\mathcal{L}_{\boldsymbol{0}}$ where $\mathcal{Q} = (\mathbb{1} - \rho_{\mathrm{st}}\operatorname{tr})$ denotes the projector to the Liouville subspace orthogonal to the stationary density operator ρ_{st}.

So far, we have defined cumulants that describe the deviation from a Gaussian distribution and, thus, feature that a Gaussian process terminates after the second order while a Poissonian process is characterized by infinite but equal orders. However, tunneling events are rather rare and resemble more to a Poissonian process. This motivates the introduction of factorial cumulants[77,110,111] which are generated from Eq. (2.3) after replacing $e^{i\chi_\alpha} \to 1 + z_\alpha$ and taking the derivative with respect to z_α. For a Poissonian process they vanish after the first order.

2.3. Energy transport, and exchange fluctuations

The moment generating function can be generalized to capture energy and heat transport,[92,93,112–114] $M(\boldsymbol{\chi}, \boldsymbol{\xi}, t) \propto \langle e^{i\boldsymbol{\chi}\cdot\boldsymbol{N} + i\boldsymbol{\xi}\cdot\boldsymbol{H}}\rangle_t$, by introducing an energy counting field $\boldsymbol{\xi} = (\xi_1, \xi_2, \ldots)$ assigned to each lead Hamiltonian, $\boldsymbol{H} = (H_1, H_2, \ldots)$. Derivation with respect to $i\xi_\alpha$ yields, thus, the energy moments at lead α. The dependence on the chemical potentials is implicitly contained in the grand canonical average. For clarity, we omitted here the normalization at initial time to unity. The corresponding master equation follows from Eq. (2.6) by substituting the dot-lead coupling $\tilde{H}_V(p\boldsymbol{\chi}, t)$ with

$$\tilde{H}_V(p\boldsymbol{\chi}, p\boldsymbol{\xi}, t) = e^{-i\frac{p}{2}(\boldsymbol{\chi}\cdot\boldsymbol{N} + \boldsymbol{\xi}\cdot\boldsymbol{H})}\tilde{H}_V(t)e^{i\frac{p}{2}(\boldsymbol{\chi}\cdot\boldsymbol{N} + \boldsymbol{\xi}\cdot\boldsymbol{H})}. \tag{2.11}$$

The cumulant generating functions obeys the exact symmetry relation,[90–93]

$$Z(\boldsymbol{\chi}, \boldsymbol{\xi}) = Z(-\boldsymbol{\chi} - i\beta\boldsymbol{\mu}, -\boldsymbol{\xi} - i\beta), \tag{2.12}$$

in the charge and energy counting field, where the replacement in the energy counting field has to be understood as $\xi_\alpha \to -\xi_\alpha - i\beta$. This symmetry relation is a variant of the exchange fluctuation theorems which relate probabilities for non-equilibrium transitions that start from a Gibbs state and reflect the time reversibility of the microscopic equations of motion.[115,116] Frequently, they are expressed by the statistics

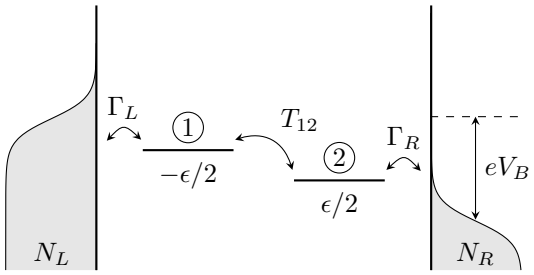

Fig. 2.3.: Double quantum dot biased by a voltage V_B and detuned by ϵ. The dot-lead tunneling rates are Γ_L and Γ_R while T_{12} denotes the inter-dot tunneling. Occupation numbers N_L and N_R refer to the left and right lead, respectively.

of work performed at a system upon time-dependent parameter variation. Taylor expansion of Eq. (2.12) at equilibrium provides relations between transport coefficients which can be verified experimentally,[94,117,118] see section 2.1.

For instance, the Johnson-Nyquist relation for lead α follows by taking the derivative of Eq. (2.12) with respect to $i\chi_\alpha$ and μ_α on both sides and evaluating the resulting expression at $\boldsymbol{\chi} = \boldsymbol{\xi} = \boldsymbol{\mu} = \mathbf{0}$, whereby one has to take into account that the cumulant generating function depends implicitly on the chemical potentials. Notice, the chemical potentials at equilibrium are defined relative to the common Fermi energy. By introducing the differential conductance $G_{\alpha,\beta} = -(\partial^2 Z/\partial i\chi_\alpha \partial\mu_\beta)|_{\boldsymbol{\chi}=\boldsymbol{\xi}=\mathbf{0}}$, this relation reads $2k_BTG^{\mathrm{eq}}_{\alpha,\alpha} = S^{\mathrm{eq}}_{\alpha\alpha}$, while the superscript "eq" indicates the evaluation at equilibrium, i.e. at equal chemical potentials. Further relations are listed in Appendix E.

Alternative definitions of the heat may refer to the energy on the leads relative to the chemical potentials, see Ref. 112. This may formally be obtained by the replacement $\chi_\alpha \to \chi_\alpha - \mu_\alpha\xi_\alpha$.[112]

2.4. Example: Double quantum dot

In this section, we look at a double quantum dot[119–123] (DQD) in contact with two leads. The purpose is twofold: To give a notion of full counting statistics and the framework of master equations, and to introduce a building block of the systems considered in the subsequent chapters. We first establish the full master equation for the DQD and provide the Taylor coefficients of the total Liouvillian which are required for calculating the cumulants. Here, we will have a closer look on the current and its differential conductance. Then, we take the high-bias limit to obtain a Lindblad form and consider the stationary current, the noise, and the Fano factor. Furthermore, we introduce the $g^{(2)}$-function to identify bunching and antibunching of electrons.

The setup of the DQD model is sketched in Fig. 2.3 and described by the Hamilto-

nian $H = H_S + H_V + \sum_\alpha H_\alpha$, where

$$H_S = \frac{\epsilon}{2}(N_2 - N_1) + T_{12}(c_1^\dagger c_2 + c_2^\dagger c_1) + U N_1 N_2 \tag{2.13}$$

models the central system with tunnel coupling T_{12}, Coulomb repulsion U, and fermionic creation operators $c_\ell^\dagger$ for an electron in dot $\ell = 1, 2$. Here, we do not consider spin effects. For strong Coulomb repulsion, at most one electron resides on the DQD and in consequence only the empty state $|0\rangle$ and the single-electron states $|\ell\rangle$ are energetically accessible, while weak Coulomb repulsion allows electrons to assume a doubly occupied state $|d\rangle$. The levels are symmetrically detuned by ϵ and their occupation numbers are given by $N_\ell = c_\ell^\dagger c_\ell$. The environment is modeled by free electrons with the Hamiltonian $H_\alpha = \sum_q \epsilon_{q\alpha} c_{q\alpha}^\dagger c_{q\alpha}$ where $c_{q\alpha}$ annihilates an electron in mode q of lead $\alpha = L, R$ with the energy $\epsilon_{q\alpha}$. Analogously, the occupation numbers $N_\alpha = \sum_q c_{q\alpha}^\dagger c_{q\alpha}$ of the left and right lead are defined. The coupling between central system and reservoirs is given by

$$H_V = \sum_{q,\alpha} V_{q\alpha}(c_{\ell_\alpha}^\dagger c_{q\alpha} + c_{q\alpha}^\dagger c_{\ell_\alpha}), \tag{2.14}$$

where we introduced the mapping ℓ_α that takes the values $\ell_L = 1$ and $\ell_R = 2$.

Inserting these Hamiltonians into Eq. (2.6) yields the master equation of the DQD $\dot\rho = \mathcal{L}_{\mathrm{DQD}}(\boldsymbol{\chi})\rho$. The counting fields only affect the fermionic operators of the leads, $\tilde c_{q\alpha}(\boldsymbol{\chi}, t) \equiv e^{i\boldsymbol{\chi}\cdot\boldsymbol{N}/2}\tilde c_{q\alpha}(t)e^{-i\boldsymbol{\chi}\cdot\boldsymbol{N}/2} = e^{-i\epsilon_{q\alpha}t - i\chi_\alpha/2}c_{q\alpha}$, since the sytstem operators commute pairwise with the lead occupation numbers. The resulting Liouvillian may be separated into $\mathcal{L}_{\mathrm{DQD}}(\boldsymbol{\chi})\rho = -i[H_S,\ \rho] + \mathcal{L}^{\mathrm{in}}(\boldsymbol{\chi})\rho + \mathcal{L}^{\mathrm{out}}(\boldsymbol{\chi})\rho$ with

$$\mathcal{L}^{\mathrm{out}}(\boldsymbol{\chi})\rho = \sum_\alpha \int dt\ F_\alpha^>(t)\Big[e^{i\chi_\alpha} J_{\ell_\alpha}^{\mathrm{out}}(t) - D_{\ell_\alpha}^{\mathrm{out}}(t)\Big], \tag{2.15}$$

where the superoperators are defined by

$$J_{\ell_\alpha}^{\mathrm{out}}(t)\rho = \frac{1}{2}\Big[\tilde c_{\ell_\alpha}(-t)\rho c_{\ell_\alpha}^\dagger + c_{\ell_\alpha}\rho\tilde c_{\ell_\alpha}^\dagger(t)\Big], \tag{2.16}$$

$$D_{\ell_\alpha}^{\mathrm{out}}(t)\rho = \frac{1}{2}\Big[c_{\ell_\alpha}^\dagger\tilde c_{\ell_\alpha}(-t)\rho + \rho\tilde c_{\ell_\alpha}^\dagger(t)c_{\ell_\alpha}\Big]. \tag{2.17}$$

The lesser and greater correlation functions[95,124] $F_\alpha^<(t) = \sum_q |V_{q\alpha}|^2\langle c_{q\alpha}^\dagger(0)c_{q\alpha}(t)\rangle = F_\alpha^>(t - i\beta)e^{\beta\mu_\alpha}$ involve the chemical potential μ_α of lead α and the common lead temperature $T = 1/k_B\beta$. The corresponding term $\mathcal{L}^{\mathrm{in}}$ follows from the substitution $\{c_\ell, F_\alpha^>(t), \chi_\alpha\} \to \{c_\ell^\dagger, F_\alpha^<(-t), -\chi_\alpha\}$.

Cumulants can be derived within the recursive scheme, Eq. (2.9) and Eq. (2.10), where only Taylor coefficients $\mathcal{W}_\alpha^k = \mathcal{W}_\alpha^{k,\mathrm{in}} + \mathcal{W}_\alpha^{k,\mathrm{out}}$ with respect to the same lead contribute, as can be seen from Eq. (2.15). Thereby $\mathcal{W}_\alpha^0 = 0$ holds, and for $k > 0$,

$$\mathcal{W}_\alpha^{k,\mathrm{out}}\rho = \frac{\partial^k}{i^k\partial\chi_\alpha^k}\mathcal{L}^{\mathrm{out}}(\boldsymbol{\chi})\rho\Big|_{\boldsymbol{\chi}=\boldsymbol{0}} = \int dt\ F_\alpha^>(t)J_{\ell_\alpha}^{\mathrm{out}}(t)\rho, \tag{2.18}$$

while $\mathcal{W}_\alpha^{k,\mathrm{in}}$ follows from the substitution above and multiplication by a factor $(-1)^k$. It is common to introduce the jump operators $\mathcal{J}_\alpha^{\mathrm{in}}$, $\mathcal{J}_\alpha^{\mathrm{out}}$ for the tunnel-in and tunnel-out events which satisfy $\mathcal{W}_\alpha^{k,\mathrm{in}} = (-1)^k \mathcal{J}_\alpha^{\mathrm{in}}$ and $\mathcal{W}_\alpha^{k,\mathrm{out}} = \mathcal{J}_\alpha^{\mathrm{out}}$. The time integral is usually solved by expressing the time evolution of the system operators in their energy eigenbasis $\{|a\rangle\}$, where $H_S|a\rangle = E_a|a\rangle$, such that it basically reduces to the Fourier transform of the lesser and greater correlation functions. Their Fourier representation yields in the wide-band limit $F_\alpha^<(\epsilon) = \Gamma_\alpha f(\epsilon - \mu_\alpha) = \Gamma_\alpha - F_\alpha^>(\epsilon)$ with $f(x) = [\exp(\beta x) + 1]^{-1}$ Fermi function and $\Gamma_\alpha(\epsilon) = (2\pi/\hbar)\sum_q |V_{q\alpha}|^2 \delta(\epsilon - \epsilon_{q\alpha}) \equiv \Gamma_\alpha$ spectral density of the dot-lead couplings, which is assumed to be energy independent. In Appendix B, we list the eigendecomposition of the DQD Liouvillian.

From the spectral decomposition of the system Hamiltonian, $H_S = (\delta/2)(|e\rangle\langle e| - |g\rangle\langle g|) + U|d\rangle\langle d|$, it can be seen that the single-electron levels hybridize in the presence of an inter-dot tunneling, where $\delta = (\epsilon^2 + 4|T_{12}|^2)^{1/2}$ denotes the level splitting. The ground and excited states $|g\rangle$ and $|e\rangle$, respectively, are parametrized by[80,125]

$$|g\rangle = -\sin\theta|1\rangle + \cos\theta|2\rangle, \quad |e\rangle = \cos\theta|1\rangle + \sin\theta|2\rangle, \tag{2.19}$$

where $\cos(2\theta) = -\epsilon/\delta$, while the doubly occupied state $|d\rangle$ is not affected by the change of basis.

Whenever a chemical potential is aligned with the hybridized levels, $\mu_\alpha = \pm\delta/2$, a transition between single electron states and the empty state occurs which exhibits resonant tunneling. Is additionally the Coulomb repulsion applied, a transition between two electron states is involved. The transitions are visualized in Fig 2.4(a), where the current through the right lead is shown with respect to a bias window $eV_B = \mu_L - \mu_R$ and a shift $\mu_L + \mu_R$. Either no current flows (white region), electrons tunnel into the system (red region) or tunnel through the right lead (blue region). Moreover, the regions in dark blue and dark red correspond to doubly occupied states, while regions with low saturation correspond to singly occupied states. The vertical line marks symmetric bias voltage, $\mu_L = -\mu_R = eV_B/2$. Panels (b) and (c) in Fig 2.4 show the differential charge and heat conductance, respectively, along this symmetric bias voltage and as a function of the detuning. They may be either computed from the charge and heat currents by derivation with respect to the bias voltage or as done here from the generalized recursive scheme which will be introduced in chapter 3. The shown conductances demonstrate that in presence of the inter-dot tunneling the ground and excited level do not cross, but rather separate by $eV_B = 4|T_{12}|$. The two-electron state below the ground state and above the excited state, respectively, requires an additional bias voltage $eV_B = \mp 2U$ to be occupied.

In the following, we consider strong Coulomb repulsion U, such that the two-electron states are shifted out of the transport window, and only single occupation occurs. The completeness relation thus reduces to $\mathbb{1} = |0\rangle\langle 0| + N_1 + N_2$.

High bias limit: For large bias voltage V_B, the DQD Liouvillian ensures unidirectional transport. This is reflected by the limit $\mu_{L,R} \to \pm\infty$ in which the lesser correlation function $F_\alpha^<(\epsilon)$ tends to Γ_L and 0, respectively. The Liouvillian reduces,

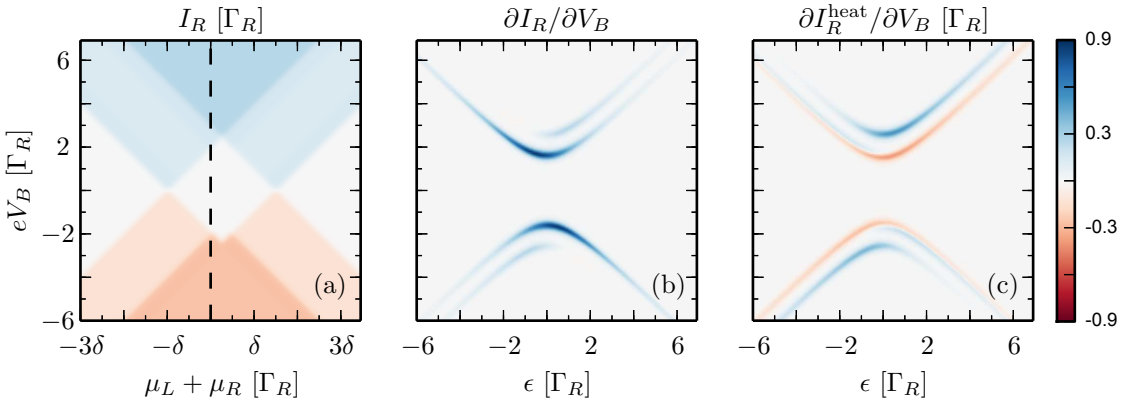

Fig. 2.4.: (a) Current through the right lead as function of $\mu_L+\mu_R$ and the bias voltage $eV_B = \mu_L - \mu_R$. Parameters are $k_BT = \Gamma_R/20$, $\epsilon = 1.2\Gamma_R$, $T_{12} = 0.8\Gamma_R$, and $\Gamma_R = \Gamma_L = 2U$. The stroked line indicates symmetric bias voltage for which in panel (b) the charge conductance, and in panel (c) the heat conductance are shown in dependence of the detuning ϵ. The step size between two neighboring ticks is $2U$ which corresponds in panel (a) to half the level splitting, $\delta/2$.

thus, to

$$\mathcal{L}_{\rm DQD}(\boldsymbol{\chi})\rho = -i[H_S,\ \rho] + \Gamma_L\Big[\mathcal{D}(c_1^\dagger)\rho + (e^{-i\chi_L} - 1)c_1^\dagger\rho c_1\Big] + \Gamma_R\Big[\mathcal{D}(c_2)\rho + (e^{i\chi_R} - 1)c_2\rho c_2^\dagger\Big], \tag{2.20}$$

with the dissipator $\mathcal{D}(x)\rho = x\rho x^\dagger - (x^\dagger x\rho + \rho x^\dagger x)/2$. The current through the right lead becomes in unidirectional transport proportional to the average occupation of the right dot, $I_R = \Gamma_R\langle N_2\rangle$, and reads

$$I_R = \frac{4|T_{12}|^2\Gamma_L\Gamma_R}{4|T_{12}|^2(2\Gamma_L + \Gamma_R) + \Gamma_L(4\epsilon^2 + \Gamma_R^2)}, \tag{2.21}$$

while the corresponding zero-frequency noise is given by[121]

$$S_{RR} = I_R\frac{16|T_{12}|^4(4\Gamma_L^2 + \Gamma_R^2) + 8|T_{12}|^2\Gamma_L^2(12\epsilon^2 - \Gamma_R^2) + \Gamma_L^2(4\epsilon^2 + \Gamma_R^2)^2}{\Big[4|T_{12}|^2(2\Gamma_L + \Gamma_R) + \Gamma_L(4\epsilon^2 + \Gamma_R^2)\Big]^2}. \tag{2.22}$$

Together with their ratio, the Fano factor, they are depicted in Fig. 2.5. For small inter-dot tunneling T_{12}, the current is quadratic in T_{12}, as can be seen from the inset, while large T_{12} corresponds to an open channel and leads to a saturation. The noise also vanishes for $T_{12} = 0$ and saturates for large inter-dot tunneling, but exhibits a local minimum which for zero detuning and symmetric dot-lead tunneling is about $T_{12} = \Gamma_R/2\sqrt{3}$. In result, the Fano factor becomes finite in the absence of the coherent tunneling, and takes the value $F = 1$ indicating a Poissonian process. For increasing inter-dot tunneling it assumes a minimum, and eventually becomes $F = (4\Gamma_L^2 + \Gamma_R^2)/(2\Gamma_L + \Gamma_R)^2$ which is sub-Poissonian for finite incoherent rates

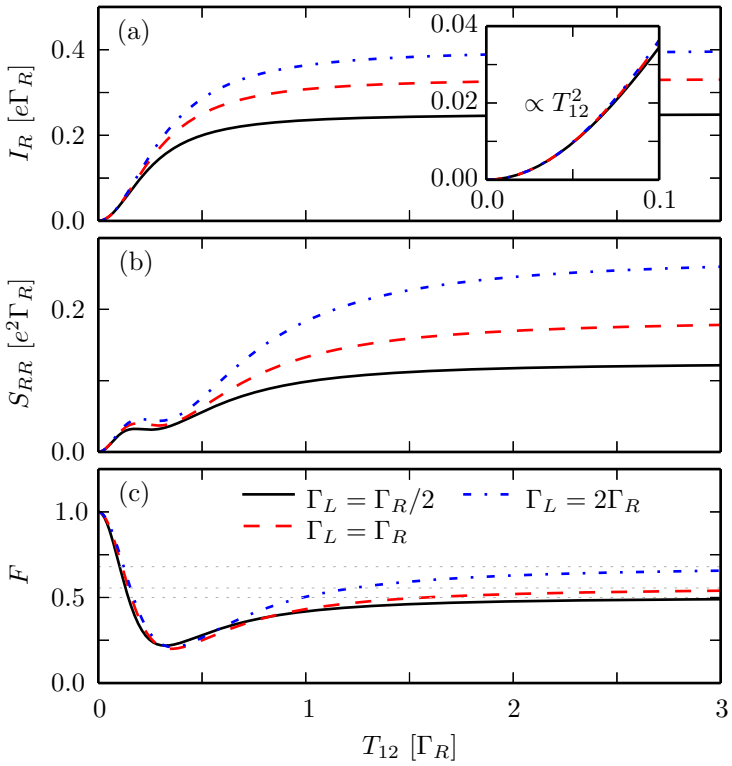

Fig. 2.5.: (a) Current, (b) noise, and (c) Fano factor $F = S_{RR}/|I_R|$ on the right lead in the high bias limit, plotted for various tunneling rates Γ_L as function of the inter-dot tunneling T_{12}. Zero detuning is assumed. The inset in panel (a) is a zoom into the current I_R. The thin dotted lines in panel (c) show the corresponding Fano factors in the rotating-wave approximation.

Γ_L and Γ_R, and approaches the Poissonian value for strongly asymmetric dot-lead coupling. The electron states for the considered parameter range correspond to a stationary density matrix $\rho_{\rm st}$ that for zero inter-dot tunneling is localized in the left state, for small inter-dot tunneling exhibits transitions between the ground and excited state, and for large values of T_{12} becomes diagonal in the occupations.

The saturations (dashed lines) in Fig. 2.5(c) have been obtained by rotating-wave approximation[105] (RWA), which states that for very weak dot-lead coupling the system dynamics is determined by the coherent time evolution. It sets the constrain on the Liouvillian than only matrix elements $[L_{\rm DQD}]_{ab,a'b'}$ contribute which fulfill the condition $E_a - E_b = E_{a'} - E_{b'}$. For a non-degenerated energy spectrum this condition can be assigned to the subscripts, $0 = \delta_{a-b,a'-b'}$, and therewith reduces the Liouvillian to the RWA Liouvillian

$$[L_{\rm DQD}^{\rm RWA}]_{ab,a'b'} = \Big[\delta_{ab}\delta_{a'b'} + (1-\delta_{a'b'})\delta_{aa'}\delta_{bb'}\Big][L_{\rm DQD}]_{ab,a'b'}. \tag{2.23}$$

Commonly, a sub-Poissonian Fano factor is associated with electron antibunching which, in general, is incorrect. To illuminate this point, we consider the second-order

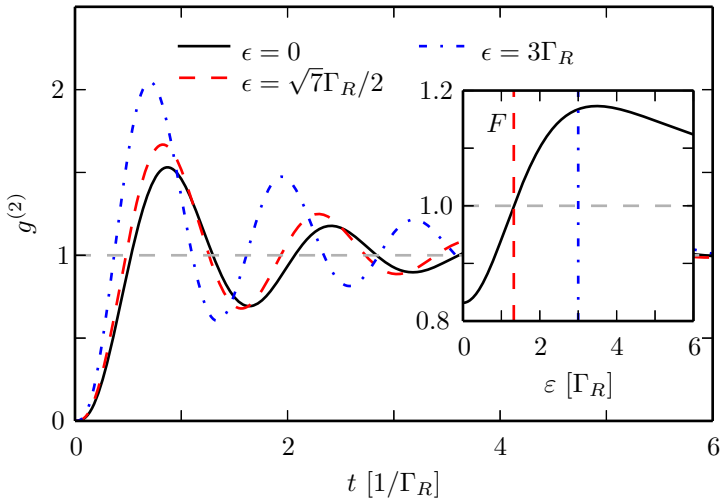

Fig. 2.6.: Second order correlation function $g^{(2)}$ propagated in time for three different values of the detuning, ϵ; see also Ref. 99. Parameters are $\Gamma_L = 10\Gamma_R$, and $T_{12} = 2\Gamma_R$. These various detunings correspond to a sub-Poissonian, Poissonian and super-Poissonian Fano factor F, as is depicted in the inset. The vertical lines mark the Poissonian, $\epsilon = (\sqrt{7}/2)\Gamma_R$, and the super-Poissonian value, $\epsilon = 3\Gamma_R$, while the Fano factor is sub-Poissonian for zero detuning. The horizontal lines indicates the saturations at unity.

correlation function[99,126]

$$g^{(2)}(t) = \frac{\langle \mathcal{J}_R^{\text{out}} \Omega(\mathbf{0}, t) \mathcal{J}_R^{\text{out}} \rangle}{\langle \mathcal{J}_R^{\text{out}} \rangle^2} \tag{2.24}$$

for the right lead, which describes the correlation between two tunnel-out events that occur after elapsed time t. It is normalized by the square of the outgoing current and, thus, tends to unity for large time. Originally, it was formulated to describe the photon counting but has been adapted by Emary et al., Ref. 99, to electron transport. It provides a criterion for electron bunching and antibunching: the condition $g^{(2)}(t) < g^{(2)}(0)$ identifies the tendency of electrons to arrive in pairs (bunching), while $g^{(2)}(t) > g^{(2)}(0)$ characterizes that electrons arrive separated (antibunching). For positive time argument, it coincides with $1 + S_{RR}(t)/I_R^2$ and, thus, is contained in the time dependent current–current auto-correlation of the right lead. A derivation of this time dependent autocorrelation is given in Sec. 3.2. Figure 2.6 shows the $g^{(2)}$-function in dependency of the time for various detunings which, due to asymmetric dot-lead couplings, correspond to a sub-Poissonian, Poissonian, and super-Poissonian Fano factor, cf. inset. However, the electron flow is antibunched since for strong Coulomb repulsion $g^{(2)}(0) = 0$ holds.

3 Formal developments of the master equation

The aim of this chapter is twofold: We provide a scheme to compute transport coefficients, see Sec. 2.3, and describe frequency dependent transport.[127–130] To tackle the former task, we extend the recursive scheme[76] discussed in chapter 2 which is used to compute the current cumulants. It is based on two facts: First, for a master equation, the zero-frequency current cumulant generating function is given by the eigenvalue of the generalized Liouvillian $\mathcal{L}_\chi$ with the smallest real value, where χ is the counting variable.[86] Second, the cumulants are the Taylor coefficients appearing in the expansion of the generating function $Z(\chi)$. Since Rayleigh-Schrödinger perturbation theory[109] provides a series expansion of eigenvalues, it can be used to compute cumulants,[76] by iteratively solving Eqs. (2.9) and (2.10).

Frequency dependent correlation functions are obtained from a generalized cumulant generating function regarding counting fields at different times. Derivation yields the corresponding cumulants which after Fourier transform provide the desired correlation functions. In particular, we consider second order correlation functions.

3.1. Generalized recursive scheme

Here, we generalize the recursive scheme in two respects. On the one hand, we want to compute also energy exchange cumulants which requires additional counting variables ξ_α for each lead α. On the other hand, we are interested in the transport coefficients, i.e., in a series expansion in the chemical potentials of the leads, μ_α, around their equilibrium value μ_0 which we set to zero for the ease of notation. While the formal aspects of the iteration scheme are the same as in its original version, the required series expansion of the Liouvillian in the variables $\boldsymbol{\chi}$, $\boldsymbol{\xi}$, and $\boldsymbol{\mu}$ is no longer that of a simple exponential.

Before extending the recursive scheme, we first have to address the inclusion of the heat counting field in the Liouvillian. Already in section 2.3 we have mentioned that Eq. (2.6) describes heat transport when including the heat counting field in the dot-lead Hamiltonian. In the case of the double or quadruple quantum dot, one can use the common master equation (2.8), with matrix elements given in Eq. (B.2), but has to modify the lesser and greater correlation functions appearing in the jump operators, i.e. in the terms accompanied by a counting phase $e^{\pm i\chi_\alpha}$. In time space, the modification consists in the replacement $t \to t - \xi_\alpha$ of the argument of these lesser and greater correlation functions. Thus, heat transport is maintained by the master equation (2.8) after the substitutions $F_\alpha^<(E) \to F_\alpha^<(E)e^{-iE\xi_\alpha}$ and $F_\alpha^>(E) \to F_\alpha^>(E)e^{iE\xi_\alpha}$, respectively, in the jump operators.

Following the idea of Ref. 76, we start by writing the generalized Liouvillian (6.2) as a series in all these variables,

$$\mathcal{L}_{\boldsymbol{\chi},\boldsymbol{\xi},\boldsymbol{\mu}} = \mathcal{L} + \sum_{\alpha} \sum_{k,k',k''=0}^{\infty} \frac{i^{k+k'}}{k!\, k'!\, k''!} \mathcal{W}_{\alpha}^{k,k',k''} \chi_{\alpha}^{k} \xi_{\alpha}^{k'} \mu_{\alpha}^{k''}, \tag{3.1}$$

with the Taylor coefficients $\mathcal{W}_{\alpha}^{0,0,0} = 0$ and $\mathcal{W}_{\alpha}^{k,k',k''} = \mathcal{W}_{\alpha,\mathrm{in}}^{k,k',k''} + \mathcal{W}_{\alpha,\mathrm{out}}^{k,k',k''}$, while for $k'' > 0$

$$\begin{aligned} \mathcal{W}_{\alpha,\mathrm{out}}^{k,k',k''} &= \partial_{i\chi_\alpha}^{k} \partial_{i\xi_\alpha}^{k'} \partial_{\mu_\alpha}^{k''} \mathcal{L}_{\boldsymbol{\chi},\boldsymbol{\xi},\boldsymbol{\mu}}^{\mathrm{out}} \Big|_{\boldsymbol{\chi},\boldsymbol{\xi},\boldsymbol{\mu}=\mathbf{0}} \\ &= \int dt\; \partial_{i\xi_\alpha}^{k'} \partial_{\mu_\alpha}^{k''} F_{\alpha}^{>}(t-\xi_\alpha)\Big|_{\boldsymbol{\xi},\boldsymbol{\mu}=\mathbf{0}} \begin{cases} J_{\ell_\alpha}^{\mathrm{out}}(t) - D_{\ell_\alpha}^{\mathrm{out}}(t) & \text{for } k = k' = 0, \\ J_{\ell_\alpha}^{\mathrm{out}}(t) & \text{else,} \end{cases} \end{aligned} \tag{3.2}$$

where the superoperators $J_{\ell_\alpha}^{\mathrm{out}}$ and $D_{\ell_\alpha}^{\mathrm{out}}$ are given by Eqs. (2.16), (2.17). The latter appear in the integrals that provide the jump operators and the dissipator, respectively, of the Liouvillian. As before, $\mathcal{W}_{\alpha,\mathrm{in}}^{k,k',k''}$ follows from the substitution $\{c_\ell, F_\alpha^{>}(t)\} \to \{c_\ell^\dagger, F_\alpha^{<}(-t)\}$ and multiplication by a factor $(-1)^k$. Notice that no cross terms between different leads emerge.

The derivatives with respect to the heat counting variables ξ_α and the chemical potentials μ_α act upon the lead correlation functions as

$$\frac{\partial^{k'}}{\partial(i\xi_\alpha)^{k'}} \frac{\partial^{k''}}{\partial \mu_\alpha^{k''}} F_{\alpha}^{>}(t-\xi_\alpha)\Big|_{\boldsymbol{\xi}=\boldsymbol{\mu}=\mathbf{0}} = \frac{\Gamma_\alpha}{2\pi} \int dE\; e^{-iEt} E^{k'} \frac{\partial^{k''}}{\partial \mu_\alpha^{k''}} [1 - f(E-\mu_\alpha)]\Big|_{\boldsymbol{\mu}=\mathbf{0}}, \tag{3.3}$$

where we have restricted ourselves to the wideband limit, $F_\alpha^{>}(E) = \Gamma_\alpha[1-f(E-\mu_\alpha)]$. The derivatives of the Fermi function at equilibrium chemical potential can be expressed as the series

$$\frac{\partial^{k''}}{\partial \mu^{k''}} f(E-\mu)\Big|_{\mu=0} = (-\beta)^{k''} \sum_{m=0}^{k''} (-1)^m m!\; S_{k'',m} [1-f(E)]^m f(E) \tag{3.4}$$

with $S_{k'',m}$ the Stirling numbers of the second kind.[131] To derive this formula, we start with the expression $\partial_x^n (e^x+1)^{-1}$ and employ Faà di Bruno's Formula[98] for the derivative of nested functions. Exploiting a relation between Stirling numbers and partial Bell polynomials, $B_{n,k}(e^x,\ldots,e^x) = e^{kx} S_{n,k}$, yields

$$\frac{\partial^n}{\partial x^n} \frac{1}{e^x+1} = \sum_{k=0}^{n} (-1)^k k!\; S_{n,k} \frac{e^{kx}}{(e^x+1)^{k+1}}, \tag{3.5}$$

by which we immediately obtain the nth derivative of the Fermi function with respect to the chemical potential and, hence, the Taylor series (3.4).

Finally, we end up with the eigenvalue problem $\mathcal{L}_{\boldsymbol{x}} \phi(\boldsymbol{x}) = \lambda(\boldsymbol{x}) \phi(\boldsymbol{x})$ with $\boldsymbol{x} = (\chi_1, \xi_1, \mu_1, \chi_2, \xi_2, \mu_2, \ldots)$ which is equivalent to the one discussed in section 2.2 but with the additional perturbations $\boldsymbol{\xi}$ and $\boldsymbol{\mu}$. Despite that the coefficients of $\mathcal{L}_{\boldsymbol{x}}$ now look more involved, we can apply the iteration scheme given by Eqs. (2.9) and (2.10)

when using the generalized Taylor coefficients $\mathcal{W}_\alpha^{k,k',k''}$. So, the transport coefficients $\lambda^{\boldsymbol{n}}$ follow from the recursion. The only peculiarity is that the stationary density operator for equal chemical potentials, $\mu_\alpha = \mu_0$, coincides with the grand canonical density operator of the central system, $\rho_{\mathrm{eq}} \propto e^{-\beta(H_S - \mu_0 N)}$, which is the equilibrium solution of the Bloch-Redfield master equation (6.2), see remark at the end of this section. Therewith the projector $\mathcal{Q}$ simplifies to $\mathcal{Q} = (\mathbb{1} - \rho_{\mathrm{eq}}\,\mathrm{tr})$.

It is worth noticing that this recursive scheme also holds for the case of distinct chemical potentials and may be applied to the calculation of conductances at finite bias voltage. This approach seems to be more stable than the determination involving numerical differentiation via finite differences.[132]

3.2. Frequency dependent transport

Current–current correlations that depend on two times can also be obtained from a cumulant generating function similar to Eq. (2.3). There are basically two strategies to treat multitimes: Either one may regard a time dependent counting field[86,133,134] which involves the Keldysh Green's function method that is usually utilized in semiclassical dynamics,[135,136] or one recovers the time dependence from the master equation, stated above, by a time-local expansion.[129,130] Here, we follow the latter strategy and notice that the formal solution of the master equation, can be expanded in time,

$$\rho(\boldsymbol{\chi}, t) = \Omega(\boldsymbol{\chi}, t - t')\rho(\boldsymbol{\chi}, t') = \Omega(\boldsymbol{\chi}, t - t')\Omega(\boldsymbol{\chi}, t')\rho(0), \quad (t > t' > 0) \tag{3.6}$$

where $\Omega(\boldsymbol{\chi}, t) = e^{\mathcal{L}(\chi)t}$ denotes the propagator. The augmented density matrix is initially assumed to be stationary. Expansion in a Fourier series allows unraveling the joint probability and expressing the time-local moment generating function by

$$M(\boldsymbol{\chi}, t; \boldsymbol{\chi}', t') = T_{\leftarrow}\langle \Omega(\boldsymbol{\chi}, t - t')\Omega(\boldsymbol{\chi} + \boldsymbol{\chi}', t')\rangle, \tag{3.7}$$

where $T_{\leftarrow}$ denotes the forward time ordering operator. The counting fields $\boldsymbol{\chi}$ and $\boldsymbol{\chi}'$ refer to the different times t and t', respectively and, thus, are affected by the time ordering. The joint probability may alternatively be obtained from Bayes formula.[51,129]

Similarly to the zero-frequency limit, Eq. (2.4) and Eq. (2.5), the time-local cumulants are defined by

$$\begin{aligned}\kappa_{\alpha\beta}(t, t') &= \frac{\partial^2}{\partial t \partial t'} \frac{\partial^2}{\partial i\chi_\alpha \partial i\chi'_\beta} \ln M(\boldsymbol{\chi}, t; \boldsymbol{\chi}', t')\Big|_{\boldsymbol{\chi}, \boldsymbol{\chi}' = \mathbf{0}} \\ &= \frac{\partial^2}{\partial t \partial t'} \Big[m_{\alpha\beta}(t, t') - m_\alpha(t, t') m_\beta(t, t') \Big],\end{aligned} \tag{3.8}$$

where $m_{\alpha\beta}(t, t') = \partial^2 M(\boldsymbol{\chi}, t; \boldsymbol{\chi}', t')/\partial i\chi_\alpha \partial i\chi'_\beta|_{\boldsymbol{\chi}, \boldsymbol{\chi}' = \mathbf{0}}$, and the moments $m_\alpha(t, t')$ and $m_\beta(t, t')$ correspond to the derivation in $i\chi_\alpha$ and $i\chi'_\beta$, respectively. Notice that $\chi'_\beta = (\boldsymbol{\chi}')_\beta$ denotes the vector components of $\boldsymbol{\chi}'$. This definition is more subtle

than in the zero-frequency limit since the moments involve now the derivation in the counting fields at different times. It is crucial to take the derivatives after the time ordering.[137] The derivation of the propagators can be carried out directly by using[138]

$$\frac{\partial}{\partial\lambda}e^{A_\lambda} = \int_0^1 ds\; e^{A_\lambda(1-s)}\frac{\partial A_\lambda}{\partial\lambda}e^{A_\lambda s}, \tag{3.9}$$

where A_λ is an arbitrary operator. After some algebra, cf. Appendix A, one finds the desired two-time cumulants which, in the stationary state, only depend on time differences, $\kappa_{\alpha\beta}(t,t') = \kappa_{\alpha\beta}(t-t',0)$. Fourier transformation yields then the frequency dependent current–current correlations,

$$\kappa_{\alpha\beta}(\omega) = \langle\mathcal{W}_{\alpha\beta}\rangle + \langle\mathcal{W}_\alpha\mathcal{R}(-i\omega)\mathcal{W}_\beta\rangle + \langle\mathcal{W}_\beta\mathcal{R}(i\omega)\mathcal{W}_\alpha\rangle. \tag{3.10}$$

The superoperators $\mathcal{W}_\alpha = (\partial\mathcal{L}/\partial i\chi_\alpha)|_{\boldsymbol{\chi}=\mathbf{0}}$ and $\mathcal{W}_{\alpha\beta} = (\partial^2\mathcal{L}/\partial i\chi_\alpha\partial i\chi_\beta)|_{\boldsymbol{\chi}=\mathbf{0}}$ are Taylor coefficients of $\mathcal{L}(\boldsymbol{\chi})$, where the first order provides the average currents $I_\alpha = \langle\mathcal{W}_\alpha\rangle$. It follows directly, that auto-correlations are symmetric while cross-correlations are not and thus may be complex. It is worth to notice that MacDonald's approach[88,128,139] also allows obtaining a frequency dependent power spectrum from equal-time cumulants, but it only yields the symmetric part.

The advantages of the presented approach to frequency dependent transport are first the treatment of unsymmetrized cross-correlations and second the possibility to apply the theory on models with non standard jump terms. The latter allows us to treat transport in a tunnel contact coupled to a double quantum dot within this scheme, as we consider in chapter 5.

4 Coherent quantum ratchets driven by tunnel oscillations

Two capacitively coupled double dots are used to study two interacting mesoscopic currents. In particular, we consider the setup of a coherent quantum ratchet, where one of the double quantum dots (driving circuit) is biased. Thus it enables coherent tunneling so that electrons perform tunnel oscillations that act as an effective ac force on the other, unbiased, double quantum dot (ratchet circuit). This introduces a net current which is known as ratchet or pump effect.[80,81] A similar setup a of double quantum dot coupled to a quantum point contact has been realized.[7] The ratchet effect is closely related to the Coulomb drag[140,141] and to the usage of a double quantum dot as noise detector.[21,82,83] For strong Coulomb repulsion, interacting channels may have the opposite effect and block each other.[142–144]

Our aim is to study the noise properties of the ratchet mechanism proposed in Ref. 80 and to analyze the full-counting statistics. Besides a numerical treatment with a master equation for the full ratchet–drive setup, we derive in the spirit of Ref. 123 an effective master equation for the ratchet and provide an analytical expression for the corresponding cumulant generating function. This approach is beyond a more heuristic elimination of the drive circuit[80] and beyond a golden-rule calculation,[82] because it includes effects stemming from delocalization and from the broadening of the ratchet levels, and therefore also holds for small ratchet detuning.

After introducing the driven ratchet model, and providing the full master equation, we discuss in section 4.2 the elimination of the drive circuit and provide our analytical results. In Sec. 4.3, we present our numerical results for the higher-order cumulants and test the quality of our approximations. The results in this chapter have been previously published by the author in Ref81.

4.1. Model and full master equation

Similar to the double quantum model in the former section, the coherent quantum ratchet, sketched in Fig. 4.1, is described by the Hamiltonian $H = H_S + H_B + H_V$, where

$$H_S = \frac{\epsilon}{2}(N_2 - N_1) - T_{\rm ra}\left(c_1^\dagger c_2 + c_2^\dagger c_1\right) - T_{\rm dr}\left(c_3^\dagger c_4 + c_4^\dagger c_3\right) + \sum_{\ell<\ell'} U_{\ell\ell'} N_\ell N_{\ell'} \qquad (4.1)$$

models the quantum dots with the electron creation and annihilation operators $c_\ell^\dagger$ and c_ℓ, and the dot occupations $N_\ell = c_\ell^\dagger c_\ell$. The ratchet circuit ($\ell = 1, 2$) has inter-dot tunneling $T_{\rm ra}$ and detuning ϵ, such that the level splitting becomes $\delta = (\epsilon^2 + 4|T_{\rm ra}|^2)^{1/2}$.

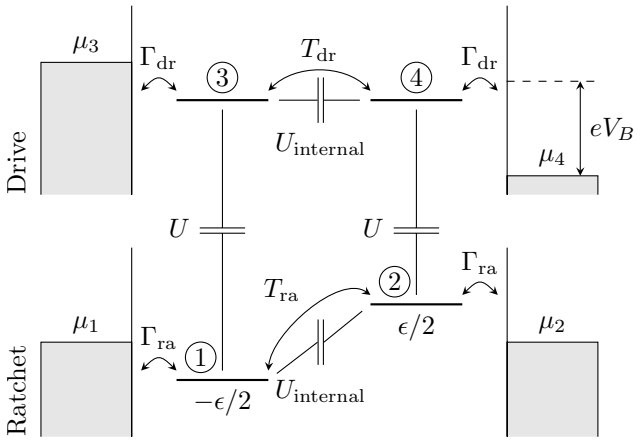

Fig. 4.1.: Quantum ratchet (lower circuit, unbiased) capacitively coupled to a drive circuit (top) biased by a voltage V_B. Each circuit is modeled as two-level system with tunnel couplings $T_{\rm ra}$ and $T_{\rm dr}$, respectively. The ratchet possess a detuning ϵ, while the drive circuit is undetuned. The dot–lead tunnel rates are $\Gamma_{\rm ra}$ and $\Gamma_{\rm dr}$, while μ_ℓ, $\ell = 1, \ldots, 4$, denotes the chemical potentials of the leads.

The levels of the drive circuit ($\ell = 3, 4$) are not detuned and possess a tunnel matrix element $T_{\rm dr}$. The setup is assumed to be symmetric, such that inter-channel Coulomb repulsion reads $U \equiv U_{13} = U_{24}$, while the internal repulsions U_{12} and U_{34} are assumed so large that each channel can be occupied with at most one electron. The inter-channel coupling U by contrast, is relatively weak but nevertheless is the relevant interaction for inducing a ratchet current.[80] We do not take into account more indirect interactions mediated by phonons[145] or by a qubit.[146]

Each dot ℓ is coupled to a lead with chemical potential μ_ℓ, where $\mu_1 = \mu_2$, while $\mu_3 > \mu_4$ with $\mu_3 - \mu_4$ so large that all levels of the drive circuit lie within the voltage window. The lead Hamiltonian and the dot-lead couplings read

$$H_B = \sum_{q\alpha} \epsilon_{q\alpha} c^\dagger_{q\alpha} c_{q\alpha}, \quad H_V = \sum_{q\alpha} \left(V_{q\alpha} c^\dagger_{q\alpha} c_{\ell_\alpha} + V^*_{q\alpha} c^\dagger_{\ell_\alpha} c_{q\alpha} \right), \tag{4.2}$$

respectively, where $c^\dagger_{q\alpha}$ and $c_{q\alpha}$ are the fermionic operators and $\epsilon_{q\alpha}$ is the corresponding single-particle energy. The system–bath interaction H_V is determined by the effective tunnel rates $\Gamma_{\rm ra}$ and $\Gamma_{\rm dr}$, which within a wide-band limit are assumed energy-independent.

Cumulant generating function and master equation: As before shown, stationary transport properties such as current and noise are encoded in the particle current cumulants,

$$\kappa^{mn}_{24} = \frac{\partial^{(m+n)}}{(\partial i\chi_2)^m (\partial i\chi_4)^n} Z \Big|_{\boldsymbol{\chi}=0} \tag{4.3}$$

which are derived from the cumulant generationg function $Z(\boldsymbol{\chi})$. Here, it is sufficient to only consider the the low-frequency properties of the currents in leads 2 and 4, which due to charge conservation are identical with those of leads 1 and 3, respectively. In particular, we focus on the ratchet current $I_{\mathrm{ra}} = e\kappa_{24}^{10}$ and the drive current $I_{\mathrm{dr}} = e\kappa_{24}^{01}$ which are first-order current cumulants, as well as the second order contributions $S_{\mathrm{ra}} = e^2\kappa_{24}^{20}$, $S_{\mathrm{dr}} = e^2\kappa_{24}^{02}$, and the cross correlation $S_{\mathrm{ra–dr}} = e^2\kappa_{24}^{11}$. Also higher order current–current cumulants of the ratchet, $\kappa^m \equiv \kappa_{24}^{m0}$, are of interest.

The cumulant generating function $Z(\boldsymbol{\chi})$ and therewith the current cumulants are obtained from the Markovian master equation

$$\dot{\rho}(\boldsymbol{\chi},t) = \Big[\mathcal{L}_0 + \sum_\alpha (e^{-i\chi_\alpha}-1)\mathcal{J}_\alpha^{\mathrm{in}} + \sum_\alpha (e^{i\chi_\alpha}-1)\mathcal{J}_\alpha^{\mathrm{out}}\Big]\rho(\boldsymbol{\chi},t), \tag{4.4}$$

which is governed by the matrix representation in Appendix B, when summing over all involved leads $\alpha = 1,\ldots,4$ and considering the eigenenergies of the system Hamiltonian, Eq. (4.1). Before discussing these results, we aim at further analytical progress.

4.2. Elimination of the drive circuit

In order to reduce the number of degrees of freedom, such that an analytically solvable master equation emerges, we eliminate the drive circuit along the lines of Ref. 123. We start by separating the master equation for $\rho(\boldsymbol{\chi},t)$, Eq. (4.4), into contributions for the ratchet, the drive circuit, and their mutual interaction,

$$\dot{\rho}(\chi_2,t) = \Big[\mathcal{L}_{\mathrm{ra}}(\chi_2) + \mathcal{L}_{\mathrm{dr}} + U\mathcal{L}_{\mathrm{ra–dr}}\Big]\rho(\chi_2,t). \tag{4.5}$$

Since we focus on the ratchet current, we keep only the counting variable χ_2 for the right lead of the ratchet circuit. The interaction Liouvillian

$$\mathcal{L}_{\mathrm{ra–dr}}\rho = -\frac{i}{2}[\Delta N_{\mathrm{dr}}\Delta N_{\mathrm{ra}},\ \rho], \tag{4.6}$$

is governed by the occupation imbalances $\Delta N_{\mathrm{ra}} = N_2 - N_1$ and $\Delta N_{\mathrm{dr}} = N_4 - N_3$, which allow one to approximately write the ratchet–drive interaction Hamiltonian as[80] $U(N_1N_3 + N_2N_4) \approx (U/2)\Delta N_{\mathrm{dr}}\Delta N_{\mathrm{ra}}$. Thereby we neglect terms that cause global shifts of all dot energies. They are not relevant here, because for all parameters considered below, the onsite energies stay far from the Fermi surfaces.

After transforming the master equation (4.5) into Laplace space, an effective Liouvillian $\mathcal{L}_{\mathrm{eff}}$ is defined by tracing over the drive circuit,[123]

$$[z - \mathcal{L}_{\mathrm{eff}}(\chi_2,z)]^{-1} \equiv \mathrm{tr}_{\mathrm{dr}}\{[z-\mathcal{L}(\chi_2)]^{-1}\rho_{\mathrm{dr}}^{\mathrm{stat}}\}, \tag{4.7}$$

where $\rho_{\mathrm{dr}}^{\mathrm{stat}}$ denotes the corresponding stationary state. This definition via an effective resolvent has the advantage that it contains fluctuations of all orders in the drive

circuit. Taylor expansion up to second order in the interaction constant U and subsequent evaluation of the partial trace yields[123]

$$\mathcal{L}_{\rm eff}(\chi_2, z) = \mathcal{L}_{\rm ra}(\chi_2) + U\mathcal{L}^{(1)}_{\rm eff}(z) + U^2\mathcal{L}^{(2)}_{\rm eff}(z). \tag{4.8}$$

Its zeroth order, $\mathcal{L}_{\rm ra}(\chi_2) = \mathcal{L}_{\rm ra} + (e^{-i\chi_2} - 1)\mathcal{J}^{\rm in} + (e^{i\chi_2} - 1)\mathcal{J}^{\rm out}$, is determined by the Liouvillian

$$\mathcal{L}_{\rm ra}\rho = -i[H_{S,\rm ra},\ \rho] + \Gamma_{\rm ra}\mathcal{D}(c_g^\dagger)\rho + \Gamma_{\rm ra}\mathcal{D}(c_e)\rho \tag{4.9}$$

with the ratchet Hamiltonian $H_{S,\rm ra}$ resembling the double quantum dot in the high bias limit, Eq. (2.20), but incorporating the fermionic operators c_g and c_e that annihilates an electron in the hybridized ground state $|g\rangle$ and the excited state $|e\rangle$, respectively. The corresponding jump operators are

$$\mathcal{J}^{\rm in}\rho = \frac{\Gamma_{\rm ra}}{2\delta}\Big[(\delta - \epsilon)\ c_g^\dagger\rho c_g + |T_{\rm ra}|\ (c_g^\dagger\rho c_e + c_e^\dagger\rho c_g)\Big], \tag{4.10}$$

$$\mathcal{J}^{\rm out}\rho = \frac{\Gamma_{\rm ra}}{2\delta}\Big[(\delta + \epsilon)\ c_e\rho c_e^\dagger + |T_{\rm ra}|\ (c_e\rho c_g^\dagger + c_g\rho c_e^\dagger)\Big], \tag{4.11}$$

which describe electron tunneling between dot 2 and the corresponding lead in the absence of the drive circuit. Since all levels are assumed to stay far from the Fermi surfaces, the impact of the interaction on the jump operators can be neglected safely. Thus, these jump operators of the effective model coincide with the ones of the full Liouvillian $\mathcal{J}_2^{\rm in/out}$.

Taking the partial trace of the interaction Liouvillian $\mathcal{L}_{\rm ra–dr}$ with respect to the drive circuit yields the linear term $\mathcal{L}^{(1)}_{\rm eff}(z) = -\frac{i}{2}\langle\Delta N_{\rm dr}\rangle[\Delta N_{\rm ra},\ \bullet]$, where we employ the superoperator notation of Ref. 147 and define $[M, \bullet]\rho \equiv [M, \rho]$. The quadratic term is given by $\mathcal{L}^{(2)}_{\rm eff}(z) = \langle\mathcal{L}_{\rm ra–dr}\mathcal{R}_{\rm dr}(z - \mathcal{L}_{ra})\mathcal{L}_{\rm ra–dr}\rangle_{\rm dr}$ with $\mathcal{R}_{\rm dr}(z)$ pseudoresolvent of the drive circuit. To perform the trace we express the ratchet Liouvillian by its spectral decomposition, $\sum_m \lambda^{(m)}_{\rm ra}|\phi^{(m)}_{\rm ra}\rangle\!\rangle\langle\!\langle\tilde{\phi}^{(m)}_{\rm ra}|$, with the eigenvalues $\lambda^{(m)} = 0, -\Gamma_{\rm ra}, -\Gamma_{\rm ra}/2 \pm i\delta$, and the left and right eigenvectors $\langle\!\langle\tilde{\phi}^{(m)}_{\rm ra}|$ and $|\phi^{(m)}_{\rm ra}\rangle\!\rangle$. Thereby a difficulty arises since the Liouvillian of a double quantum dot in the zero-bias limit is defective, and does not possess a complete set of eigenvectors, see Appendix C. Nevertheless, one may proceed either by constructing a generalized eigenbasis or by introducing a small perturbation that lifts the defectiveness, and finally consider the limit of vanishing perturbation.[148] Here, we choose the former strategy and find that the trace over the drive circuit involves the Laplace transformed auto correlation function of the population imbalance

$$C(t) = \langle\Delta\tilde{N}_{\rm dr}(t)\Delta N_{\rm dr}\rangle - \langle\Delta N_{\rm dr}\rangle^2 \tag{4.12}$$

evaluated at the eigenvalues of the ratchet Liouvillian, $C(z - \lambda^{(m)}_{\rm ra})$. Below we will find that the poles of $C(z)$ are related to the extrema of the ratchet current. This correlation function fulfills $C^*(z) = C(z^*)$, see Appendix C, and enables us to

formulate the quadratic correction as

$$\begin{aligned}\mathcal{L}^{(2)}_{\text{eff}}(z) =& -\frac{1}{4}[\Delta N_{\text{ra}},\ \bullet]C(z-\mathcal{L}_{ra})[\Delta N_{\text{ra}},\ \bullet]\\ =& -\frac{1}{4}\sum_m C(z-\lambda^{(m)}_{\text{ra}})[\Delta N_{\text{ra}},\ \bullet]|\phi^{(m)}_{\text{ra}}\rangle\!\rangle\langle\!\langle\tilde{\phi}^{(m)}_{\text{ra}}|[\Delta N_{\text{ra}},\ \bullet]\\ &+\frac{1}{4}C'(z-\lambda^{(2)}_{\text{ra}})[\Delta N_{\text{ra}},\ \bullet]|\phi^{(1)}_{\text{ra}}\rangle\!\rangle\langle\!\langle\tilde{\phi}^{(2)}_{\text{ra}}|[\Delta N_{\text{ra}},\ \bullet].\end{aligned} \tag{4.13}$$

The generalized eigenvectors $|\phi^{(1)}_{\text{ra}}\rangle\!\rangle$ and $|\phi^{(2)}_{\text{ra}}\rangle\!\rangle$ correspond to the defective eigenvalue $-\Gamma_{\text{ra}}$. To evaluate the action of $[\Delta N_{\text{ra}},\ \bullet]$ on the generalized eigenvectors, we change to the Fock basis $\{|0\rangle\langle 0|, |1\rangle\langle 1|, |2\rangle\langle 2|, |2\rangle\langle 1|, |1\rangle\langle 2|\}$ and obtain the expression

$$\mathcal{L}^{(2)}_{\text{eff}}(z) = \begin{pmatrix} 0 & 0 & 0 & 0 & 0\\ 0 & 0 & 0 & 0 & 0\\ 0 & 0 & 0 & 0 & 0\\ 0 & 0 & 0 & A(z) & B^*(z^*)\\ 0 & 0 & 0 & B(z) & A^*(z^*)\end{pmatrix}, \tag{4.14}$$

where the terms

$$\begin{aligned}A(z) =& -\frac{|T_{\text{ra}}|^2}{\delta^2}\Big[2C(z+\Gamma_{\text{ra}}) - \Gamma_{\text{ra}}C'(z+\Gamma_{\text{ra}})\Big]\\ &-\sum_{s=\pm}\frac{(\delta+s\epsilon)^2}{4\delta^2}C(z+\Gamma_{\text{ra}}/2+si\delta),\end{aligned} \tag{4.15}$$

$$\begin{aligned}B(z) =& \frac{T^2_{\text{ra}}}{\delta^2}\Big[2C(z+\Gamma_{\text{ra}}) - \Gamma_{\text{ra}}C'(z+\Gamma_{\text{ra}})\\ &- C(z+\Gamma_{\text{ra}}/2+i\delta) - C(z+\Gamma_{\text{ra}}/2-i\delta)\Big]\end{aligned} \tag{4.16}$$

contain a non-Markovian correction through the Laplace variable z.

The linear contribution to the effective Liouvillian, $\mathcal{L}^{(1)}_{\text{eff}}$ merely provides a small additional bias for the ratchet circuit, but does not induce any non-equilibrium effect. Thus, we omit this term and focus on the impact of the quadratic term. For the resulting effective ratchet Liouvillian, $\mathcal{L}_{\text{ra}}(\chi_2) + U^2\mathcal{L}^{(2)}_{\text{eff}}(z)$, the cumulant generating function can be obtained by computing the eigenvalue that vanishes for $\chi_2 \to 0$. This yields a somewhat bulky expression and, thus, we restrict ourselves to the Markovian limit obtained by $z \to 0$. By differentiation with respect to χ_2, we obtain the current and the zero-frequency noise as

$$I_{\text{ra}} = e\frac{2b\epsilon}{\delta}\,\text{Im}\Big[\Big(-\Gamma_{\text{ra}}/2+i\delta\Big)C\Big(\Gamma_{\text{ra}}/2+i\delta\Big)\Big], \tag{4.17}$$

$$S_{\text{ra}} = e^2\frac{b}{\delta^2}\,\text{Im}\Big[(-\Gamma_{\text{ra}}\epsilon^2 + i\delta\epsilon^2 + i\delta^3)C(\Gamma_{\text{ra}}/2+i\delta)\Big], \tag{4.18}$$

where $b = 4|T_{\text{ra}}|^2U^2/\delta(4\delta^2+\Gamma^2_{\text{ra}})$. Both expressions are proportional to the auto correlation function (4.12) of the drive circuit in Laplace space, which underlines

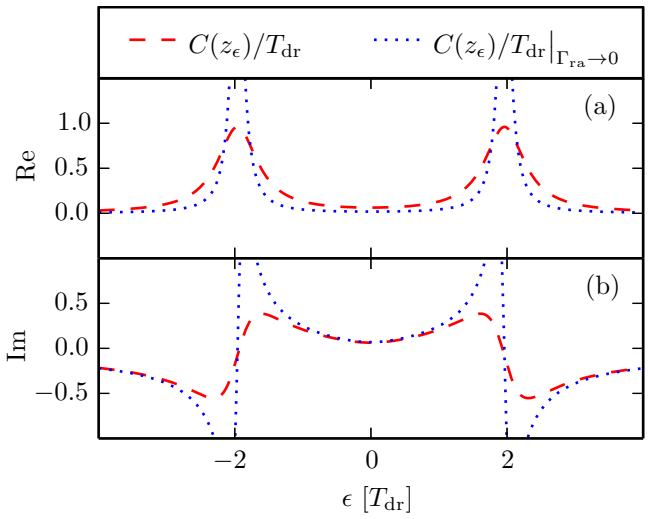

Fig. 4.2.: (a) Real and (b) imaginary part of the auto correlation function (dashed lines) of the drive population imbalance in Laplace representation, $C(z_\epsilon)$, evaluated at the broadened resonance of the ratchet Liouvillian, $z_\epsilon = \Gamma_{\rm ra}/2 + i(\epsilon^2 + 4|T_{\rm ra}|^2)^{1/2}$ with $\Gamma_{\rm ra} = 0.5\,T_{\rm dr}$ and $T_{\rm ra} = 0.2\,T_{\rm dr}$, as function of the detuning ϵ. The dotted lines correspond to the limit $\Gamma_{\rm ra} \to 0$. The dot–lead coupling is $\Gamma_{\rm dr} = T_{\rm ra}$.

that the current is induced by non-equilibrium fluctuations of the drive circuit acting upon the ratchet.

Equations (4.17) and (4.18) allow us to simplify the cumulant generating function and to obtain

$$Z^{(I)}_{\rm eff}(\chi_2) = \frac{i(I_{\rm ra}/e)\sin(\chi_2) + (S_{\rm ra}/e^2)[\cos(\chi_2) - 1]}{1 + \frac{b\Gamma^2_{\rm ra}}{2\delta U^2}[\cos(\chi_2) - 1]}, \tag{4.19}$$

which within the present approximation contains the full information about the low-frequency properties of the ratchet current. The presence of the counting variable χ_2 in the denominator, however, renders the actual calculation of higher-order cumulants a formidable task. Only in the golden-rule limit, i.e., to lowest order in $\Gamma_{\rm ra}$, the denominator becomes independent of χ_2, so that $Z^{(I)}_{\rm eff}(\chi_2) = i(I^{(0)}_{\rm ra}/e)\sin(\chi_2) + (S^{(0)}_{\rm ra}/e^2)[\cos(\chi_2) - 1]$. Consequently, we obtain the current cumulants

$$\kappa^m = \frac{\partial^m}{\partial(i\chi_2)^m} Z^{(I)}_{\rm eff}(\chi_2)\Big|_{\chi_2=0} = \begin{cases} I^{(0)}_{\rm ra}/e & \text{for odd } m \\ S^{(0)}_{\rm ra}/e^2 & \text{for even } m \end{cases} \tag{4.20}$$

where the upper index (0) refers to the limit $\Gamma_{\rm ra} \to 0$. It turns out to be a good approximation, unless universal cumulant oscillations set in, as we will discuss in Sec. 4.3.2.

Before testing the quality of this approximation and the parameter dependence of the results, we close this section by a remark on a formal aspect of the perturbation theory. Both the current (4.17) and the zero-frequency noise (4.18) are proportional

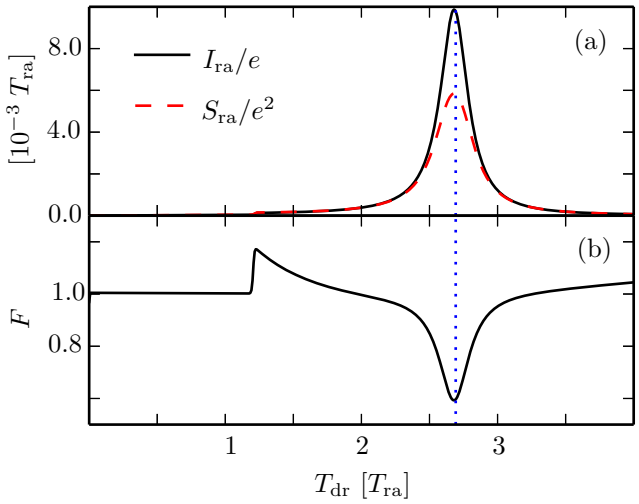

Fig. 4.3.: (a) Ratchet current $I_{\rm ra}$, its zero-frequency noise $S_{\rm ra}$, and (b) the resulting Fano factor $F = S_{\rm ra}/e|I_{\rm ra}|$ as function of the tunnel matrix element of the drive circuit. The results are computed with the full master equation. The other parameters are $\Gamma_{\rm ra} = \Gamma_{\rm dr} = 0.1\ T_{\rm ra}$, $U = 0.5\ T_{\rm ra}$, and $\epsilon = 5\ T_{\rm ra}$. The vertical dotted line marks the resonance condition $4|T_{\rm dr}|^2 = \epsilon^2 + 4|T_{\rm ra}|^2$.

to the auto correlation function of the population imbalance, $C(z)$, evaluated at the broadened level splitting of the ratchet, where the Laplace variable reads $z_\epsilon = \Gamma_{\rm ra}/2 + i(\epsilon^2 + 4|T_{\rm ra}|^2)^{1/2}$. Thus we expect the ratchet current to exhibit resonance peaks. Taking into account the broadening distinguishes the present result from that of Ref. 80. There the ratchet current has been computed from the golden-rule rates for noise-induced transitions between ratchet eigenstates. While this treatment accounts properly for delocalization effects, it predicts too pronounced resonance peaks. Formally, the golden-rule solution is restored by the replacement $C(\Gamma_{\rm ra}/2 + i\delta) \to C(i\delta)$ in Eq. (4.17). Figure 4.2 visualizes that for ratchet detunings close to resonances, the difference between the two approximations may be significant.

4.3. Characterization of the ratchet current

Before starting with the analysis of the ratchet current fluctuations, let us compare the present case to that of a ratchet driven by an ac field. There, the current exhibits resonance peaks with a large current and low zero-frequency noise.[108,149] For large driving amplitudes, the same behavior is visible at multi-photon resonances. Figure 4.3 shows the corresponding result for the present driving by tunnel oscillations. When the level splitting of the ratchet matches the tunnel frequency of the drive circuit, we indeed observe the qualitatively same behavior. Here however, we do not find higher-order resonances and, moreover, the Fano factor does not reach the extremely small values found in Ref. 149. The reason for this is that for realistic parameters, the driving via Coulomb interaction with the upper circuit is much weaker than direct ac driving by, e.g., a high-frequency gate voltage.[29] The kink in

the Fano factor stems from a small step in the current and can be attributed to an energy difference of many-particle states that crosses the Fermi level of the ratchet.[80] This confirms our picture in which the tunnel oscillations of electrons in the drive circuit act like an ac driving with (angular) frequency $\Omega = |2T_{\rm dr}|$ determined by the tunnel splitting.

4.3.1. Zero-frequency noise and Fano factor

If the tunnel coupling of the ratchet is smaller than that of the drive circuit, $T_{\rm ra} < T_{\rm dr}$, one can adjust the ratchet bias ϵ such, that the resonance condition $\epsilon^2 + 4|T_{\rm ra}|^2 = 4|T_{\rm dr}|^2$ is met. By contrast, for $T_{\rm ra} > T_{\rm dr}$ this is not the case. In order to first sketch the global behavior, we first consider the current, the zero-frequency noise, and the resulting Fano factor in dependence of the ratchet bias. We compare numerical results obtained from the full master equation with the analytical solution of Sec. 4.2. Moreover, we also discuss the analytical expressions (4.17) and (4.18) to lowest order in $\Gamma_{\rm ra}$, because this restores the golden-rule results of Ref. 80.

Figure 4.4 provides an overview to the behavior. The current which is depicted in the first row, exhibits the expected resonance peaks provided that $T_{\rm ra} < T_{\rm dr}$. If the tunnel matrix element is rather small ($T_{\rm ra} = 0.2\,T_{\rm dr}$), we witness also the small peaks at small values of ϵ, which we predicted within our analytical treatment. Upon increasing the inter-dot tunneling $T_{\rm ra}$, the current peaks naturally increase as well. Once $T_{\rm ra} > T_{\rm dr}$, the resonance peaks fade away while the structure at $\epsilon \approx 0$ becomes rather pronounced. In all regimes, the analytical result (4.17) for the current is well confirmed. The main difference is the absence of the slight asymmetry with respect to reverting the detuning, $\epsilon \to -\epsilon$. Nevertheless, the characteristics of the current as function of ϵ is by and large antisymmetric, which implies a current reversal close to zero detuning. To capture also the lack of perfect antisymmetry, we would have to consider the linear perturbation $\mathcal{L}^{(1)}_{\rm eff}$ which, however, would impede concise analytical results. For the parameters used in Fig. (4.4), the golden-rule expression of Ref. 80, i.e., Eq. (4.17) to lowest order in $\Gamma_{\rm ra}$, reproduces the behavior only qualitatively. It predicts too sharp peaks, because this approximation does not account for the level broadening of the ratchet. The deviation is quite significant in the non-resonant case $T_{\rm ra} > T_{\rm dr}$.

The main features such as the location of the peaks are also found for the zero-frequency noise plotted in the middle row. An important difference is found only close to $\epsilon = 0$, where the current vanishes for symmetry reasons. The noise nevertheless remains finite and may even have a peak. This behavior is reflected by the Fano factor which stays close to the Poissonian value $F = 1$ for detunings far from the current reversal point $\epsilon = 0$. There the current vanishes, while the noise remains finite, such that F diverges. The reason for this universal behavior can be understood from the analytical results for the current and the noise. Both $I_{\rm ra}$ and $S_{\rm ra}$ depend on the drive circuit via the drive correlation function $C(z)$ which, thus, cancels in their ratio, i.e., in the Fano factor. On a smaller scale, we observe in the Fano factor occasional kinks in less important regions in which the current is rather small. There

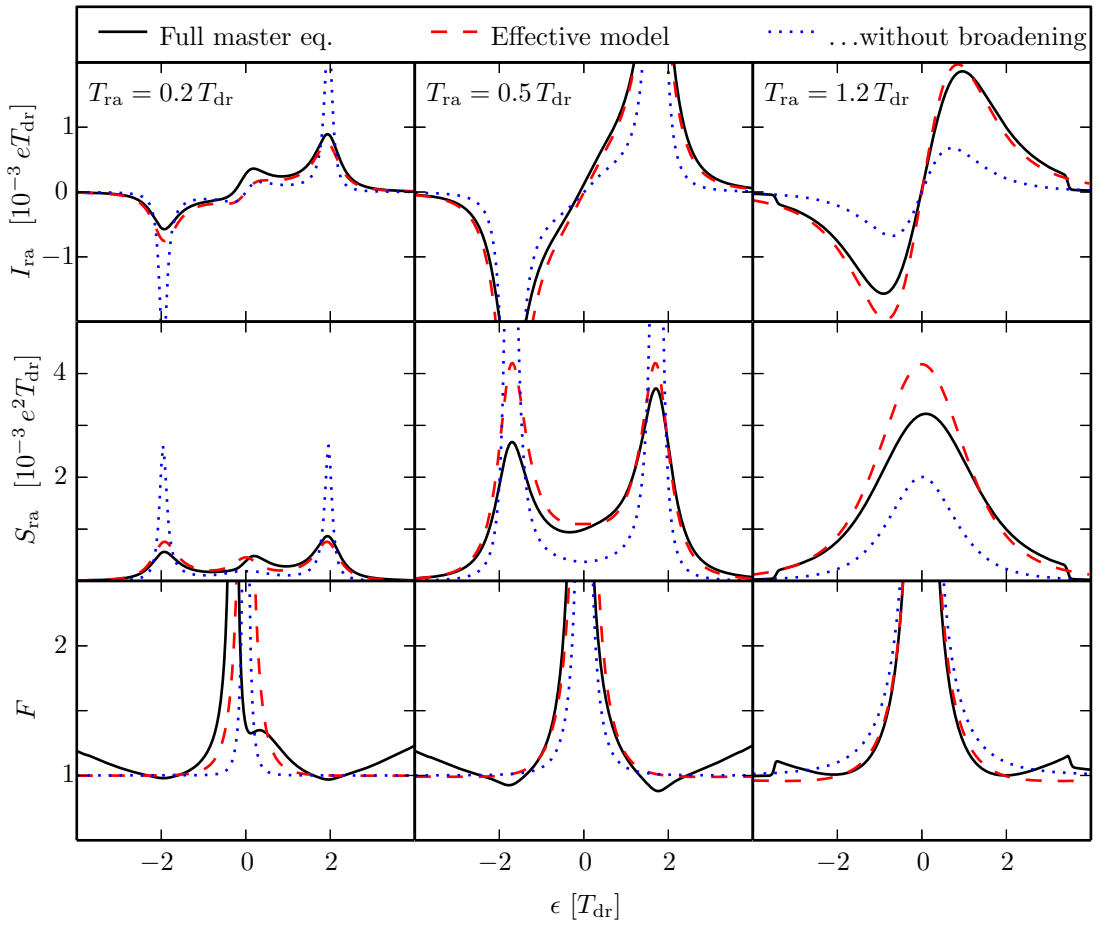

Fig. 4.4.: Ratchet current (upper row), zero-frequency noise (middle), and Fano factor (lower row) as function of the ratchet detuning ϵ for various tunnel couplings $T_{\rm ra}$. Results for the full master equation (solid lines) are compared to the analytical results (4.17) and (4.18) (dashed). Dotted lines mark the golden-rule results which ignore the broadening $\Gamma_{\rm ra}$. The dot-lead tunneling rates are $\Gamma_{\rm ra} = 0.5\,T_{\rm dr}$ and $\Gamma_{\rm dr} = 0.2\,T_{\rm dr}$, while the inter-channel coupling reads $U = 0.2\,T_{\rm dr}$.

a small change in the denominator of $F = S_{\rm ra}/e|I_{\rm ra}|$ may have a strong effect.

4.3.2. Higher-order cumulants

For a refined study of the current noise, we investigate also the cumulants of higher order, where we express the results in terms of the ratio between subsequent cumulants, $|\kappa^{n+1}/\kappa^n|$. For this quantity, the limit of small $\Gamma_{\rm ra}$ is rather interesting, because our analytical result (4.20) implies that the cumulant ratio alternates between the Fano factor and its reciprocal. Such behavior is characteristic for a bi-directional Poisson process,[150] i.e., a superposition of a forward and a backward Poisson process with rates $\gamma^{\pm}$. The resulting cumulants read[77] $\kappa^{n,(\pm)} = (\pm 1)^n\gamma^{\pm}$, where the sign reflects the direction of the backward current. The net transport is given by the difference of

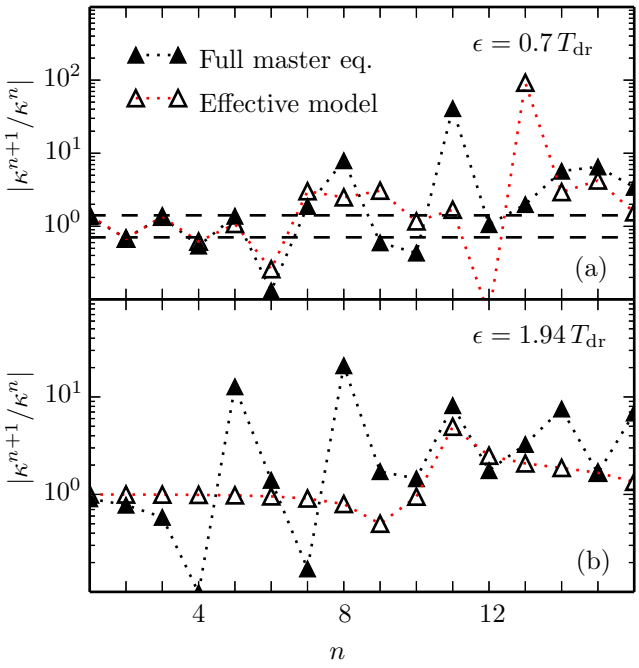

Fig. 4.5.: Cumulant ratio $|\kappa^{n+1}/\kappa^n|$ versus order n for the parameters used in the second column of Fig. 4.4 for two values of the detuning ϵ. The value $\epsilon \approx 1.94\,T_{\rm dr}$ corresponds to the resonance between ratchet and drive circuit. The horizontal lines in panel (a) mark the analytical result (4.20) valid to lowest order in $\Gamma_{\rm ra}$, i.e., F and $1/F$. The dotted lines serve as guide to the eye.

both processes such that its cumulants read $\kappa^n = \gamma^+ + (-1)^n\gamma^-$, provided that the two Poisson processes are statistically independent. The alternating cumulant ratio follows straightforwardly. The usual Poisson process with $|\kappa^{n+1}/\kappa^n| = 1$ emerges as special case if the backward current is negligible. The higher-order cumulants of the effective Liouvillian for larger values of $\Gamma_{\rm ra}$ can be evaluated from the generating function (4.19), but the expressions become rather bulky, so that one has to resort to a numerical evaluation.

Figure 4.5 shows a comparison of these two approximations together with the result of the full master equation. For a small ratchet detuning below the resonance [panel (a)], we find that all three solutions agree quite well and that the first few cumulants exhibit the predicted alternation between the values F and $1/F$. For higher orders, the generic universal cumulant oscillations set in,[103] which obviously is beyond our analytical approach. At the resonance, the universal oscillations start even already at lower order and Eq. (4.20) no longer holds. This is in agreement with our earlier observation that the broadening of the ratchet levels plays a significant role for resonant driving.

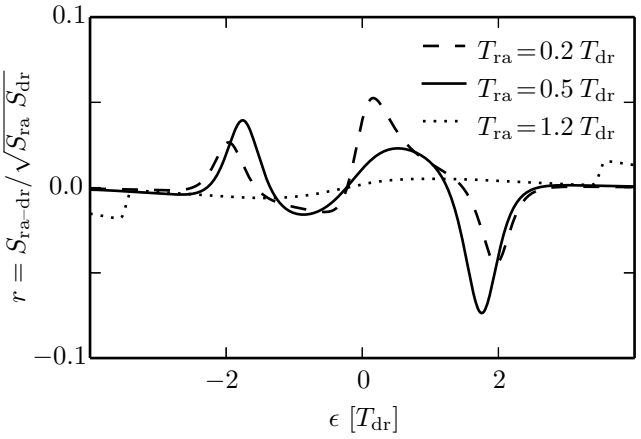

Fig. 4.6.: Correlation coefficient r versus detuning ϵ for the parameters used in Fig. 4.4.

4.3.3. Cross correlations

Let us finally consider the cross correlations between the drive current and the ratchet current. They can be characterized by the cumulant $\kappa_{1,1}$, which is equivalent to the covariance of the transported charge in the two circuits. As a dimensionless measure, we introduce the correlation coefficient $r \equiv S_{\rm ra-dr}/\sqrt{S_{\rm ra}\,S_{\rm dr}}$, which is bounded by $-1 \leq r \leq 1$. The results depicted in Fig. 4.6 demonstrate that the correlation between the two currents is rather low. While it can be up to $|r| \sim 0.1$ at the resonances, it is hardly noticeable in the non-resonant case $T_{\rm ra} > T_{\rm dr}$.

4.4. Main results

A double quantum dot with detuned energy levels but zero bias voltage may act as a quantum ratchet or a quantum pump when driven out of equilibrium. Application of an external force with zero net bias can locally influence such a system and induce a dc current. Here, we investigated a quantum ratchet with a particular driving, namely one that stems from the capacitive coupling to a further double quantum which, however, is strongly biased. Electrons flowing through the drive circuit perform tunnel oscillations which indeed induce phenomena similar to those induced by deterministic ac driving. In this study, we mainly focused on the fluctuations of the emerging ratchet current.

Besides a numerical solution with a master equation for all four quantum dots, we derived an effective ratchet Liouvillian by eliminating the drive circuit. In this way, we obtained analytical results even for higher-order cumulants, which agree well with those of the full master equation provided that the tunnel splitting of the drive circuit is larger than that of the ratchet.

As a common feature of driving by tunnel oscillations and driving by an ac field, we found resonance peaks at which the ratchet current assumes a maximum, while the relative noise characterized by the Fano factor is minimal. However, clearly

sub-Poissonian noise is only found for large detuning of the ratchet levels. This noise reduction should be measurable, even though it is not as pronounced as in the case of ac driving, mainly because it requires large driving amplitudes which here cannot be achieved with realistic parameters. For less detuned ratchet levels, the Fano factor is typically of the order one, unless the detuning is so small that its orbitals are fully delocalized. Then the lack of sufficiently strong asymmetry keeps the current at a low value, while the zero-frequency noise stays finite. Thus, the Fano factor being the ratio of these two quantities assumes very large values. This generic behavior of the Fano factor is explained by our analytical results which reveal that both the current and the zero-frequency noise are proportional to the correlation function of the drive circuit. Thus the Fano factor depends only on the shape of the ratchet eigenfunctions, while the correlation function cancels.

The higher-order cumulants tend to alternate between two values. This indicates a bi-directional Poisson process and implies that a backward current becomes relevant. With increasing order, however, universal oscillations with ever larger amplitude dominate. The onset of the universal oscillations marks the point at which our analytically obtained higher-order cumulants significantly deviate from those for the full master equation. Nevertheless, the physically relevant cumulants of lower order are well within our analytical treatment.

The more global picture is such that the noise is close to the Poissonian level, whenever the current is relatively large. Thus possible applications and measurements of a ratchet current induced by tunnel oscillations, should not be hindered by current fluctuations.

5 Monitoring quantum transport

The conductance of a quantum point contact can be influenced significantly by the capacitive interaction with a nearby electron. Thus it can act as detector for the charge state of a quantum dot in its vicinity and enables monitoring of single-electron tunneling through a quantum dot.[69–73] Commonly, quantum point contacts are used to measure charging diagrams with high precision.[25,151] Alternative detector concepts base on shifting a level across the Fermi energy of a lead[152] or tuning a DQD into and out of resonance.[59] On the formal level, the measurement quality of such charge detection can be expressed by the correlation between the detector current and the dot occupation.[153] In contrast to a single quantum dot, a DQD with strong inter-dot coupling possesses delocalized electron states which suffer from decoherence when their charge distribution is probed. An example is the coherent quantum ratchet in chapter 4. Such measurement backaction has been investigated theoretically for the readout of charge qubits[56,59,152,154] and the adiabatic passage of electrons.[155] Typically a charge detector is strongly biased and, thus, entails non-equilibrium noise to the system to which it couples. Thus it can induce pump currents[7,81] and phonon-assisted tunneling.[19] This complex interplay between measurement, decoherence, and non-equilibrium dynamics raises interest in correlations between the detector currents, the charge, and the current in a DQD.

We study a quantum point contact in the tunnel regime acting as charge monitor for a DQD, as is sketched in Fig. 5.1. Focusing on the correlations between the detector current and DQD observables, we reveal under which conditions the former correlates with both the charge and the current of the DQD. After introducing the full quantum mechanical model for the DQD and the detector in Sec. 5.1, we follow two different paths for the specific calculations: First, we consider the classical limit in which the inter-dot tunneling is fully incoherent. Hence, correlation functions can be expressed in terms of conditional probabilities. Second we tackle the full quantum mechanical problem within a Bloch-Redfield equation approach, which allows us to identify genuine quantum features such as decoherence and measurement backaction. Comparing both limits provides the effective parameters and the range of validity of the classical description. This chapter bases on the results published in Ref. 63. The alternative method for solving the classical limit, see Appendix D, was derived in collaboration with Jorge Gómez-García.[156]

5.1. DQD coupled to a charge detector

The setup consists of a double quantum dot in the high bias limit, see Sec. 2.4, where the Coulomb repulsion represents the largest energy scale. Therewith double

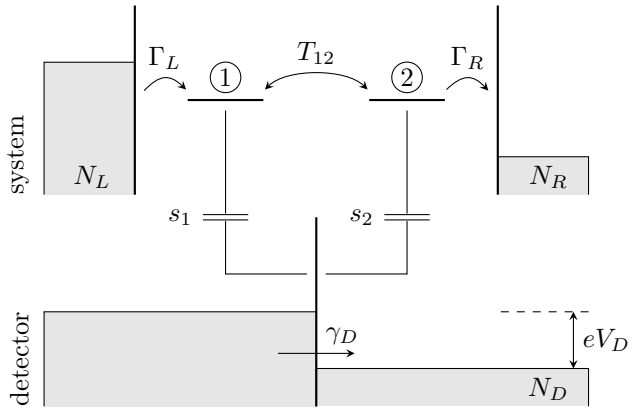

Fig. 5.1.: Quantum point contact in the tunnel regime acting as charge monitor for an undetuned but biased DQD. Electrons on the latter increase the tunnel barrier and, thus, reduce the detector current.

occupation is inhibited and spin effects play a minor role and will be ignored. Energetically, only the empty state $|0\rangle$ and the single-electron states $|\ell\rangle$ are assumed to be accessible, where $\ell = 1, 2$ labels the dots. This setup is described by the Hamiltonian $H_{\mathrm{DQD}} + H_{\mathrm{DQD,leads}}$, where $H_{\mathrm{DQD}} = T_{12}(c_1^\dagger c_2 + c_2^\dagger c_1)$ models the DQD with vanishing onsite energies, see Eq. (2.13). For ease of notation we consider particle currents. The coupling to the electron source and drain is given by

$$H_{\mathrm{DQD,leads}} = \sum_{q,\alpha} V_{q\alpha}(c_{\ell_\alpha}^\dagger c_{q\alpha} + c_{q\alpha}^\dagger c_{\ell_\alpha}) + \sum_{q,\alpha} \epsilon_q N_{q\alpha}, \tag{5.1}$$

where $c_{q\alpha}^\dagger$ are the fermionic creation operators for an electron in mode q of lead $\alpha = L, R$ with the energy ϵ_q. The mapping ℓ_α takes the values $\ell_L = 1$ and $\ell_R = 2$, respectively. Tunneling between the DQD and the leads is determined by the spectral densities $\Gamma_\alpha(\epsilon) = (2\pi/\hbar)\sum_q |V_{q\alpha}|^2 \delta(\epsilon - \epsilon_q) \equiv \Gamma_\alpha$ which we assume within a wideband limit energy independent.

We restrict ourselves to a fully symmetric DQD with equal barrier capacitances. Then according to the Ramo-Shockley theorem,[4,157] the displacement currents in the double dot circuit are such that the experimentally measured current is the average of the currents through the left and the right tunnel barrier, $I = \frac{1}{2}I_L - \frac{1}{2}I_R$. Its noise spectrum computed below depends on the charge fluctuations of the DQD and reads[4,158,159]

$$C_{II}(\omega) = \frac{1}{2}C_{I_L I_L}(\omega) + \frac{1}{2}C_{I_R I_R}(\omega) - \frac{\omega^2}{4}C_{NN}(\omega). \tag{5.2}$$

Motivated by recent experiments,[25,69–73,151] we assume that the detector consists of a tunnel barrier with a transmission that depends on the charge state of the DQD. We model its leads by the Hamiltonian $H_D = \sum_k \epsilon_k c_k^\dagger c_k + \sum_{k'} \epsilon_{k'} c_{k'}^\dagger c_{k'}$ with the fermionic creation operators of the left and the right lead, $c_k^\dagger$ and $c_{k'}^\dagger$, respectively. The tunnel coupling depends on the DQD occupation and reads[160–162]

$$H_D^{\mathrm{tun}} = (1 - s_1 N_1 - s_2 N_2) \sum_{kk'} t_{kk'}(c_k^\dagger c_{k'} + c_{k'}^\dagger c_k), \tag{5.3}$$

where $t_{kk'}$ denotes the tunnel matrix elements which we replace in a continuum limit by the conductance $G(\epsilon,\epsilon') = 2\pi \sum_{kk'} |t_{kk'}|^2 \delta(\epsilon-\epsilon_k)\delta(\epsilon-\epsilon_{k'}) \equiv G_D$ in units of e^2/h, which is also assumed energy independent. The number operators N_ℓ in the prefactor reflect the fact that an electron on the DQD increases the potential barrier of the tunnel contact and, thus, reduces the tunnel amplitudes. The strength of this reduction depends on the interaction with the DQD which is quantified by the dimensionless parameters s_1 and s_2. For consistency, it must obey $s_1 N_1 + s_2 N_2 \leq 1$ for all DQD occupations considered.

5.2. DQD in the classical limit

Within a classical approximation, we assume that the inter-dot tunneling is small such that H_{DQD} practically commutes with the occupation operators N_ℓ. Then the DQD dynamics can be neglected for the computation of the tunnel rates. Thus, we can adopt the golden-rule treatment of Ref. 163 by which we obtain that an electron in state k of the left lead may tunnel to state k' of the right lead with probability $(2\pi/\hbar)|t_{kk'}|^2\delta(\epsilon_k-\epsilon_{k'})(1-s_1N_1-s_2N_2)^2$. Expressing the probability for the initial many-body state in terms of Fermi functions and integrating over ϵ_k and $\epsilon_{k'}$, we find that for $N_1 = N_2 = 0$ the detector current can be described by a Poisson process with a rate $\gamma_0 = G_D|V_D|$ proportional to the bias voltage applied to the detector, V_D.[4,163] Thus, while in our model γ_0 is not restricted, we will see that good measurement correlations require it to be much larger than the dot-lead tunneling. If an electron resides on the DQD, Coulomb repulsion reduces the tunnel rates according to $\gamma_0 \to \gamma \equiv \gamma_0(1-\tilde{s}_1N_1-\tilde{s}_2N_2)$, where $\tilde{s}_\ell = s_\ell(2-s_\ell)$ reflects the detector sensitivities.[153]

Subsuming these two cases, we can conclude that the tunnel process at the detector inherits an additional randomness from the DQD occupation. In more technical terms, the Poisson process turns into a Cox process[164] with a rate

$$\gamma = \gamma_0(1-\tilde{s}_1N_1-\tilde{s}_2N_2) \tag{5.4}$$

which depends on the transport process of the DQD. Thus, the average current through the detector, $\langle j\rangle$, can be expressed in terms of the DQD occupations. While the same is true for the detector-DQD correlations, auto-correlations of the detector current contain also a (white) shot noise contribution, such that the power spectrum becomes[164]

$$C_{jj}(\omega) = \langle j\rangle + \gamma_0^2 \sum_{\ell,\ell'=L,R} \tilde{s}_\ell \tilde{s}_{\ell'} C_{N_\ell N_{\ell'}}(\omega). \tag{5.5}$$

For a derivation of the shot noise term, see Ref. 159. The fluctuations of the detector current are characterized by the frequency-dependent Fano factor $F(\omega) = C_{jj}(\omega)/\langle j\rangle$. In consistency with Ref. 153, we find that good measurement correlations are accompanied by $F(\omega) \gg 1$, see Fig. 5.2(a) and discussion below.

5.2.1. Master equation for uni-directional transport

We consider a DQD with large bias such that electrons can enter exclusively from the left lead with tunnel rate Γ_L, while leaving to the right lead with tunnel rate Γ_R. For our numerical study, we focus on a symmetric situation with $\Gamma_L = \Gamma_R \equiv \Gamma$. Moreover, if the onsite energies of both dots are equal as well, inter-dot tunneling is direction independent with a rate Γ_{12}. This rate description corresponds to situations in which $\Gamma_{12} \ll \Gamma$ such that the influence of the leads dominates or in which coherence is destroyed by environmental effects beyond our model.[163] Then electrons are always localized on one dot and quantum coherence does not play any role, which is the main requirement for a classical description. Then the natural basis is given by localized states and coherences can be ignored. Within the full quantum mechanical description of Sec. 5.3, we will investigate for which parameters this assumption is fulfilled.

If at most one electron can reside in the DQD, we have to take into account the states $\ell = 0, 1, 2$, referring to an empty DQD, one electron on the left dot, and one the right dot, respectively. Then the corresponding occupation probabilities obey the master equation $\dot{P} = \mathcal{M}P$, with

$$\mathcal{M} = \begin{pmatrix} -\Gamma_L & 0 & \Gamma_R \\ \Gamma_L & -\Gamma_{12} & \Gamma_{12} \\ 0 & \Gamma_{12} & -\Gamma_{12} - \Gamma_R \end{pmatrix}, \tag{5.6}$$

and $P = (P_0, P_1, P_2)^{\mathsf{T}}$, where T denotes transposition. P^{st} denotes with $\mathcal{M}P^{\mathrm{st}} = 0$ the stationary solution of the master equation. Our central quantity for the computation of correlation functions is the conditional probability

$$P(\ell, t|\ell', t') = [e^{\mathcal{M}(t-t')}]_{\ell\ell'}, \tag{5.7}$$

for the DQD being in state ℓ at time t provided that it was in state ℓ' at the earlier time $t' < t$. It is equivalent to the propagator of the master equation[165] and to lowest order in dt it obeys $P(\ell, t + dt|\ell', t) = \delta_{\ell\ell'} + \mathcal{M}_{\ell\ell'}dt$.

5.2.2. DQD-detector correlations

The stationary correlation of any DQD variable X with the detector current j can be obtained from the stochastic part of the rate γ given by Eq. (5.4) and reads

$$C_{jX} = -\gamma_0(\tilde{s}_1 C_{N_1 X} + \tilde{s}_2 C_{N_2 X}). \tag{5.8}$$

Since we are interested in the degree of correlation rather than in absolute values, we focus on the normalized correlation at a given measurement frequency ω which we define as

$$r_{ab}(\omega) = \frac{C_{ab}(\omega)}{\sqrt{C_{aa}(\omega)\, C_{bb}(\omega)}}\,. \tag{5.9}$$

Its absolute value is a figure of merit for the detection quality and in the ideal case is of order unity. In turn, for $|r_{jX}| \ll 1$, the detector current is practically independent of X.

In order to quantify the detection of the charge in dot $\ell = 1, 2$, we consider the correlation coefficient r_{jN_ℓ}. According to Eqs. (5.5) and (5.8), it can be expressed in terms of stationary correlation functions of the DQD populations which in the time domain read

$$C_{N_\ell N_{\ell'}}(t - t') = \langle N_\ell(t) N_{\ell'}(t') \rangle - \langle N_\ell \rangle \langle N_{\ell'} \rangle. \tag{5.10}$$

Since N_ℓ can assume only the values 0 and 1, the first term on the right-hand side is given by the joint probability $P(\ell, t; \ell', t')$ for the DQD being in the states ℓ and ℓ' at the respective times. Bayes' theorem relates this joint probability in the stationary limit to P^{st} and the conditional probability (5.7) so that we obtain for $t \geq t'$ the expression

$$C_{N_\ell N_{\ell'}}(t - t') = P(\ell, t|\ell' t') P^{\mathrm{st}}_{\ell'} - P^{\mathrm{st}}_{\ell} P^{\mathrm{st}}_{\ell'}, \tag{5.11}$$

while the opposite time ordering $t < t'$ follows by relabeling.

The conditional probabilities required for the current–current correlations and the correlations between currents and occupations are provided in Appendix D.

5.2.3. Alternative solution of the classical model and Fano factor

Albeit the treatment of frequency dependent correlation functions via Bayes' theorem is the most instructive approach, for numerical calculations a more direct method is desirable. To this end, we employ the method introduced in section 2.2 to compute second order correlation functions between currents in a unified manner. In particular, correlations involving the total current and correlations between occupations are comparably derived from a generalized Liouvillian, see the subsequent section 5.3 treating the full quantum mechanical problem.

The classical master equation is formally an equation of motion for the diagonal matrix elements of the full density matrix in the localized basis. Since in the DQD Liouvillian the dissipative term that describes the influence of the detector, see Eq. (5.20), is also diagonal in this basis, we merely have to replace the augmented Liouvillian $\mathcal{L}(\boldsymbol{\chi})$ by

$$\mathcal{M}(\boldsymbol{\chi}) = \mathcal{M} + \Gamma_L(e^{-i\chi_1} - 1)\mathcal{J}_L + \Gamma_R(e^{i\chi_2} - 1)\mathcal{J}_R + \gamma_0(e^{i\chi_D \operatorname{sgn} V_D} - 1)\mathcal{J}_D \tag{5.12}$$

with $\mathcal{M}$ as in Eq. (5.6) and the DQD-lead jump operators

$$\mathcal{J}_L = \begin{pmatrix} 0 & 0 & 0 \\ 1 & 0 & 0 \\ 0 & 0 & 0 \end{pmatrix}, \qquad \mathcal{J}_R = \begin{pmatrix} 0 & 0 & 1 \\ 0 & 0 & 0 \\ 0 & 0 & 0 \end{pmatrix}, \tag{5.13}$$

while the detector jump operator

$$\mathcal{J}_D = \begin{pmatrix} 1 & 0 & 0 \\ 0 & 1 - \tilde{s}_1 & 0 \\ 0 & 0 & 1 - \tilde{s}_2 \end{pmatrix} \tag{5.14}$$

follows from Eq. (5.20) by ignoring non-diagonal contributions. We have confirmed all results for the classical limit with the method relying on the conditional probabilities provided in Appendix D.

This alternative method is rather convenient for obtaining an analytical expression for the detector Fano factor in the classical limit. For this purpose, we compute the pseudoresolvent of $\mathcal{M}$ so that we can directly evaluate the auto-correlation function of the detector, $C_{jj}(\omega)$. Thus, with the average current $\langle j \rangle$, we find the frequency-dependent Fano factor $F_D(\omega) = C_{jj}(\omega)/\langle j \rangle$. For $\Gamma_L = \Gamma_R \equiv \Gamma$ and small inter-dot rates $\Gamma_{12} \ll \Gamma$, it becomes

$$F_D(\omega) = 1 + \frac{2\gamma_0\Gamma_{12}}{\Gamma^2+\omega^2} \frac{\frac{3\Gamma^2+\omega^2}{\Gamma^2+\omega^2}\tilde{s}_1(\tilde{s}_1-\tilde{s}_2)+\tilde{s}_2^2}{1-\tilde{s}_1} \tag{5.15}$$

and assumes rather large values in the zero-frequency limit $\omega \ll \Gamma$. For $\omega \gtrsim \Gamma$, we approximate the last factor in Eq. (5.15) by $\max(\tilde{s}_1, \tilde{s}_2)$ and obtain $F_D(\omega) = 1 + (\omega_{\max}/\omega)^2$ with $\omega_{\max}$ given by Eq. (5.16).

5.2.4. Numerical results

For the numerical evaluation of the correlation coefficients, we diagonalize the matrix (5.6) to obtain a bi-orthonormal set of left and right eigenvectors, u_i^{T} and v_i, as well as the eigenvalues $-\lambda_i$, which for proper $\mathcal{M}$ have non-negative real part. Then $\exp(\mathcal{M}t) = \sum_i v_i u_i^{\mathsf{T}} e^{-\lambda_i t}$ for $t > 0$. We obtain for each correlation function a sum of decaying exponentials and a formal expression for the Fourier transformed of the propagator $P(\ell, t|\ell', 0)$.

Investigating various correlation functions, we found that one has to distinguish three frequency regimes which can be characterized by the frequency-dependent Fano factor of the detector current derived in Appendix D and depicted in the inset of Fig. 5.2(a). First, if the measurement frequency is small, $\omega \lesssim \Gamma$, all correlation functions assume their zero-frequency value. Typically the detector Fano factor is several orders of magnitude above the shot noise level, where its precise value depends much on the coupling strengths $\tilde{s}_1$ and $\tilde{s}_2$. Such low measurement frequencies correspond to static DQD properties, i.e., time-averaged expectation values. The crossover to the high-frequency limit occurs at

$$\omega_{\max} = (2\gamma_0\Gamma_{12})^{1/2} \max(\tilde{s}_1, \tilde{s}_2), \tag{5.16}$$

which reflects the largest relevant frequency. For $\omega \gtrsim \omega_{\max}$, the Fano factor assumes the Poissonian value $F(\omega) \approx 1$ while all DQD-detector correlations practically vanish. Thus, on such large frequency scales and on the corresponding short time scales, the detector cannot provide information about the DQD. The proportionality of the upper limit, $\omega_{\max} \propto \gamma_0^{1/2}$, has also been found for detecting the charge state of a single quantum dot.[153] For intermediate frequencies, we find $F(\omega) \propto \omega^{-2}$, a behavior typical for a dichotomic process[77] such as alternating between an empty and an occupied DQD. correlation coefficients provide information about the possibility of time-resolved measurement. This generic global behavior of the detector-DQD

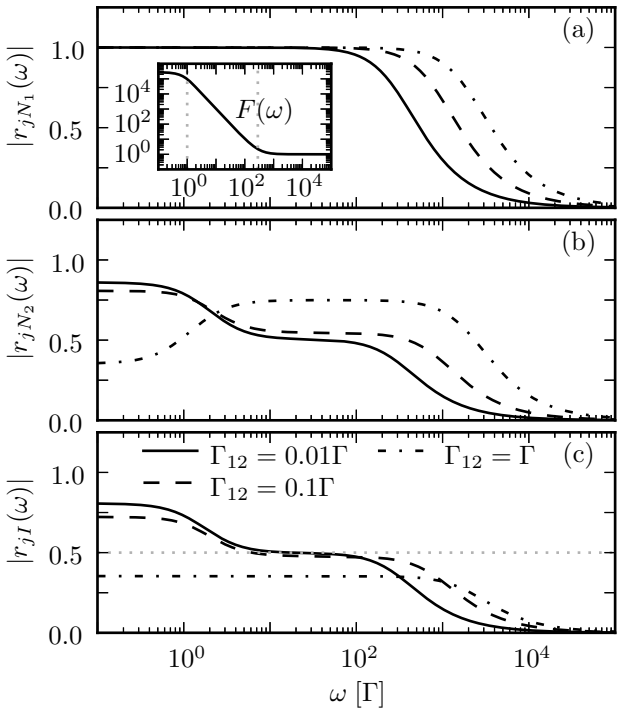

Fig. 5.2.: Classical frequency-dependent correlation coefficients between the detector current and (a) the occupation of the left dot, (b) the occupation of the right dot, and (c) the symmetrized current through the DQD for various inter-dot rates Γ_{12}. The detector is characterized by a bare rate $\gamma_0 = 10^8\Gamma$ and the sensitivities $\tilde{s}_1 = 0.2$ and $\tilde{s}_2 = 0$, i.e., it couples to only the left dot. The inset in panel (a) shows the frequency dependent Fano factor of the detector current for $\Gamma_{12} = 0.01\,\Gamma$, where the dashed lines mark the crossover region between the plateaus. The horizontal line in panel (c) marks the upper limit 1/2 discussed in the text.

correlations relates the possibility of charge detection to the emergence of super-Poissonian detector noise. Physically, this reflects switching between two values of the detector current and the associated bunching of the electrons flowing through the detector.

Charge detection

Figures 5.2 and 5.3 show the correlations between the detector current j and the DQD for the coupling to only the left quantum dot. Then for frequencies below $\omega_{\max}$, the measurement correlation with the occupation of the left dot [panel (a) in each figure] assumes the ideal value $r_{jN_1} = 1$. This indicates the possibility of time-resolved detection of the charge on the left dot, as long as the Fano factor stays significantly above the shot noise level. Thus the time resolution of our charge detection scheme is limited by $\omega_{\max}$.

Since an electron on the right quantum dot originates from the left lead, it must

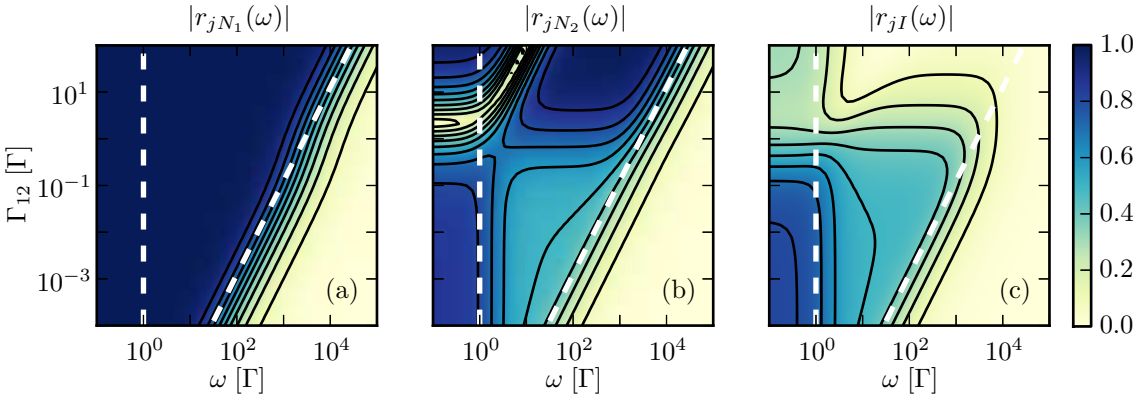

Fig. 5.3.: Classical correlation coefficients depicted in Fig. 5.2 as function of the frequency ω and the inter-dot rate Γ_{12} while all other parameters are the same. The dashed lines at $\omega = \Gamma$ and at $\omega = \omega_{\max}$ mark the crossover between the different regimes discussed in the text.

have occupied the left dot at some earlier stage. Then one naturally expects some remnant correlation between the occupations of both dots. As a consequence, the detector not only correlates with the dot to which it couples, but also with the other dot as can be appreciated in Figs. 5.2(b) and 5.3(b). In the regime of weak inter-dot tunneling, $\Gamma_{12} \lesssim \Gamma$, this correlation decays as a function of ω via an intermediate plateau limited by the crossover frequencies Γ and $\omega_{\max}$. For $\omega \lesssim \Gamma$, we find $r_{jN_2} \approx 0.8$, i.e., the detector notices the average population of dot 2 to some extent. In the intermediate regime, $\Gamma \lesssim \omega \lesssim \omega_{\max}$, the correlation coefficient drops down to a value 1/2. Interestingly enough, for a strong inter-dot rate $\Gamma_{12} \gtrsim \Gamma$, the intermediate plateau starts to decay at slightly larger frequencies, while the correlation coefficient always stays clearly below unity.

In a realistic setup, a charge detector at a DQD is sensitive not only to the closer dot, but to some extent also to the other dot. This raises the question whether the influence of the latter affects the measurement quality. Being interested in time-resolved measurement, we focus on the intermediate frequency regime. Figure 5.4(a) shows the correlation coefficient of the detector current with the occupation of the left dot as a function of both sensitivities. It demonstrates that (almost) perfect correlation requires $\tilde{s}_1 \gtrsim 2\tilde{s}_2$, i.e., the left dot must couple at least twice as strong as the right dot. An extreme case of very small correlation is found for $\tilde{s}_2 \approx 2\tilde{s}_1$. There the behavior is even counter-intuitive since reducing the coupling to the left dot increases the correlation. Finally, the correlation with the population of the right dot (not shown) behaves accordingly. It can be obtained by interchanging the labels 1 and 2, which is non-trivial since reflection symmetry is absent owing to the bias voltage applied to the DQD.

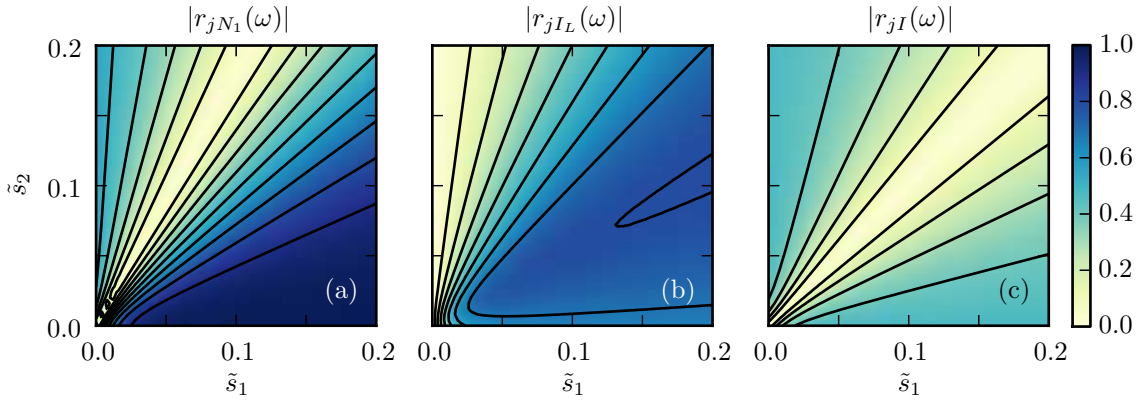

Fig. 5.4.: Classical correlation coefficients between the detector and (a) the occupation of the left dot, (b) the current through the left DQD barrier, and (c) the Ramo-Shockley current as a function of the detector sensitivities $\tilde{s}_1$ and $\tilde{s}_2$. The frequency $\omega = 50\Gamma$ corresponds to the middle of the second plateau at which time-resolved measurement is possible. The inter-dot rate is $\Gamma_{12} = 0.1\Gamma$, while all other parameters are as in Fig. 5.2.

Current detection

Even though the detector couples to the charge degree of freedom, it has been employed to reconstruct the corresponding time-resolved current[69,71] and its full-counting statistics.[103] A later theoretical investigation[153] revealed that nevertheless the correlation coefficient between the detector current and the measured current stays significantly below unity. Thus, knowledge about the transport mechanism must provide missing information.

Figure 5.4(b) depicts the correlation of the detector current with the current entering the DQD from the left lead at an intermediate measurement frequency. It assumes its maximum $r_{jI_L} \approx 0.8$ for $\tilde{s}_1 \approx 2\tilde{s}_2$. Surprisingly, this value is slightly above the limit of $\sqrt{1/2}$ found for a detector coupled to a single quantum dot.[153] A remarkable difference to the single quantum dot is also found for the Ramo-Shockley current $I = \frac{1}{2}I_L - \frac{1}{2}I_R$ which for a symmetric single quantum dot is fully uncorrelated with the detector current.[153] Figure 5.4(c), by contrast, reveals that this is not the case for a DQD unless both dots couple equally strongly to the detector. If one coupling dominates, the correlation can be up to $r_{jI} = 1/2$.

5.3. Quantum mechanical description

In order to obtain the quantum mechanical detector-DQD correlations, we employ the generalized master equation (2.6) discussed in section 2.2. This formulation is capable to treat the detector current operator which, in contrast to previous applications of this approach to quantum transport,[129,130,166,167] is not a usual "electron jump term" between the system and a lead. Since this master equation is Markovian, it allows us to compute two-time expectation values of system variables via the quantum regression theorem.[79,168,169]

5.3.1. Bloch-Redfield master equation

To setup the Liouvillian, we start from the full DQD-lead-detector Hamiltonian and separate it into the DQD contribution H_S, the lead terms, and the tunneling terms from and to the four leads. Thus, we can apply equation (2.6) and end up with a Markovian master equation that captures the DQD-lead tunneling and the detector tunneling to second order. Owing to strict conservation of the total lead charge in the detector circuit, one counting variable for the detector is sufficient. Thus we only consider the counting field $\boldsymbol{\chi} = (\chi_L, \chi_R, \chi_D)$ referring to the left and the right lead of the DQD and to the right lead of the detector, respectively. By contrast, the total lead electron number in the DQD circuit fluctuates due to charging and discharging of the DQD. As a consequence, a full time-dependent description requests two independent counting variables. By tracing out the leads, mixing terms between DQD and detector vanish and we obtain the master equation $\dot{\rho} = \mathcal{L}(\boldsymbol{\chi})\rho$ with the generalized Liouvillian $\mathcal{L}(\boldsymbol{\chi})\rho = -i[H_S,\ \rho] + \mathcal{L}_S(\boldsymbol{\chi})\rho + \mathcal{L}_D(\boldsymbol{\chi})\rho$. The density operator ρ relates to the moment-generating function for the lead electrons which allows us to determine frequency dependent correlations. As in the previous section discussed, the moment-generating function obeys interesting symmetry properties known as exchange fluctuation theorems.[91,93] Recently they have been investigated for capacitively coupled conductors like the present models.[84,141,162,170] Moreover, such coupling may influence Kondo effects.[171]

For the DQD-lead tunneling in the large-bias limit we find

$$\mathcal{L}_S(\boldsymbol{\chi})\rho = \Gamma_L\Big[\mathcal{D}(c_1^\dagger)\rho + (e^{-i\chi_1} - 1)c_1^\dagger\rho c_1\Big] + \Gamma_R\Big[\mathcal{D}(c_2)\rho + (e^{i\chi_2} - 1)c_2\rho c_2^\dagger\Big], \quad (5.17)$$

see Eq. (2.20) The tunnel Hamiltonian of the detector, Eq. (5.3), contains besides lead terms the system operator $X \equiv \mathbb{1} - \sum_\ell s_\ell N_\ell$ which determines the generalized detector Liouvillian

$$\mathcal{L}_D(\boldsymbol{\chi})\rho = Y_-(\boldsymbol{\chi})\rho X + X\rho Y_+(\boldsymbol{\chi}) - XY_-\rho - \rho Y_+ X, \quad (5.18)$$

where in the zero-temperature limit and for large bias voltage, $|V_D| > 2|T_{12}|$,

$$Y_\pm(\boldsymbol{\chi}) = e^{i\chi_D \operatorname{sgn} V_D}\frac{G_D}{2}\Big(|V_D|X \pm [H_S,\ X]\Big). \quad (5.19)$$

The commutator in Eq. (5.19) is proportional to the inter-dot tunnel amplitude T_{12} and, thus, can be neglected for large detector bias voltage, $|V_D| \gg 2|T_{12}|$. Therefore, we proceed with

$$\mathcal{L}_D(\boldsymbol{\chi})\rho = \gamma_0\Big[\mathcal{D}(X)\rho + (e^{i\chi_D \operatorname{sgn} V_D} - 1)X\rho X\Big], \quad (5.20)$$

where $\gamma_0 = G_D|V_D|$ is the tunnel rate of the detector in the absence of the DQD. For typical parameters[69,71,72] of $V_D = 1\,\mathrm{mV}$, $G_D \lesssim 0.1\,e^2/h$, DQD-lead rates Γ of a few kHz, and inter-dot tunneling up to $T_{12} = 100\,\mu\mathrm{eV}$, this corresponds to detector rates in the range 10^5–$10^8\,\Gamma$.

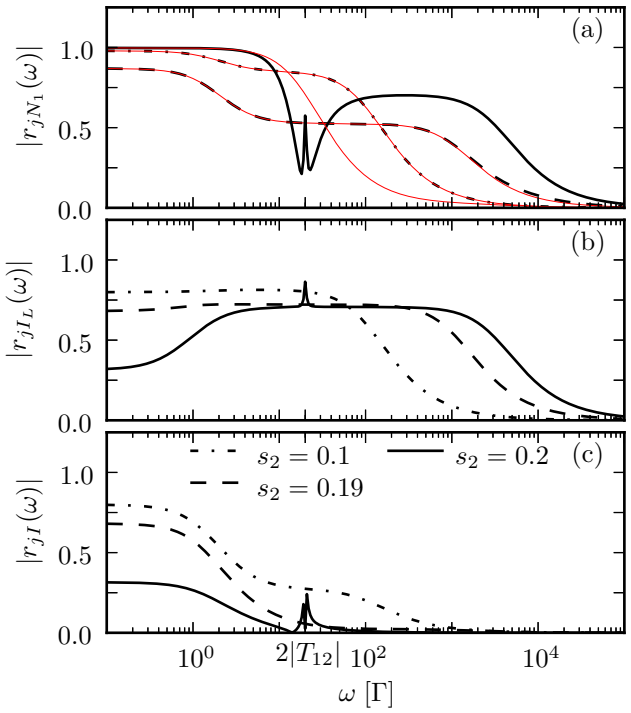

Fig. 5.5.: Quantum mechanical version of the correlation coefficients between the detector current and (a) the occupation of the left dot, (b) the current through the left DQD barrier, and (c) the symmetrized current through the DQD for various values of the sensitivity s_2 while $s_1 = 0.2$ is fixed. The inter-dot tunnel coupling is $T_{12} = 10\Gamma$, while all other parameters are as in Fig. 5.2. The thin red lines in panel (a) show the corresponding classical correlation coefficients for Γ_{12} determined by the quantum-to-classical mapping in Eq. (5.27).

5.3.2. Charge and current correlations

Also here we characterize the measurement by normalized correlation coefficients defined in Eq. (5.9), but with the corresponding quantum mechanical expressions on the right-hand side. Thus, we have to compute auto-correlations and cross correlations of the DQD occupations and the detector current.

For the dot occupations, we define $C_{N_\ell N_{\ell'}}$ as in Eq. (5.10). From the quantum regression theorem[79,168,169] follows the frequency-dependent correlation function

$$C_{N_\ell N_{\ell'}}(\omega) = \mathrm{tr}[N_\ell \mathcal{R}(-i\omega) N_{\ell'} \rho_{\mathrm{st}} + N_{\ell'} \mathcal{R}(i\omega) \rho_{\mathrm{st}} N_\ell]. \tag{5.21}$$

In order to formally perform the Fourier transformation, we have introduced the pseudoresolvent $\mathcal{R}(z) = \mathcal{Q}(z - \mathcal{L})^{-1}\mathcal{Q}$ with $\mathcal{Q} = (\mathbb{1} - \rho_{\mathrm{st}}\,\mathrm{tr})$ the projector to the part of Liouville space orthogonal to the stationary state ρ_{st} of the DQD.

In contrast to the classical case, our master equation formalism allows us to treat all currents on equal footing, namely by computing derivatives of the generalized Liouvillian $\mathcal{L}(\boldsymbol{\chi})$ with respect to the corresponding counting variable. Then we

find[129,130,166,167]

$$C_{I_\alpha I_\beta}(\omega) = \langle \mathcal{W}_{\alpha\beta} \rangle + \langle \mathcal{W}_\alpha \mathcal{R}(-i\omega) \mathcal{W}_\beta \rangle + \langle \mathcal{W}_\beta \mathcal{R}(i\omega) \mathcal{W}_\alpha \rangle, \tag{5.22}$$

where $\alpha, \beta \in \{L, R, D\}$ label the leads. The superoperators $\mathcal{W}_\alpha = (\partial \mathcal{L}/\partial i\chi_\alpha)|_{\boldsymbol{\chi}=\mathbf{0}}$ and $\mathcal{W}_{\alpha\beta} = (\partial^2 \mathcal{L}/\partial i\chi_\alpha \partial i\chi_\beta)|_{\boldsymbol{\chi}=\mathbf{0}}$ are Taylor coefficients of $\mathcal{L}(\boldsymbol{\chi})$, where the first expression provides the average currents $I_\alpha = \langle \mathcal{W}_\alpha \rangle$. Formally, expression (5.22) follows by substituting in Eq. (5.21) the number operators by jump operators and adding the shot noise contribution $\langle \mathcal{W}_{\alpha\beta} \rangle$ which vanishes unless $\alpha = \beta$. The charge correlations satisfy $C_{I_\alpha I_\beta}(\omega) = C_{I_\beta I_\alpha}(-\omega) = C^*_{I_\beta I_\alpha}(\omega)$ and exhibit therewith symmetric auto-correlations while the cross correlations may contain complex contributions. Notice that in accordance with Ref. 167, $2\,\mathrm{Re}\langle \mathcal{W}_\alpha \mathcal{R}(i\omega) \mathcal{W}_\alpha \rangle = \langle \mathcal{W}_\alpha [\mathcal{R}(i\omega) + \mathcal{R}(-i\omega)] \mathcal{W}_\alpha \rangle$.

The frequency-dependent fluctuations (5.2) of the Ramo-Shockley current[4,157] $I = \frac{1}{2} I_L - \frac{1}{2} I_R$ are linear combination of the above expressions. They can also be obtained directly from the generalized density operator by transforming the counting fields according to[130] $\chi_L \to \chi_A + \chi_T/2$ and $\chi_R \to \chi_A - \chi_T/2$, where χ_T refers to the total current I, while χ_A accounts for temporary charge accumulation on the DQD. Notice that we follow the sign convention of Ref. 172, where the currents are positive when electrons flow from the lead to the DQD.

For the cross correlations between currents and DQD occupations, we define the according expression

$$C_{I_\alpha N_\ell}(\omega) = \mathrm{tr}[N_\ell \mathcal{R}(-i\omega) \mathcal{W}_\alpha \rho_{\mathrm{st}} + \mathcal{W}_\alpha \mathcal{R}(i\omega) \rho_{\mathrm{st}} N_\ell]. \tag{5.23}$$

Since we did not derive the latter correlation function in terms of a measurement procedure, it is an operationally defined quantity rather than an observable. For ease of notation we henceforth replace the subscript I_D by j.

5.3.3. Classical limit of the quantum master equation

The classical limit of the Bloch-Redfield equation can be obtained by eliminating the coherences between the left and the right quantum dot in the limit of small inter-dot tunneling T_{12}. This task is hampered by the fact that the natural basis of the Bloch-Redfield equation is given by the eigenstates of H_S which, owing to the absence of a detuning, are always delocalized irrespective of how small T_{12} is. However, there exists a way out based on the comparison of the average currents in both limits. While comparing the DQD currents yields an effective Γ_{12} in terms of T_{12}, the detector current provides a relation between the coupling strengths of the quantum mechanical model, s_ℓ, and the classical couplings $\tilde{s}_\ell$.

A straightforward computation of the stationary state of the classical master equation, see Eq. (5.6), yields the occupation numbers

$$\langle N_1 \rangle = \frac{\Gamma_L(\Gamma_R + \Gamma_{12})}{\Gamma_L \Gamma_R + (2\Gamma_L + \Gamma_R)\Gamma_{12}}, \tag{5.24}$$

$$\langle N_2 \rangle = \frac{\Gamma_L \Gamma_{12}}{\Gamma_L \Gamma_R + (2\Gamma_L + \Gamma_R)\Gamma_{12}}, \tag{5.25}$$

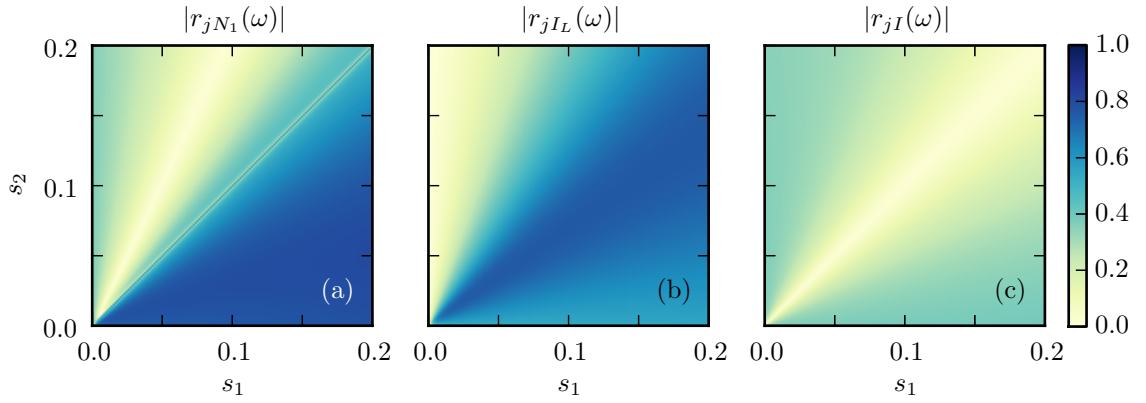

Fig. 5.6.: Quantum mechanical version of the correlation coefficients shown in Fig. 5.4 as a function of the detector sensitivities s_1 and s_2. The frequency is $\omega = 50\Gamma$, the tunnel rate is $T_{12} = 10\Gamma$, while all other parameters are as in Fig. 5.5. Notice that in the regime depicted, the classical and the quantum mechanical detector sensitivities relate as $s_\ell \approx \tilde{s}_\ell/2$.

from which by use of $I^{\rm cl}_{\rm DQD} = \Gamma_R \langle N_2 \rangle$ immediately follows [see Eq. (2.21)]

$$I^{\rm cl}_{\rm DQD} = \frac{\Gamma_L \Gamma_R \Gamma_{12}}{\Gamma_L \Gamma_R + (2\Gamma_L + \Gamma_R)\Gamma_{12}}. \tag{5.26}$$

Comparison with the corresponding expression for the quantum master equation, $\langle \mathcal{W}_R \rangle$, provides the effective classical inter-dot rate

$$\Gamma_{12} = \frac{4|T_{12}|^2}{\Gamma_R + \gamma_0 (s_1 - s_2)^2}. \tag{5.27}$$

Obviously, the DQD current assumes its maximum for $s_1 = s_2$, while it becomes much smaller when the two couplings are different (notice that typically $\gamma_0 \ggg \Gamma_{L,R}$). The reason for this current reduction is the fact that for $s_1 \neq s_2$, the detector performs a position measurement of the DQD electrons. Therefore, it destroys the coherence between the left dot and the right dot and, thus, forces the electron into the corresponding pointer states, which leads to localization. This localization is manifest in a current suppression which represents the main measurement backaction of the charge sensor to the DQD. In the limiting case $s_1 = s_2$, the measured quantity is the total electron number of the DQD which commutes with H_S and therefore does not affect the coherences. Below we will find that in a large part of parameter space, the classical treatment with Γ_{12} given by Eq. (5.27) agrees very well with the full quantum mechanical solution.

For the detector current, we insert the populations (5.24) and (5.25) into Eq. (5.4) to obtain

$$j_{\rm cl} = G_D V_D (1 - \tilde{s}_1 \langle N_1 \rangle - \tilde{s}_2 \langle N_2 \rangle), \tag{5.28}$$

where the prefactor relates to the tunnel rate of the detector, $\gamma_0 = G_D |V_D|$. Comparison with the quantum mechanical expression and using the above result for

Γ_{12} provides a relation between the classical and the quantum mechanical detector sensitivities,

$$\tilde{s}_\ell = s_\ell(2 - s_\ell), \tag{5.29}$$

where for the small couplings considered in our numerical studies, $\tilde{s}_\ell \approx 2s_\ell$.

5.3.4. Numerical results

We already discussed above that the presence of the detector causes backaction which reduces the effective inter-dot rate Γ_{12}. In particular, this rate becomes smaller with a larger difference between the two detector couplings, $|s_1 - s_2|$. Consequently, we expect that the frequency $\omega_{\max}$ beyond which all DQD-detector correlations vanish [see Eq. (5.16)] also depends on the coupling strength as well as on the bare detector rate γ_0. The quantum mechanical correlation coefficients for different values of s_2 depicted in Fig. 5.5 confirm this expectation.

Charge detection

Figures 5.5(a) and 5.6(a) show the correlation coefficient between the occupation of the left quantum dot and the detector current. The former is compared with the classical result with the effective Γ_{12} given by Eq. (5.27). We find that as long as the two couplings differ, the values obtained from the quantum-to-classical mapping are practically the same as those of the quantum case. A minor difference is visible at large frequencies for $s_2 = 0.19$. Only when both couplings are equal, the quantum mechanical solution becomes rather different and is beyond the classical approach. This corresponds to the situation discussed above in which the detector is sensitive to the total number of electrons on the DQD. Then the DQD-detector Hamiltonian commutes with H_S and, thus, it measures a good quantum number.

This behavior is also found for the correlation for an intermediate frequency as a function of the couplings shown in Fig. 5.6(a). The main difference to the corresponding classical solution (not shown) is found in a narrow region at $s_1 = s_2$. As in the classical case, fulfilling the condition for good charge detection at dot 1, $r_{jN_1} \approx 1$, requires $s_1 \gtrsim 2s_2$.

Current detection

Figure 5.5 also shows the correlation coefficients with the DQD current through the left barrier [panel (b)] and with the Ramo-Shockley current [panel (c)]. Besides the global behavior already discussed for the correlation with the DQD occupations, we find for $s_1 = s_2$ a sharp peak at a measurement frequency $2|T_{12}|$ which corresponds to the level splitting of the DQD. As soon as both couplings differ minimally, this peak vanishes. Since we consider $\gamma_0 \ggg \Gamma$, a tiny difference of much less than one percent is already sufficient to suppress the peak. This demonstrates that the detector by and large destroys the quantum features of the DQD unless it couples to a good quantum number.

Figures 5.6(b) and 5.6(c) show the correlations of the detector and the DQD currents as a function of the sensitivities for an intermediate frequency. It confirms the predictions from the classical treatment (cf. the corresponding panels of Fig. 5.4). In particular, it shows that also quantum mechanically the current through the individual barriers may correlate strongly with the detector, while the Ramo-Shockley current always correlates weakly.

5.4. Main results

We have studied a tunnel contact employed as charge sensor for a strongly biased DQD such that electrons are detected while being transported. The central idea of this scheme is a capacitive coupling between the two subsystems by which electrons on the DQD reduce the transmission of the tunnel contact. We have characterized this measurement by correlation coefficients of the detector current and DQD observables both in the classical limit and within a full quantum mechanical approach. The comparison of these limits allowed us to investigate the backaction on the coherence of DQD electrons.

The key ingredient to the classical description is a phenomenological incoherent inter-dot transition rate between the localized electron states on the DQD. It determines the conditional probabilities of the DQD and, thus, the joint probabilities that enter the two-time correlations under investigation. This approach represents a generalization of the one used for calculating current-current correlations[127] and measurement correlations[153] for a single electron transistor.

The correlation coefficients studied provide a limiting frequency beyond which measurement is no longer possible and which determines the time-resolution of the detection scheme. This limit increases with the detector rate, the inter-dot rate, and the detector sensitivity. The possibility of charge detection depends also crucially on the ratio between the capacitive couplings to each dot: A charge on a particular dot can be monitored reliably only if it couples to the detector at least twice as strong as an electron on the other dot. With the time-resolved DQD populations at hand, one can reconstruct the corresponding time-dependent current, at least under the assumption of unidirectional transport. This is reflected by a significant, but not perfect correlation between the detector and the DQD currents. Rather surprisingly, this correlation is slightly larger than for the corresponding setup with a single-electron transistor, despite the more complicated transport mechanism of the present case.

On the quantum mechanical level, we used a method based on a Bloch-Redfield master equation augmented by a counting field. In order to capture also the detector current, we generalized this method to the presence of "jump terms" that do not alter the DQD occupation, but describe the detector current. A main issue for such quantum mechanical position measurement is its backaction to the coherence of the measured system. Here it is manifest in an additional localization of the DQD electrons. On the one hand, this leads to a significant reduction of the DQD current, on the other hand, it pushes the system towards its classical limit. Indeed

our quantitative analysis revealed that the classical description is adequate whenever the detector current correlates strongly with one of the DQD occupations. A natural expectation is that this tendency should be even stronger in the presence of couplings to external degrees of freedom such as the electronic circuitry or substrate phonons.

Even though we restricted ourselves to a narrow part of parameter space, we observed a rather rich behavior. Thus, a full understanding of the detection scheme may requires taking further ingredients into account. Besides the already mentioned influence of external degrees of freedom, this could be a detuning which also cause localization.

6 Exchange fluctuations

Exchange fluctuation theorems are exact relations between probabilities for non-equilibrium transitions emerging from a Gibbs state.[115,116] In section 2.3, we briefly introduced a variant thereof concerning charge and heat exchange in quantum transport between equal and distinct leads[90–93] which can be verified experimentally.[94,117,118] In practice, theoretical studies of quantum transport often rely on approximations such as perturbation theory in the tunneling between system and electron reservoirs to obtain a master equation approach.[120] On the one hand, it has been demonstrated that a careless application of master equations may predict spurious currents at equilibrium[173] and thus may violate fluctuation theorems. On the other hand, the validity of exchange fluctuation theorems has been verified for master equation descriptions of various specific situations.[117,141,162,170,174,175] Thus, the question arises whether any general statement for a whole class of master equations is possible. In particular, we consider the Bloch-Redfield formalism provided in section 2.2 which is a widely employed Markovian master equation for quantum systems weakly coupled to environmental degrees of freedom.[78] It is equivalent to various common master equations.

We briefly present the exact fluctuation theorem and demonstrate afterwards that the Bloch-Redfield master equation is consistent with exchange fluctuation theorems only to some extent. Then, we consider the rotating-wave approximation and show that the resulting RWA master equation complies within the fluctuation theorem (2.12) despite contriving a further approximation. Moreover, we predict for the fluctuation theorem violation of the Bloch-Redfield equation a scaling behavior which we confirm by a numerical study on a four terminal double quantum dot. Complementary, we regard a four terminal quadruple quantum dot. The author has previously published the results of this chapter in Ref84.

6.1. Model and exchange fluctuation theorem

As introduced in chapter 2, we consider a general transport setup of quantum dots modeled by the Hamiltonian $H = H_S + V + \sum_\alpha H_\alpha$. Thereby, the central system, H_S, is in contact with fermionic leads formed by free electron gases, $H_\alpha = \sum_q \epsilon_{q\alpha} c^\dagger_{q\alpha} c_{q\alpha}$. Initially the leads are in a Gibbs ensemble at a common temperature $T = 1/k_B\beta$, while the chemical potentials μ_α are shifted from their equilibrium values $\mu_\alpha = 0$ by externally applied voltages. In contrast to Refs.115,176, our system Hamiltonian H_S may contain Coulomb repulsion terms which in most quantum dots represent the largest energy scale. Thus for the decomposition of the density operator, we

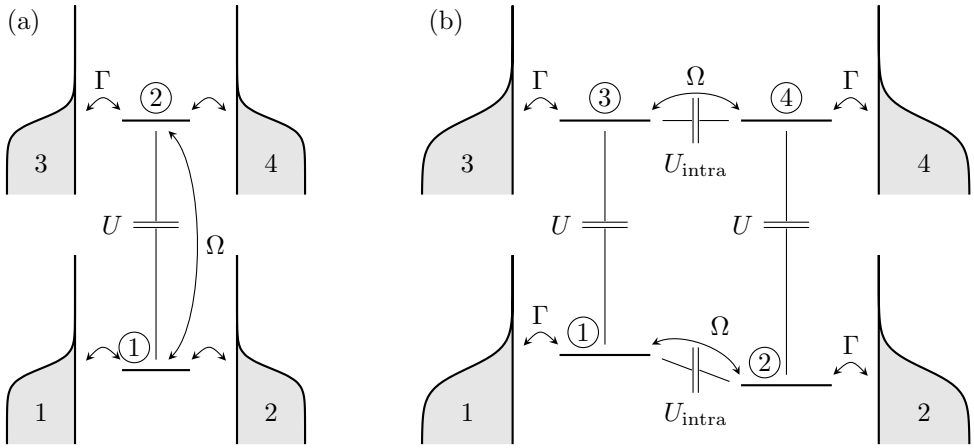

Fig. 6.1.: (a) Double quantum dot in contact with four leads $\alpha = 1, \ldots, 4$, used to exemplify our analytical results and the scaling of the deviations from the exact exchange fluctuation theorem (6.1). (b) Quadruple quantum dot in contact with four leads. The system can be considered as two coupled transport channels, each formed by a double quantum dot and interacting capacitively with the other.

will have to work in a many-body basis. Each lead α is tunnel coupled to one quantum dot N_{ℓ_α} via a Hamiltonian $V_{q\alpha}(c^\dagger_{\ell_\alpha} c_{q\alpha} + c^\dagger_{q\alpha} c_{\ell_\alpha})$, which is fully determined by the spectral density $\Gamma_\alpha(\epsilon)$. In our numerical calculations, we assume within a wide-band limit energy-independent couplings, $\Gamma_\alpha(\epsilon) \equiv \Gamma_\alpha$, while our analytical results are valid beyond. For numerical evaluation, we consider the four terminal double quantum dot sketched in Fig. 6.1(a) and the four terminal quadruple quantum dot sketched in Fig. 6.1(b). The latter model has been studied in the previous chapter in the configuration of a coherent quantum ratchet—here we assume equal inter-dot tunneling $\Omega = T_{\rm dr} = T_{\rm ra}$, and consider the leads at finite temperatures and at zero bias voltages.

Not only the stationary current and its low-frequency fluctuations are obtained from a cumulant generating function $Z(\boldsymbol{\chi})$ but also transport coefficients, i.e., derivatives of the current and its cumulants with respect to the applied voltages. In particular, $I_\alpha = (\partial Z/\partial i\chi_\alpha)|_{\boldsymbol{\chi}=\boldsymbol{\mu}=\mathbf{0}}$, the conductance $G_{\alpha,\beta} = -(\partial^2 Z/\partial i\chi_\alpha \partial\mu_\beta)|_{\boldsymbol{\chi}=\boldsymbol{\mu}=\mathbf{0}}$, while the zero-frequency limit of the current correlation function $\langle I_\alpha, I_\beta\rangle_{\omega\to 0}$ reads[4] $S_{\alpha\beta} = (\partial^2 Z/\partial i\chi_\alpha \partial i\chi_\beta)|_{\boldsymbol{\chi}=\mathbf{0}}$. The cumulant generating function implicitly depends on the chemical potentials μ_α.

Using an exact formal solution of the dot-lead dynamics, one can demonstrate that the cumulant generating function obeys the exchange fluctuation theorem[93]

$$Z(\boldsymbol{\chi}) = Z(-\boldsymbol{\chi} - i\beta\boldsymbol{\mu}). \tag{6.1}$$

Its practical use is to derive relations between different transport coefficients, see section 2.3. To first order, $I_\alpha = 0$, while to second order one, e.g., obtains the Johnson-Nyquist relation $2k_BTG^{\rm eq}_{\alpha,\alpha} = S^{\rm eq}_{\alpha\alpha}$. For a proof of Eq. (6.1), one introduces a counting variable ξ for the total lead energy[92,93,177,178] to obtain the relation

$Z(\boldsymbol{\chi},\xi) = Z(-\boldsymbol{\chi} - i\beta\boldsymbol{\mu}, -\xi + i\beta)$. Then one argues that, provided that the energy of the central system is negligible, the total lead energy is conserved and, thus, Z is independent of ξ. Notice, that we introduced in section 2.3 the more general definition of the cumulant generating function covering local energy exchange. Here, we are rather interested in the dissipation of the total energy which is formally obtained by setting for all leads $\xi_\alpha = \xi$. In the following, we explore up to which extent a Bloch-Redfield theory for quantum transport complies with this exact statement.

6.2. Bloch-Redfield master equation

The generalized Liouvillian describing charge and heat cumulants is of the form

$$\mathcal{L}_{\boldsymbol{\chi},\xi} = -i[H_S,\rho] - \mathcal{D} + \sum_\alpha \Big[e^{-i\chi_\alpha}\mathcal{J}_\alpha^{\text{in}}(\xi) + e^{i\chi_\alpha}\mathcal{J}_\alpha^{\text{out}}(\xi)\Big], \tag{6.2}$$

where $\mathcal{J}_\alpha^{\text{in/out}}$ describe dot-lead tunneling and $\mathcal{D}$ subsumes all other dissipative terms. For vanishing counting variables, $\mathcal{L}_{\mathbf{0},0}$ represents the physical Liouvillian. For numerical purpose the density operator and therewith the Liouvillian is decomposed into the many-body eigenstates of the quantum dots. Thus, the tunneling-in jump operator of lead α becomes

$$\begin{aligned}[\mathcal{J}_\alpha^{\text{in}}(\xi)]_{ab,a'b'} = \frac{1}{2}\Big[&F_\alpha^<(E_a - E_{a'})e^{-i(E_a-E_{a'})\xi} + F_\alpha^<(E_b - E_{b'})e^{-i(E_b-E_{b'})\xi}\Big] \\ &\times \langle a|c_{\ell_\alpha}^\dagger|a'\rangle\langle b'|c_{\ell_\alpha}|b\rangle,\end{aligned} \tag{6.3}$$

as stated in chapter 3. The corresponding tunneling-out term $[\mathcal{J}_\alpha^{\text{out}}(\xi)]_{ab,a'b'}$ follows from the replacement $\{c_\ell, F^<(\epsilon)\} \to \{c_\ell^\dagger, F^>(-\epsilon)\}$, and $\mathcal{L}_{\mathbf{0},0}$ is given by Eq. (B.3), where the appearing jump operators are evaluated at zero counting fields. Notice the dependence on energy differences of the many-body states, $E_a - E_{a'}$. Only for non-interacting systems, this difference becomes a single-particle energy.

Since $\operatorname{tr}\rho_{\boldsymbol{\chi},\xi}$ is the moment generating function for the leads electron number, the current cumulant generating function reads $Z_{\text{BR}}(\boldsymbol{\chi},\xi) = \lim_{t\to\infty}\frac{\partial}{\partial t}\ln\operatorname{tr}\rho_{\boldsymbol{\chi},\xi}$. A generalized iteration scheme for the computation of its cumulants and corresponding transport coefficients is provided in chapter 3.

A rather important feature of the Bloch-Redfield master equation (6.2) is that in the absence of any bias voltage, i.e., for all $\mu_\alpha = \mu_0$, its stationary solution is the grand canonical state of the central system, $\rho_{\text{eq}} \propto \exp[-\beta(H_S - \mu_0 N)]$. While within the RWA discussed below, this is quite obvious, the proof for the full master equation is more involved and can be found in section 6.3. Moreover, our master equation is generally not of Lindblad form[179,180] so that it may violate the positivity of the reduced density operator. Studies of specific systems, however, indicate that generally this occurs only far from equilibrium and during short a transient stage at which the reduced dynamics is non-Markovian.[181] Therefore we do not expect any problem of this kind as long as we stay close to the thermal state ρ_{eq}. Let us also emphasize that there are cases such as a double quantum dot with small inter-dot

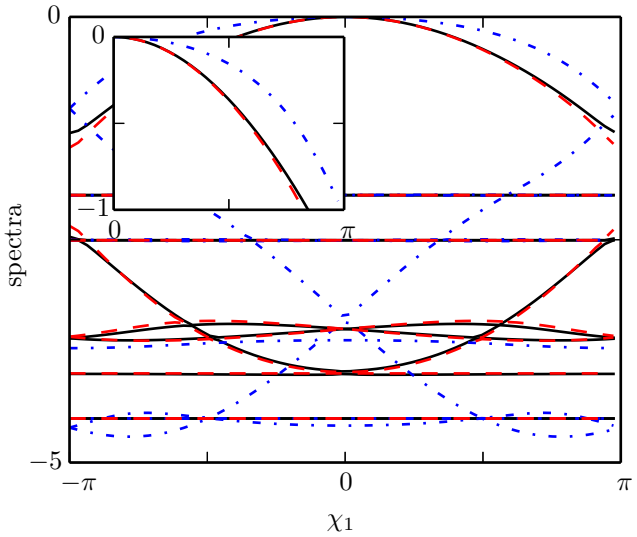

Fig. 6.2.: Real part of the eigenvalues of the Liouvillians $\mathcal{L}_{\boldsymbol{\chi},0}$ (solid lines), $\mathcal{L}_{-\boldsymbol{\chi}-i\beta\boldsymbol{\mu},i\beta}$ (dashed, hidden by solid lines), and $\mathcal{L}_{-\boldsymbol{\chi}-i\beta\boldsymbol{\mu},0}$ (dash-dotted) [see Eq. (6.2)] of the double quantum dot model as function of the counting variable χ_1 while all other $\chi_\alpha = 0$. The parameters are: inter-dot tunneling $\Omega = 0.75\Gamma$, temperature $k_BT = 0.1\Gamma$, onsite energies $\epsilon_1 = 2\,\epsilon_2 = \Gamma$, and chemical potentials $\mu_1 = -\mu_2 = -\mu_3 = -\mu_4 = 0.25\,\Gamma$. The inset shows an enlargement of the "zero" eigenvalues revealing the slight difference between $\mathcal{L}_{\boldsymbol{\chi},0}$ and $\mathcal{L}_{-\boldsymbol{\chi}-i\beta\boldsymbol{\mu},i\beta}$.

tunneling and vanishing interaction in which a RWA leads to significant deviations from the exact scattering solution while a treatment beyond RWA yields the exact stationary current.[182] Thus it is essential to keep the non-RWA terms.

A first glance of the results derived below, is provided by the spectra of $\mathcal{L}_{\boldsymbol{\chi},\xi}$, $\mathcal{L}_{-\boldsymbol{\chi}-i\beta\boldsymbol{\mu},-\xi+i\beta}$, and $\mathcal{L}_{-\boldsymbol{\chi}-i\beta\boldsymbol{\mu},\xi}$ at $\xi = 0$ given in Fig. 6.2. One notices that the former and the latter clearly disagree, which demonstrates that for Z_{BR}, it is not sufficient to consider only the number counting variable $\boldsymbol{\chi}$. Thus, Z_{BR} does not fulfill Eq. (6.1), i.e., the full Bloch-Redfield equation violates the exchange fluctuation theorem. When also the energy counting variable is substituted as $\xi \to -\xi + i\beta$, the difference between the spectra becomes significantly smaller, which indicates that the fluctuation theorem violation relates to the total lead energy.

6.2.1. RWA master equation for many-body states

If after an irrelevant transient stage, the density operator becomes practically diagonal in the energy basis, one may employ the RWA ansatz $\rho_{ab} = P_a\delta_{ab}$, where the populations P_a obey $\dot{P}_a = \sum_{a'} w_{a\leftarrow a'}P_{a'}$. The transition rates $w_{a\leftarrow a'}$ consist of the tunnel-in contributions for each lead,

$$w^{\alpha,\mathrm{in}}_{a\leftarrow a'}(\boldsymbol{\chi},\xi) = e^{-i\chi_\alpha}[\mathcal{J}^{\mathrm{in}}_\alpha(\xi)]_{aa,a'a'} = e^{-i\chi_\alpha}e^{-i(E_a-E_{a'})\xi}F^<_\alpha(E_a-E_{a'})|\langle a|c^\dagger_{\ell_\alpha}|a'\rangle|^2, \quad (6.4)$$

and the corresponding $w^{\alpha,\mathrm{out}}_{a\leftarrow a'}$. Adding both contributions and using the Kubo-Martin-Schwinger relation[95,124] $F^{<}_{\alpha}(\epsilon)e^{\beta(\epsilon-\mu_\alpha)} = F^{>}_{\alpha}(\epsilon)$, we find

$$w_{a'\leftarrow a}(\boldsymbol{\chi},\xi) = w_{a\leftarrow a'}(-\boldsymbol{\chi} - i\beta\boldsymbol{\mu}, -\xi + i\beta), \tag{6.5}$$

i.e., the substitution $\boldsymbol{\chi},\xi \to -\boldsymbol{\chi} - i\beta\boldsymbol{\mu}, -\xi + i\beta$ corresponds to the transposition of the RWA Liouvillian. Moreover, the ξ-dependence can be removed via the similarity transformation $w \to S^{-1}wS$ with $S_{a,a'} = \delta_{aa'}e^{iE_a\xi}$. Since both the transposition and the transformation with S leave the spectrum unchanged, we can draw two conclusions for the generating function being the lowest eigenvalue: First, Z_{RWA} is ξ-independent which implies that the lead energy is conserved in the long-time limit. Second, $Z_{\mathrm{RWA}}(\boldsymbol{\chi})$ fulfills Eq. (6.1).

The validity of the exchange fluctuation theorem relates to the local detailed balance condition[117,162,170,175] for the incoherent transitions between the states $|a\rangle$ and $|a'\rangle$ manifest in Eq. (6.5). Notice that the full Bloch-Redfield master equation contains coherent quantum oscillations and, thus, is beyond a description with transition rates.

6.2.2. RWA class of master equations

The above statement about the Bloch-Redfield master equation in RWA can be applied also to master equations that are seemingly not of that form. Moreover, the cases of vanishing Coulomb interaction and of infinitely strong repulsion emerge as single-particle limits of our statements. In that sense, we can identify a whole "RWA class" of master equations for which Eq. (6.1) holds.

A most relevant case is a master equation for capacitively coupled, but electrically isolated quantum dots, each modeled as single level. Owing to the lack of coherent tunneling, the Hamiltonian of this system is diagonal in the onsite basis, while no quantum coherence emerges. Thus, off-diagonal density matrix elements vanish exactly, so that the resulting master equation in a localized basis assumes the form of the RWA limit of the Bloch-Redfield equation. Recently, the validity of the exchange fluctuation theorem has been exemplified for various particular situations of this kind.[141,162,170,174,175] They represent special cases of our generic statement.

Moreover, there are limits in which our many-body master equation becomes in fact a single-particle particle equation. This is naturally the case for very strong inter-dot Coulomb repulsion, such that at most one electron can enter the system. Then only eigenstates with one electron play a role and the energy differences in the jump operator (6.3) become single particle energies. In the opposite limit of non-interacting electrons, the many-body states $|a\rangle$ are Slater determinants of single-particle states, while all E_a are sums of single-particle energies, a case that has been considered, e.g., in Ref. 115. Again only the single-particle energies appear in the decomposition of the jump operators. We emphasize that genuine many-body effects or correlation effects typically emerge for intermediate interaction and, thus, are beyond those limits.

6.3. Johnson-Nyquist relation and equilibrium solution

Even though the Bloch-Redfield master equation beyond RWA does not fulfill the fluctuation theorem exactly, the resulting conductance $G^{\rm eq}_{\alpha,\alpha} = -\partial I_\alpha/\partial\mu_\alpha|_{\boldsymbol{\mu}=\mathbf{0}}$ and the zero-frequency noise $S_{\alpha\alpha} = \partial^2 Z/\partial\chi_\alpha^2|_{\boldsymbol{\chi}=\boldsymbol{\xi}=\mathbf{0}}$ at equilibrium nevertheless obey the Johnson-Nyquist relation $2G^{\rm eq}_{\alpha,\alpha} = \beta S^{\rm eq}_{\alpha\alpha}$. For a proof, we perform the iteration described above up to second order which yields the expressions

$$S^{\rm eq}_{\alpha\alpha} = \langle \mathcal{W}^{2,0,0}_\alpha\rangle + 2\langle \mathcal{W}^{1,0,0}_\alpha \mathcal{R}_0 \mathcal{W}^{1,0,0}_\alpha\rangle, \tag{6.6}$$

$$G^{\rm eq}_{\alpha,\alpha} = -\langle \mathcal{W}^{1,0,1}_\alpha\rangle - \langle \mathcal{W}^{1,0,0}_\alpha \mathcal{R}_0 \mathcal{W}^{0,0,1}_\alpha\rangle - \langle \mathcal{W}^{0,0,1}_\alpha \mathcal{R}_0 \mathcal{W}^{1,0,0}_\alpha\rangle, \tag{6.7}$$

where the angular brackets denote the expectation value with respect to the equilibrium density operator $\rho_{\rm eq}$ and $\mathcal{R}_0$ defines the pseudoresolvent of the Liouvillian at zero frequency.

We proceed by showing that in Eq. (6.7), the first two terms obey the relations $2\langle \mathcal{W}^{1,0,1}_\alpha\rangle = -\beta\langle \mathcal{W}^{2,0,0}_\alpha\rangle$ and $\mathcal{W}^{0,0,1}_\alpha\rho_{\rm eq} = -\beta \mathcal{W}^{1,0,0}_\alpha\rho_{\rm eq}$, respectively, while the last term vanishes, $\mathrm{tr}\,\mathcal{W}^{0,0,1}_\alpha = 0$. The latter relation follows from the fact that the trace condition of the Liouvillian is independent of the lead chemical potential, so that the corresponding Taylor expansion vanishes to all orders.

The proof for the other two relations is more involved. It is based on the Kubo-Martin-Schwinger relation for the lead correlation functions,[95,124]

$$F^{>}_\alpha(t) = e^{-\beta\mu_\alpha}\, F^{<}_\alpha(t+i\beta). \tag{6.8}$$

and a related detailed balance relation for the interaction picture operators,

$$\tilde{c}_{\ell_\alpha}(t) e^{-\beta(H_S-\mu_0 N)} = e^{\beta\mu_0} e^{-\beta(H_S-\mu_0 N)} \tilde{c}_{\ell_\alpha}(t-i\beta). \tag{6.9}$$

The latter holds for fermionic annihilation operators in the interaction picture with respect to H_S, i.e., for any $\tilde{c}_{\ell_\alpha}(t) = e^{iH_S t} c_{\ell_\alpha} e^{-iH_S t}$ of the system, owing to the commutator relation $[N, c_{\ell_\alpha}] = -c_{\ell_\alpha}$. From this relation follow detailed balance relations for the jump operators,

$$D^{\rm in}_{\ell_\alpha}(t)\rho_{\rm eq} = e^{-\beta\mu_0} J^{\rm out}_{\ell_\alpha}(-t-i\beta)\rho_{\rm eq}, \tag{6.10}$$

$$D^{\rm out}_{\ell_\alpha}(t)\rho_{\rm eq} = e^{\beta\mu_0} J^{\rm in}_{\ell_\alpha}(-t-i\beta)\rho_{\rm eq}, \tag{6.11}$$

which we use to transform the superoperators appearing in $S^{\rm eq}_{\alpha\alpha}$.

We start with the tunnel-out contribution of the first term of Eq. (6.7),

$$\mathrm{tr}\,\mathcal{W}^{1,0,1}_{\alpha,\rm out}\rho_{\rm eq} = \mathrm{tr}\int dt\, \frac{\partial}{\partial\mu_\alpha} F^{>}_\alpha(t) J^{\rm out}_{\ell_\alpha}(t)\Big|_{\mu_\alpha=\mu_0}\rho_{\rm eq}, \tag{6.12}$$

insert Eqs. (6.8), (6.10), (6.11) and substitute the integration variable $t \to -t - i\beta$. Again we use that $\mathcal{W}^{0,0,1}_{\alpha,\rm out}$ is trace free and obtain

$$\langle \mathcal{W}^{1,0,1}_{\alpha,\rm out}\rangle = -\beta\langle \mathcal{W}^{2,0,0}_{\alpha,\rm in}\rangle - \langle \mathcal{W}^{1,0,1}_{\alpha,\rm in}\rangle. \tag{6.13}$$

This relation together with the corresponding expression for the tunnel-in term, $\langle \mathcal{W}^{1,0,1}_{\alpha,\mathrm{in}} \rangle = -\beta \langle \mathcal{W}^{2,0,0}_{\alpha,\mathrm{out}} \rangle - \langle \mathcal{W}^{1,0,1}_{\alpha,\mathrm{out}} \rangle$, yields $\langle \mathcal{W}^{1,0,1}_{\alpha} \rangle = -(\beta/2) \langle \mathcal{W}^{2,0,0}_{\alpha} \rangle$, which links the first term of Eq. (6.6) to the first term of Eq. (6.7).

Following the same path for the second term, we find

$$\mathcal{W}^{0,0,1}_{\alpha,\mathrm{out}} \rho_{\mathrm{eq}} = \int dt \, \frac{\partial}{\partial \mu_\alpha} F^{>}_{\alpha}(t) [J^{\mathrm{out}}_{\ell_\alpha}(t) - D^{\mathrm{out}}_{\ell_\alpha}(t)\Big|_{\mu_\alpha = \mu_0} \rho_{\mathrm{eq}} = \left[\mathcal{W}^{1,0,1}_{\alpha} - \beta \mathcal{W}^{1,0,0}_{\alpha,\mathrm{in}} \right] \rho_{\mathrm{eq}}, \quad (6.14)$$

as well as $\mathcal{W}^{0,0,1}_{\alpha,\mathrm{in}} \rho_{\mathrm{eq}} = (-\mathcal{W}^{1,0,1}_{\alpha} - \beta \mathcal{W}^{1,0,0}_{\alpha,\mathrm{out}}) \rho_{\mathrm{eq}}$. Thus, also the second terms in Eqs. (6.6) and (6.7) differ only by a factor $\beta/2$, which completes our proof that the conductivity and the zero-frequency noise computed with the full Bloch-Redfield master equation (6.2) obey the Johnson-Nyquist relation $S^{\mathrm{eq}}_{\alpha\alpha} = 2 k_B T G^{\mathrm{eq}}_{\alpha,\alpha}$.

Finally, let us remark that Eqs. (6.8), (6.10) and (6.11) can be used to demonstrate that the grand canonical state of the central system, $\rho_{\mathrm{eq}} \propto \exp[-\beta(H_S - \mu_0 N)]$, represents the equilibrium solution of the Bloch-Redfield master equation (6.2) both within RWA and beyond. Thus, $\mathcal{L} \rho_{\mathrm{eq}} = 0$ and $\mathcal{L}_{\mathrm{RWA}} \rho_{\mathrm{eq}} = 0$ provided that no bias voltages are applied so that all lead chemical potentials are equal. As further consequence, for both master equations the current vanishes at equilibrium as expected.

6.4. Exchange fluctuation theorem violation

6.4.1. Charge fluctuations

Having seen that the full Bloch-Redfield equation violates the fluctuation theorem, we turn to a quantitative analysis of the deviations. To this end, we introduce as measure the $(m+n)$th order Taylor coefficients of the difference between the terms appearing in Eq. (6.1),

$$R^{\alpha_1 \cdots \alpha_m}_{\beta_1 \cdots \beta_n} = \frac{(-i)^m \partial^{m+n}}{\partial \chi_{\alpha_1} \cdots \partial \mu_{\beta_n}} \left[Z_{\mathrm{BR}}(\boldsymbol{\chi}) - Z_{\mathrm{BR}}(-\boldsymbol{\chi} - i\beta \boldsymbol{\mu}) \right] \Big|_{\boldsymbol{\chi} = \boldsymbol{\mu} = \mathbf{0}}, \quad (6.15)$$

which are constructed such that they vanish if the exchange fluctuation theorem (6.1) is fulfilled. An alternate definition is discussed in Appendix E. Notice that Z_{BR} possesses also an implicit $\boldsymbol{\mu}$ dependence, so that generally the contribution of the first term does not vanish. Since, the r.h.s of Eq. (6.15) consists of derivatives of current cumulants evaluated at equilibrium $\boldsymbol{\mu} = \mathbf{0}$, the fact that $R^{\alpha_1 \cdots \alpha_m}_{\beta_1 \cdots \beta_n}$ must vanish provides a relation between transport coefficients.[93] For example, the mentioned Johnson-Nyquist relation is of second order and reads $R^{\alpha}_{\alpha} = 0 = \beta S^{\mathrm{eq}}_{\alpha\alpha} - 2 G^{\mathrm{eq}}_{\alpha,\alpha}$. This rather important relation represents an interesting special case of Eq. (6.15) because it is fulfilled also by the full Bloch-Redfield equation beyond RWA, as we prove in section 6.3.

Before entering numerical calculations, we like to conjecture the scaling behavior of the deviations (6.15) as function of (i) the incoherent tunnel rates Γ and (ii) the coherent tunnel coupling Ω. In each case, we depart from a limit in which the

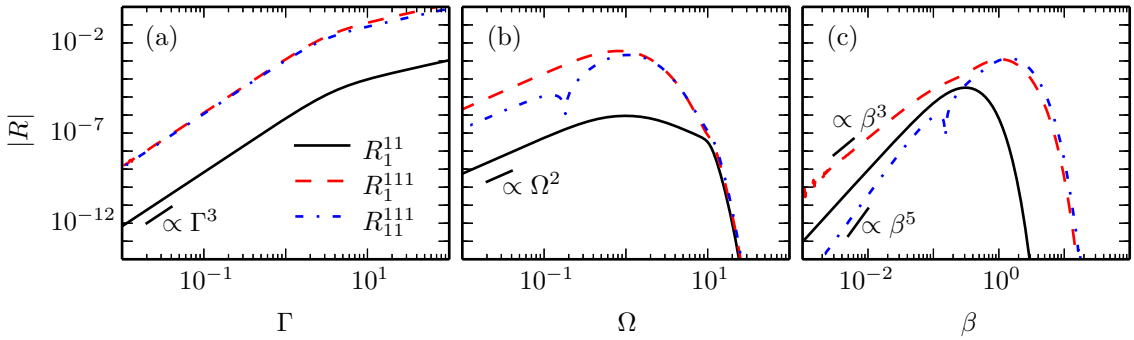

Fig. 6.3.: Violation of the exchange fluctuation theorem by the Redfield master equation beyond RWA for the double quantum dot sketched in Fig. 6.1(a) as function of (a) the dot-lead coupling Γ, (b) the inter-dot tunneling Ω, and (c) the inverse temperature $\beta = 1/k_B T$ for the parameters $\Gamma = 0.5\,\Omega = k_B T$ and $\epsilon_\alpha = \mu_\alpha = 0$. The scaling behavior verifies the conjecture (6.16) for the selected generalized Casimir-Onsager relations $R_1^{11} = 0$ (solid line), $R_1^{111} = 0$ (dashed), and $R_{11}^{111} = 0$ (dash-dotted).

fluctuation theorem (6.1) is fulfilled, so that all R indeed vanish. Concerning (i) we recall that the master equation (6.2) is based on a perturbation theory in the dot-lead coupling which cannot capture the Lorentzian broadening of the quantum dot resonance denominator $\propto (\epsilon^2 + \Gamma^2)^{-1}$. Thus, corrections to the exact equilibrium density matrix should be of the order Γ^2. Moreover, since all transport coefficients inherit a prefactor Γ from the jump operators [see Eq. (6.3)], we expect $R \propto \Gamma^3$. For case (ii) we notice that for $\Omega = 0$, no coherent tunneling is present and the full Bloch-Redfield falls into the RWA class identified above, so that the fluctuation theorem holds exactly. Since expectation values typically depend only on even powers of tunnel matrix elements, we anticipate deviations of order Ω^2. Assuming that the deviations from $R = 0$ depend on the smaller of both parameters, we can conjecture the generic behavior

$$R \propto \begin{cases} \Gamma^3 & \text{for } \Gamma \ll \Omega, \\ \Omega^2 & \text{for } \Omega \ll \Gamma. \end{cases} \tag{6.16}$$

For the verification of this hypothesis for systems such as the ones sketched in Fig. 6.1, we apply the generalized iteration scheme mentioned before. In this section we focus on the double quantum dot while the quadruple quantum dot is discussed in the following section. Figures 6.3(a) and 6.3(b) depict the scaling behavior of three different deviations as functions of Γ and Ω, which confirms the conjecture (6.16). In some particular cases, we found that R vanishes even faster with small Γ or Ω which means that Eq. (6.16) is a rather conservative estimate. For particular R's (e.g. for R_1^1 as discussed above) or particular systems, the scaling may even be more favorable. As an example, we present below results for the quadruple quantum dot.

As function of the temperature $k_B T = 1/\beta$, the deviations behave even more interestingly, because they vanish in both the high-temperature and the low-temperature limit [see Fig. 6.3(c)]. For the high-temperature limit $\beta \to 0$, this is expected since

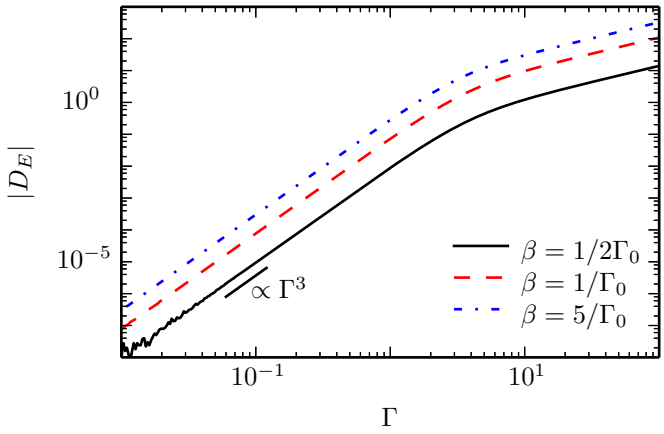

Fig. 6.4.: Fluctuations of the total lead energy manifest in the energy diffusion constant $D_E = \lim_{t\to\infty}\langle \Delta E^2_{\text{leads}}\rangle/t$ as function of the dot-lead tunnel rate Γ and various temperatures. The chemical potentials at the upper quantum dot are $\mu_1 = -\mu_2 = 3\,\Gamma_0$, while all other parameters are as in Fig. 6.3(a).

the substitution $\xi \to -\xi + i\beta$ by and large cures the fluctuation theorem violation, while being irrelevant for $\beta = 0$. Quantitatively we find the scaling $R \propto \beta^3$ or even higher powers. For the experimentally rather relevant low-temperature limit $\beta \to \infty$, we find that the deviations turn rather rapidly to zero, but do not follow a power law. Once $k_B T \lesssim \Gamma/10, \Omega/10$, all deviations from $R = 0$ are already many orders smaller than the individual terms of R.

6.4.2. Energy fluctuations

In the exact treatment, the total energy is conserved while the central system can only ingest a finite amount. Therefore, cumulants of the lead energy cannot grow indefinitely, so that the energy current cumulants must vanish.[93] For the RWA master equation, they vanish as well owing to the ξ-independence of the generating function, see discussion after Eq. (6.4). Beyond RWA this need not be the case, because the full Bloch-Redfield equation allows electrons to lose coherence while residing on the central system. Such coherence loss can cause transitions between states with different energy, e.g., between bonding and anti-bonding states. Therefore the variance of the total lead energy might grow diffusively, as is confirmed by the results shown in Fig. 6.4. The scaling with the dot-lead rate is $\propto \Gamma^3$, i.e., equal to that of the generic deviations from $R = 0$. For the usual dot-lead models, this seems to be a consequence of the approximations underlying the Bloch-Redfield equation.

6.5. Numerical results for a quadruple quantum dot

As a special system for which the deviations from the fluctuation theorem scale even more favorable as the behavior given by Eq. (6.15), we present numerical results for a quadruple quantum dot coupled to four leads, as is sketched in Fig. 6.1(b).

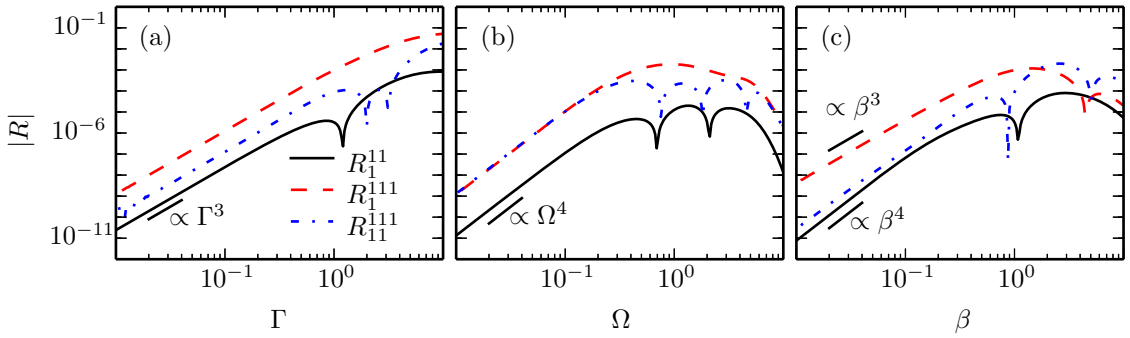

Fig. 6.5.: Deviation of the exchange fluctuation theorem for the quadruple quantum dot as function of (a) the dot-lead coupling Γ, (b) the inter-dot tunneling Ω, and (c) the inverse temperature $\beta = 1/k_B T$ for the parameters $\Gamma = 0.5\,\Omega = k_B T = 10\epsilon_1 = -10\epsilon_2$ and $\mu_\alpha = 0$. The selected generalized Casimir-Onsager relations are those of Fig. 6.3, i.e., $R_1^{11} = 0$ (solid line), $R_1^{111} = 0$ (dashed), and $R_{11}^{111} = 0$ (dash-dotted).

The deviation from $R = 0$ as function of the dot-lead coupling Γ and the inverse temperature $\beta = 1/k_B T$ [Figs. 6.5(a) and 6.5(c)] is the generic one, i.e., $R \propto \Gamma^3$, while R vanishes in the high-temperature limit $\propto \beta^3$ or faster. In the low-temperature limit $\beta \to \infty$, the deviations decay rapidly without following any power law. Also for the lead energy variance behaves generically, as can be appreciated in Fig. 6.6. The main difference to the generic behavior is found as function of the coherent inter-dot tunneling Ω: We observe a decay $R \propto \Omega^4$, i.e., faster than the generic $\propto \Omega^2$ discussed in the main text.

6.6. Main results

By studying exchange fluctuation theorems for quantum transport, we have identified a class of master equations for which these theorems hold exactly. Equations of this class are characterized by an equivalence to a RWA master equation for some many-body basis for which we proved the validity of the fluctuation theorem. The many-body aspect is rather crucial for the direct application to coupled quantum dots given that Coulomb interaction represents the largest energy scale in these systems. Interestingly, various previous studies[141,162,170,174] represent special cases of our more generic statements. Moreover we studied quantitatively the scaling behavior of the violation of the Bloch-Redfield master equation on two specific capacitively coupled quantum dots.

Despite that the RWA version of the Bloch-Redfield master equation obeys the fluctuation theorem (6.1) exactly and, thus, possesses a desirable formal property, it is not necessarily the preferential choice, because coherences may be of the same order as the populations so that neglecting coherences may lead to even qualitatively wrong predictions.[182] Going beyond RWA, we quantified the degree of fluctuation theorem violation of the full Bloch-Redfield master equation, in particular its scaling

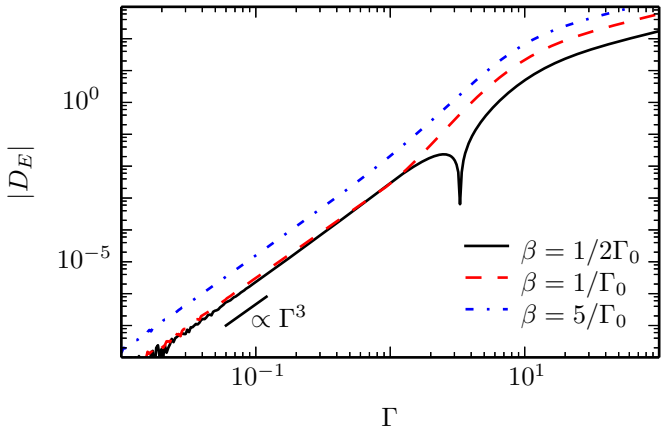

Fig. 6.6.: Diffusion constant $D_E = \lim_{t\to\infty}\langle\Delta E^2_{\text{leads}}\rangle/t$ of the total lead energy for the setup sketched in Fig. 6.1(b) as function of the dot-lead tunnel rate $\Gamma \equiv \Gamma_\alpha$ and various temperatures. The chemical potential of leads 1 and 2 read $\mu_1 = -\mu_2 = 3\,\Gamma_0$, while all other parameters are as in Fig. 6.5(a).

behavior as function of the coherent and the incoherent tunneling. Most important for the application of the Bloch-Redfield master equation to real experiments is the fact that at low temperatures, the discrepancies become rather tiny.

Moreover, we have shown that the Bloch-Redfield master equation fulfills two particular exchange fluctuation theorems exactly: It always predicts a vanishing equilibrium current and a zero-frequency noise that complies with the Johnson-Nyquist relation.

Even though our investigation already provides a general proof for the consistency of a whole class of master equations with exchange fluctuations theorems, two further generalizations seem desirable. On the one hand, one should consider also spin effects, which requires a refined treatment of time-reversal symmetry.[175] On the other hand, one may include quantum dissipation for which in the absence of electron reservoirs, similar conclusions about the compliance of master equations with fluctuation theorems can be drawn,[183] while for the combination of transport and dissipation the fluctuation theorem holds at least to some extent.[184]

7 Conclusions and outlook

We have studied quantum transport in different capacitively coupled quantum circuits. Therefore, we introduced the Bloch-Redfield formalism which has been generalized to some extent and illustrated the concepts of full-counting statistics on the double quantum dot model. Then, we turned to specific transport problems. In particular, we investigated the full-counting statistics of a coherent quantum ratchet formed by two coupled double quantum dots. Charge and current monitoring of a double quantum dot have been studied by employing a nearby quantum point contact as detector. Further, formal aspects of Markovian Bloch-Redfield master equations have been explored with regard to their compliance with exact exchange fluctuation relations. Numerical and analytical results have been illustrated for a double and quadruple quantum dot.

In chapter 4, we studied a driven quantum ratchet where the driving stemming from tunnel oscillations induces a dc current. It is mainly controlled by the detuning of the ratchet levels and exhibits current reversals about zero detuning. Far from this reversal point, its Fano factor (noise-to-current ratio) reflects a nearly Poissonian behavior while it diverges at the reversal point since its zero-frequency noise always remains finite. The enhancement of the Fano factor for small detuning is further associated to a bi-directional Poisson process expressing the competition between incoming and outgoing tunneling processes. The generic behavior of the Fano factor can be explained by our analytical model revealing that both the ratchet current and the corresponding noise are proportional to the correlation function of the drive circuit—the Fano factor, thus, is independent of the drive correlation function which cancels. Moreover, resonant driving has been investigated. It causes resonance peaks in the ratchet current but minimizes the Fano factor. This noise reduction leads for large detuning to sub-Poissonian statistics.

In chapter 5, we employed a quantum point contact as charge and current sensor for a strongly biased double quantum dot. Good measurement correlations between detector and DQD observables can be found for large frequency dependent Fano factor of the detector. However, for a Poissonian value the detector becomes insensitive. This condition relates to a limiting frequency beyond which measurement no longer is possible. Reliable charge measurement of a particular charge is assured if it couples at least twice as strong to the detector as an electron on the other dot. For unidirectional transport the time-dependent detector current, thus, can be reconstructed from time-resolved DQD populations. A main issue of such quantum measurement is its backaction on the measured system. In our case, the detector localizes the charges on the double quantum dot, and thus, reduces significantly the

DQD current. On the other hand, this fact enables a faithful description within a classical master equation approach possessing an effective incoherent tunneling, whenever the detector current correlates strongly with one of the DQD occupations.

Chapter 6 was devoted to study exchange fluctuations and to identify a class of master equations which obey these relations. Equations of this class are characterized by an equivalence to a RWA master equation in some basis. This covers the limits of the Bloch-Redfield master equation in which electrons experience strong Coulumb repulsion or, on the contrary, are non interacting. The full Bloch-Redfield master equation, however, generally does not fulfill the exact exchange fluctuation theorem but nevertheless satisfy the Johnson-Nyquist relation. Further, we found that for low temperatures, the fluctuation theorem violation of the full Bloch-Redfield master equation is of minor relevance.

On the formal side, we generalized the Bloch-Redfield master equation formalism to capture heat transport and to cover exchange fluctuation relations. In particular, we extended the common recursive scheme for calculating stationary current cumulants to provide transport coefficients also for finite voltage bias. Beside its numerical benefit, this generalization has been used in chapter 6 to analytically proof the validity of the Johnson-Nyquist relation within the Bloch-Redfield formalism. Additionally, it has been shown that Bloch-Redfield master equations of the form of Eq. (6.2) recover the correct thermalization of the density matrix whenever the chemical potentials of all arising leads are equal. In other words, their stationary solutions coincide in equilibrium with the grand canonical state of the corresponding central system.

Moreover, we derived frequency dependent current–current cross-correlations which are applicable to models in which electron transport may not be described in terms of usual non-diagonal jump operators. In chapter 5, we thus have been able to obtain current correlations involving a quantum point contact as detector. In the classical limit, the results have been affirmed by comparison with calculations relying on conditional probabilities. A further peculiarity of our derivation is that, in contrast to the MacDonald approach, it is not restricted to symmetrized cross-correlations.

Future directions may include spin effects and regard additional dissipative sources such as dissipation stemming from electron-phonon scattering that are known to be experimentally relevant at low temperatures. As possible continuation of ac effects induced by tunnel oscillations, one may study a heat pump or a quantum refrigerator. A quadruple quantum dot coupling to two unbiased leads at different temperatures may be a possible candidate. In Ref. 185, such a model has been exposed to ac driving to transfer heat from a cold to a hot reservoir. One may aim at employing tunnel oscillations stemming from a biased DQD as source of nonequilibrium fluctuations. The interplay of electron transport and heat transfer as well as the efficiency of the cooling mechanism would be of interest. Moreover, while several alternative charge detector schemes have been proposed, their formal properties have been studied barely. One may compare different detector schemes with respect to the loss of coherence and identify such schemes that are suitable for nondemolition measurements under certain conditions. The four terminal relations derived in Ref. 186 for an arbitrary coherent conductor in the limit of negligible phase loss may serve as figure of merit.

8 Conclusiones y perspectivas

Hemos estudiado transporte cuántico en diferentes circuitos de puntos cuánticos acoplados capacitivamente. Para ello, hemos introducido el formalismo de Bloch-Redfield generalizado y hemos expuesto los conceptos de *full-counting statistics* en el modelo de un doble punto cuántico (DPC). Luego, nos hemos centrado en problemas específicos de transporte. En concreto, hemos investigado el *full-counting statistics* de un trinquete cuántico coherente constituido por dos DPCs acoplados. La monitorización de carga de un DPC se ha estudiado empleando como detector un contacto de punto cuántico (CPC). Además, se han estudiado a que nivel los aspectos formales de las ecuaciones maestras Markovianas de Bloch-Redfield cumplen las relaciones exactas de fluctuación. Presentamos resultados numéricos y analíticos para un doble y un cuádruple punto cuántico.

En el capítulo 4, hemos estudiado un trinquete cuántico forzado donde el forzamiento es causado por las oscilaciones de túnel que inducen una corriente continua. Esto está controlado principalmente por el *detuning* de los niveles del trinquete manifestando inversión de la corriente para *detuning* cero. Lejos de este punto de inversión, su factor Fano (*noise-to-current ratio*) evidencia un comportamiento aproximadamente poissoniano. El factor Fano diverge en el punto de inversión debido a que el ruido a frecuencia cero siempre se mantiene finito. El incremento del factor Fano para un pequeño *detuning* está asociado a un proceso de Poisson bidireccional reflejando la competición entre un proceso túnel entrante y otro saliente. El comportamiento general del factor Fano se explica con nuestro modelo analítico revelando que tanto la corriente del trinquete como el correspondiente ruido son proporcionales a la función de correlación del circuito forzado—el factor Fano, por lo tanto, es independiente de la función de correlación forzada que se cancela. Por otra parte, se ha estudiado el forzamiento resonante, causando picos resonantes en la corriente del trinquete y minimizando el factor Fano. Esta reducción del ruido lleva a la estadística sub-poissoniana para *detunings* grandes.

En el capítulo 5, para un punto cuántico con un *bias* grande hemos empleado como sensor de corriente y de carga un CPC. Se pueden encontrar buenas medidas de correlación entre los detectores y los observables del DPC para el factor Fano del detector a frecuencias grandes. De todas formas, para un valor poissoniano el detector se vuelve insensible. Esta condición proporciona una frecuencia límite a partir de la cual ya no es posible medir. Se aseguran medidas fiables de una carga particular si el acoplamiento con el detector es por lo menos tan fuerte como dos veces el acoplamiento del electrón con el otro punto cuántico. Para transporte unidireccional la dependencia temporal del detector de corriente puede ser reconstruida con las

resoluciones temporales de las ocupaciones del DPC. El principal problema en la medición es el *backaction* sobre el sistema medido. En nuestro caso, el detector localiza la carga en el DPC, y por lo tanto reduce significativamente la corriente. Por otro lado, este hecho permite en la aproximación clásica una descripción precisa de la ecuación maestra dominada por un túnel efectivo incoherente, siempre que el detector de la corriente esté fuertemente correlacionado con una de las ocupaciones del DPC.

En el capítulo 6 se estudia el intercambio de fluctuaciones y la identificación de la clase de ecuación maestra que obedece estas relaciones. Las ecuaciones de esta clase se caracterizan por una equivalencia en la aproximación de onda rotante. Esto abarca los límites de la ecuación maestra de Bloch-Redfield en la cual los electrones experimentan una fuerte repulsión de Coulomb o por el contrario no son interactuantes. Generalmente la ecuación maestra completa de Bloch-Redfield no cumple el intercambio exacto del teorema de fluctuación, pero sin embargo satisface la relación de Johnson-Nyquist. Además hemos obtenido que para bajas temperaturas la violación del teorema de la fluctuación por la ecuación de Bloch-Redfield tiene una relevancia mínima.

En la parte formal, generalizamos el formalismo de la ecuación de Bloch-Redfield para conseguir transporte de calor y las relaciones de fluctuaciones de intercambio. En particular, ampliamos el esquema recursivo común para calcular cumulantes de corrientes estacionarias que proporcionan los coeficientes del transporte para *bias* finito. Además de los beneficios numéricos, esta generalización ha sido usada en el capítulo 6 para demostrar analíticamente la validez de la relación de Johnson-Nyquist en el formalismo de Bloch-Redfield. Adicionalmente, se ha mostrado que la ecuación maestra de Bloch-Redfield en la forma de Eq. (6.2) recupera la correcta termalización de la matriz densidad cuando el potencial químico de todos los contactos son iguales. En otras palabras, las soluciones estacionarias en equilibrio coinciden con el estado gran canónico del correspondiente sistema central.

Por otra parte, obtenemos la correlación cruzada corriente–corriente dependiente de la frecuencia que se aplica a modelos en los cuales el transporte electrónico no puede ser descrito en términos de los típicos operadores no diagonales de salto. En el capítulo 5 hemos sido capaces de obtener correlaciones de corriente donde se usaban CPCs como detectores. En el límite clásico, los resultados han sido avalados por comparación con los cálculos basados en probabilidades condicionales. Una peculiaridad adicional de nuestro desarrollo es que a diferencia de la aproximación de MacDonald, esta no está restringida a correlaciones cruzadas simetrizadas.

Las líneas de investigación a desarrollar en el futuro pueden incluir efectos de espín y considerar fuentes disipativas adicionales tales como disipación debido al *scattering* de electrones con fonones, que son consideradas experimentalmente relevantes a bajas temperaturas. Una posible continuación a los efectos tipo c.a. inducidos por las oscilaciones de túnel, puede ser el estudio de bombeo de calor o un refrigerador cuántico. Como candidato se podría proponer un punto cuádruple acoplado a dos contactos sin *bias* con diferentes temperaturas. En la referencia Ref. 185 se expone este modelo para transferir calor de un reservorio frio a otro caliente mediante forzamiento

con c.a. Uno podría emplear oscilaciones de túnel de un DPC con *bias* como una fuente de fluctuaciones fuera del equilibrio. La interacción del transporte electrónico y la corriente de calor así como la eficiencia del mecanismo de enfriamiento serían de gran interés. A pesar de que se han propuesto diferentes sistemas de detección de carga alternativos, sus propiedades formales no han sido prácticamente estudiadas. Sería posible comprobar respecto a la pérdida de coherencia diferentes sistemas de detección e identificar bajo ciertas condiciones aquellos que son apropiados para medidas no invasoras. Las correlaciones de cuatro terminales obtenidas en Ref. 186 para un conductor coherente arbitrario, en el límite de pérdida de fase despreciable, puede servir como *figure of merit*.

A Two-time correlation functions

In this section, we derive the frequency dependent current–current correlations, Eq. (3.10), from the defining expression (3.8). The main task is to apply the operator derivative, Eq. (3.9), on the propagator of the augmented density matrix to acquire the moments. It is instructive to first rederive in this scheme the corresponding cumulants at equal times which complements the iteration approach, Eq. (2.9) and Eq. (2.10). The emerging second order moment can be recycled when we finally regard distinct times. The derivation of the current–current correlations at distinct times follows the same approach and only differs in another moment generating function, (3.7).

A.1. Cumulants at equal times

The master equation (2.8) can either be regarded as eigenvalue problem or solved by propagation in time.[187] In the latter case the formal solution reads $\rho(\boldsymbol{\chi},t) = \Omega(\boldsymbol{\chi},t)\rho_{\mathrm{st}}$ which is initially assumed to be stationary. The moment generating function $M(\boldsymbol{\chi},t) = \operatorname{tr}\rho(\boldsymbol{\chi},t)$ follows by tracing out the system degrees of freedom and their Taylor coefficients are moments that relate via Eq. (2.4) to the current–current correlations,

$$\kappa_{\alpha\beta}(t) = \frac{\partial}{\partial t}\Big[m_{\alpha\beta}(t) - m_{\alpha}(t)m_{\beta}(t)\Big]. \tag{A.1}$$

To evaluate the moments, we consider $\rho_{\alpha}(t) = \partial\rho(\boldsymbol{\chi},t)/\partial i\chi_{\alpha}|_{\boldsymbol{\chi}=\mathbf{0}}$. Application of Eq. (3.9) on the propagator $\Omega(\boldsymbol{\chi},t) = e^{\mathcal{L}(\boldsymbol{\chi})t}$ yields

$$\rho_{\alpha}(t) = \int_0^1 ds\; e^{\mathcal{L}_{\mathbf{0}}t(1-s)}\mathcal{W}_{\alpha}\rho_{\mathrm{st}}|_{\boldsymbol{\chi}=\mathbf{0}}t. \tag{A.2}$$

Obviously, the first moments $m_{\alpha}(t) = \langle\mathcal{W}_{\alpha}\rangle t$ follow directly by taking the trace. In addition, the Taylor coefficient (A.2) can be computed by series expansion of the matrix exponential such that

$$\int_0^1 ds\; e^{\mathcal{L}_{\mathbf{0}}t(1-s)} = \int_0^1 ds\; e^{\mathcal{L}_{\mathbf{0}}ts} = \mathcal{P} + \mathcal{Q}\Big(\mathcal{L}_{\mathbf{0}}t\Big)^{-1}\mathcal{Q}\Big(e^{\mathcal{L}_{\mathbf{0}}t} - 1\Big)\mathcal{Q}, \tag{A.3}$$

where $\mathcal{P} = \mathbb{1} - \mathcal{Q}$ denotes the projector into the nullspace of $\mathcal{L}_{\mathbf{0}}$. This projector $\mathcal{P} = \mathcal{P}^2$ is orthogonal to $\mathcal{Q} = \mathcal{Q}^2$ such that their product $\mathcal{P}\mathcal{Q} = \mathcal{Q}\mathcal{P}$ vanishes. Inserting this expression in Eq. (A.2) yields

$$\rho_{\alpha}(t) = \mathcal{P}\mathcal{W}_{\alpha}\rho_{\mathrm{st}}t - \mathcal{R}_0\Big(e^{\mathcal{L}_{\mathbf{0}}t} - 1\Big)\mathcal{Q}\mathcal{W}_{\alpha}\rho_{\mathrm{st}}, \tag{A.4}$$

where $\mathcal{R}_0 = \mathcal{Q}(0 - \mathcal{L}_\mathbf{0})^{-1}\mathcal{Q}$ refers to the pseudoresolvent. The second order moment similarly reduces to

$$m_{\alpha\beta}(t) = \langle \mathcal{W}_{\alpha\beta}\rangle t + \langle \mathcal{W}_\alpha \Big(\int_0^1 \int_0^1 ds\, ds'\, e^{\mathcal{L}_\mathbf{0} tss'} t^2 s \Big) \mathcal{W}_\beta \rangle + \langle \mathcal{W}_\beta \Big(\int_0^1 \int_0^1 ds\, ds'\, e^{\mathcal{L}_\mathbf{0} tss'} t^2 s \Big) \mathcal{W}_\alpha \rangle, \tag{A.5}$$

after deriving the propagator with respect to $i\chi_\alpha$ and $i\chi_\beta$, taking the trace, and variable substitution $s \to 1 - s$ and $s' \to 1 - s'$, respectively. Applying Eq. (A.3) on the integral over s' yields

$$\int_0^1 \int_0^1 ds\, ds'\, e^{\mathcal{L}_\mathbf{0} tss'} t^2 s = \frac{1}{2}\mathcal{P}t^2 - \mathcal{R}_0 \Big(\int_0^1 ds e^{\mathcal{L}_\mathbf{0} ts} - 1 \Big) \mathcal{Q}t, \tag{A.6}$$

which eventually leads to

$$m_{\alpha\beta}(t) = m_\alpha(t) m_\beta(t) - \mathrm{tr}\left[\mathcal{W}_\alpha \mathcal{R}_0 \rho_\beta(t)\right] - \mathrm{tr}\left[\mathcal{W}_\beta \mathcal{R}_0 \rho_\alpha(t)\right] + \langle \mathcal{W}_{\alpha\beta}\rangle t + \langle \mathcal{W}_\alpha \mathcal{R}_0 \mathcal{W}_\beta \rangle t + \langle \mathcal{W}_\beta \mathcal{R}_0 \mathcal{W}_\alpha \rangle t. \tag{A.7}$$

By inserting this expression into Eq. (A.1), the term $m_\alpha(t) m_\beta(t) = \langle \mathcal{W}_\alpha \mathcal{P} \mathcal{W}_\beta \rangle t^2 = \mathrm{tr}\left[\mathcal{W}_\alpha \mathcal{P} \rho_\beta(t)\right] t$ cancels out the counter term. Then taking the time derivative yields the current–current correlation

$$\kappa_{\alpha\beta}(t) = \langle \mathcal{W}_{\alpha\beta}\rangle + \mathrm{tr}\left[\mathcal{W}_\alpha \mathcal{Q} \rho_\beta(t)\right] + \mathrm{tr}\left[\mathcal{W}_\beta \mathcal{Q} \rho_\alpha(t)\right], \tag{A.8}$$

by regarding that $\dot{\rho}_\alpha(t) = \mathcal{L}_\mathbf{0}\rho_\alpha(t) + \mathcal{W}_\alpha \rho_\mathrm{st}$ and $\mathcal{R}_0 \mathcal{L}_\mathbf{0} = -\mathcal{Q}$. The stationary limit may be obtained by exploiting the final value theorem, $\lim_{t\to\infty} \kappa_{\alpha\beta}(t) = \lim_{z\to 0} z\kappa_{\alpha\beta}(z)$, where the Laplace transform of the former differential equation yields the central expression $z\mathcal{Q}\rho_\alpha(z) = \mathcal{R}(z)\mathcal{W}_\alpha \rho_\mathrm{st}$.

A.2. Cumulants at different times

The treatment of the current–current correlation at distinct times follows the derivation above but is based on the time-local cumulant generating function Eq. (3.7). Again, we exploit Eq. (3.9) to find the first order moments

$$m_\alpha(t, t') = \langle \mathcal{W}_\alpha \rangle t, \quad m_\beta(t, t') = \langle \mathcal{W}_\beta \rangle t', \tag{A.9}$$

where the former is obtained by derivation with respect to $i\chi_\alpha$ while the latter is derived with respect to $i\chi'_\beta$. Their product simply yields $m_\alpha(t, t') m_\beta(t, t') = \langle \mathcal{W}_\alpha \rangle \langle \mathcal{W}_\beta \rangle t t'$. The second order moment is of the form $m_{\alpha\beta}(t, t') \equiv \Theta_{t,t'} m^{>}_{\alpha\beta}(t, t') + \Theta_{t',t} m^{<}_{\alpha\beta}(t, t')$ while the Heaviside functions $\Theta_{t,t'} = \Theta(t - t')$ and $\Theta_{t',t}$ stem from the two contributions of the time ordering. The former part yields

$$m^{>}_{\alpha\beta}(t, t') = \langle \mathcal{W}_\alpha \mathcal{R}_0 \Big(e^{\mathcal{L}_\mathbf{0}(t-t')} - 1 \Big) \mathcal{R}_0 \Big(e^{\mathcal{L}_\mathbf{0} t'} - 1 \Big) \mathcal{Q} \mathcal{W}_\beta \rangle + \langle \mathcal{W}_\alpha \rangle \langle \mathcal{W}_\beta \rangle (t - t') t' + m_{\alpha\beta}(t'), \tag{A.10}$$

after applying Eq. (3.9) twice. The latter part satisfies $m^{<}_{\alpha\beta}(t,t') = m^{>}_{\beta\alpha}(t',t)$ which allow us to deduce that the lesser and greater second order moments reduce at equal times to $m^{<}_{\alpha\beta}(t,t) = m^{>}_{\alpha\beta}(t,t) = m_{\alpha\beta}(t)$. This condition enables us to cancel two terms in the next step in which we evaluate the time derivatives in Eq. (3.8) while holding the moments unevaluated. By applying the identity $1 = \Theta_{t,t'} + \Theta_{t',t}$ on the product $m_\alpha(t,t')m_\beta(t,t')$, one finds

$$\begin{aligned}\kappa_{\alpha\beta}(t,t') = &+ \Theta_{tt'}\partial_t\partial_{t'}\Big[m^{>}_{\alpha\beta}(t,t') - m_\alpha(t,t')m_\beta(t,t')\Big] + \delta_{t,t'}\partial_{t'}\Big[m^{>}_{\alpha\beta}(t,t') - m^{<}_{\alpha\beta}(t,t')\Big] \\ &+ \Theta_{t't}\partial_t\partial_{t'}\Big[m^{<}_{\alpha\beta}(t,t') - m_\alpha(t,t')m_\beta(t,t')\Big]. \end{aligned} \tag{A.11}$$

Application of Eq. (A.10) and Eq. (A.7) yields finally

$$\kappa_{\alpha\beta}(t,t') = \delta_{t,t'}\langle\mathcal{W}_{\alpha\beta}\rangle + \Theta_{tt'}\langle\mathcal{W}_\alpha\mathcal{Q}e^{\mathcal{L}_\mathbf{0}(t-t')}\mathcal{Q}\mathcal{W}_\beta\rangle + \Theta_{t't}\langle\mathcal{W}_\beta\mathcal{Q}e^{\mathcal{L}_\mathbf{0}(t'-t)}\mathcal{Q}\mathcal{W}_\alpha\rangle, \tag{A.12}$$

which only depends on the time difference.

B Eigendecomposition of the master equation

For the evaluation of the time integral in Eq. (2.18), it is convenient to work in the eigenbasis of the system Hamiltonian which is defined by $H_S|a\rangle = E_a|a\rangle$. Thus, the time dependent system operators in $J^{\text{out}}_{\ell_\alpha}(t)$ transform as, for instance,

$$\int dt\; F^{>}_{\alpha}(t)\tilde{c}^{\dagger}_{\ell_\alpha}(t) = \sum_{ab} |a\rangle\langle b| F^{>}_{\alpha}(E_a - E_b)\langle a|c^{\dagger}_{\ell_\alpha}|b\rangle, \tag{B.1}$$

where $\tilde{c}^{\dagger}_{\ell_\alpha}(t) = e^{iH_S t}c^{\dagger}_{\ell_\alpha}e^{-iH_S t}$. The energy arguments in the greater correlation indicate its Fourier representation. This eigendecomposition allows us to write the master equation in the energy basis, $\dot{\rho}_{ab} = \sum_{a'b'}[\mathcal{L}(\boldsymbol{\chi})]_{ab,a'b'}\;\rho_{a'b'}$, such that the Liouvillian

$$[\mathcal{L}(\boldsymbol{\chi})]_{ab,a'b'} = [\mathcal{L}_0]_{ab,a'b'} + \sum_{\alpha}(e^{-i\chi_\alpha}-1)[\mathcal{J}^{\text{in}}_{\alpha}]_{ab,a'b'} + \sum_{\alpha}(e^{i\chi_\alpha}-1)[\mathcal{J}^{\text{out}}_{\alpha}]_{ab,a'b'} \tag{B.2}$$

can be expressed as[81]

$$\begin{aligned}
[\mathcal{L}_0]_{ab,a'b'} = &-i\delta_{a'a}\delta_{b'b}(E_a - E_b) + \sum_{\alpha}[\mathcal{J}^{\text{in}}_{\alpha}]_{ab,a'b'} + \sum_{\alpha}[\mathcal{J}^{\text{out}}_{\alpha}]_{ab,a'b'} \\
&- \frac{1}{2}\delta_{b'b}\sum_{\alpha,c} F^{<}_{\alpha}(E_c - E_{a'})\langle a|c_{\ell_\alpha}|c\rangle\langle c|c^{\dagger}_{\ell_\alpha}|a'\rangle \\
&- \frac{1}{2}\delta_{a'a}\sum_{\alpha,c} F^{<}_{\alpha}(E_c - E_{b'})\langle b'|c_{\ell_\alpha}|c\rangle\langle c|c^{\dagger}_{\ell_\alpha}|b\rangle \\
&- \frac{1}{2}\delta_{b'b}\sum_{\alpha,c} F^{>}_{\alpha}(E_{a'} - E_c)\langle a|c^{\dagger}_{\ell_\alpha}|c\rangle\langle c|c_{\ell_\alpha}|a'\rangle \\
&- \frac{1}{2}\delta_{a'a}\sum_{\alpha,c} F^{>}_{\alpha}(E_{b'} - E_c)\langle b'|c^{\dagger}_{\ell_\alpha}|c\rangle\langle c|c_{\ell_\alpha}|b\rangle,
\end{aligned} \tag{B.3}$$

with the matrix elements of jump operators

$$[\mathcal{J}^{\text{in}}_{\alpha}]_{ab,a'b'} = \frac{1}{2}\Big[F^{<}_{\alpha}(E_a - E_{a'}) + F^{<}_{\alpha}(E_b - E_{b'})\Big]\langle a|c^{\dagger}_{\ell_\alpha}|a'\rangle\langle b'|c_{\ell_\alpha}|b\rangle, \tag{B.4}$$

$$[\mathcal{J}^{\text{out}}_{\alpha}]_{ab,a'b'} = \frac{1}{2}\Big[F^{>}_{\alpha}(E_{a'} - E_a) + F^{>}_{\alpha}(E_{b'} - E_b)\Big]\langle a|c_{\ell_\alpha}|a'\rangle\langle b'|c^{\dagger}_{\ell_\alpha}|b\rangle, \tag{B.5}$$

where δ_{ab} is the Kronecker delta function.

The matrix elements of the fermionic operators in the eigenbasis may be evaluated by expressing them in terms of N-particle states that are defined by the prescription

$$|k_N, \ldots, k_2, k_1\rangle = \left(c^{\dagger}_N\right)^{k_N} \ldots \left(c^{\dagger}_2\right)^{k_2}\left(c^{\dagger}_1\right)^{k_1}|0\rangle, \tag{B.6}$$

where $|0\rangle$ denotes the vacuum state and the k_ℓ are either zero or one. This prescription corresponds to the Jordan-Wigner transform[188,189] of the annihilation operators that for $\ell = 1, \ldots, N$ reads

$$c_\ell = \left(\bigotimes_{k=1}^{N-\ell} \sigma_z \right) \otimes \sigma_+ \otimes \left(\bigotimes_{k=1}^{\ell-1} \mathbb{1}_{2\times 2} \right), \tag{B.7}$$

where $\sigma_+ = \frac{1}{2}(\sigma_x + i\sigma_y)$, and σ_x, σ_y, σ_z are Pauli matrices. In particular, we obtain for the double quantum dot the matrix representations

$$c_1 = \begin{pmatrix} 0 & 1 & 0 & 0 \\ 0 & 0 & 0 & 0 \\ 0 & 0 & 0 & -1 \\ 0 & 0 & 0 & 0 \end{pmatrix}, \quad c_2 = \begin{pmatrix} 0 & 0 & 1 & 0 \\ 0 & 0 & 0 & 1 \\ 0 & 0 & 0 & 0 \\ 0 & 0 & 0 & 0 \end{pmatrix}. \tag{B.8}$$

C Contributions of the effective quantum ratchet

The effective ratchet Liouvillian in Sec. 4.2 can be constructed from the ratchet and the drive Liouvillian, therein. While the eigenbasis of the ratchet Liouvillian determines its vector structure, the drive Liouvillian is needed to express occurring fluctuations of the environment. Both Liouvillians are special cases of the full double quantum dot model which is introduced in chapter 2 and is described in Appendix B. They are both of Lindblad form and correspond to the zero bias and infinite bias limit, respectively. Hereby, the eigenrepresentation of the ratchet Liouvillian is defective and requires generalized eigenvectors to be treated correctly.

First we address the spectral decomposition of the ratchet Liouvillian. Then we consider the drive circuit and provide the correlation function of the occupation imbalance.

C.1. Spectral decomposition of the ratchet Liouvillian

The ratchet Liouvillian reads in the energy basis $\{|0\rangle\langle 0|, |e\rangle\langle e|, |g\rangle\langle g|, |g\rangle\langle e|, |e\rangle\langle g|\}$ and in absence of the counting variable $\chi_2 \to 0$, Eq. (4.9),

$$\mathcal{L}_{\mathrm{ra}} = \begin{pmatrix} -\Gamma_{\mathrm{ra}} & \Gamma_{\mathrm{ra}} & 0 & 0 & 0 \\ 0 & -\Gamma_{\mathrm{ra}} & 0 & 0 & 0 \\ \Gamma_{\mathrm{ra}} & 0 & 0 & 0 & 0 \\ 0 & 0 & 0 & -\frac{\Gamma_{\mathrm{ra}}}{2} + i\delta & 0 \\ 0 & 0 & 0 & 0 & -\frac{\Gamma_{\mathrm{ra}}}{2} - i\delta \end{pmatrix}. \tag{C.1}$$

Within the perturbative treatment of Sec. 4.2, we need to compute functions $f(\mathcal{L}_{\mathrm{ra}})$ of this matrix involving the propagator $\exp(\mathcal{L}_{\mathrm{ra}}t)$ or the resolvent $(z - \mathcal{L}_{\mathrm{ra}})^{-1}$, which is usually achieved by spectral decomposition of the Liouvillian. Here however this is hindered by the fact that $\mathcal{L}_{\mathrm{ra}}$ is defective, i.e., it does not possess a complete set of eigenvectors. The problem arises from the upper block

$$L \equiv \begin{pmatrix} -\Gamma_{\mathrm{ra}} & \Gamma_{\mathrm{ra}} & 0 \\ 0 & -\Gamma_{\mathrm{ra}} & 0 \\ \Gamma_{\mathrm{ra}} & 0 & 0 \end{pmatrix}, \tag{C.2}$$

which we transform via

$$S = \begin{pmatrix} 0 & -1 & 0 \\ 0 & 0 & -1/\Gamma_{\mathrm{ra}} \\ 1 & 1 & 1/\Gamma_{\mathrm{ra}} \end{pmatrix}, \tag{C.3}$$

to the Jordan canonical form[148,190]

$$J = S^{-1}LS = \begin{pmatrix} 0 & 0 & 0 \\ 0 & -\Gamma_{\mathrm{ra}} & 1 \\ 0 & 0 & -\Gamma_{\mathrm{ra}} \end{pmatrix}. \tag{C.4}$$

Its eigenvalues obviously are 0 and the twofold degenerate $-\Gamma_{\mathrm{ra}}$, and one immediately finds two vectors that obey the eigenvalue equation, namely $L|0\rangle = 0|0\rangle$, $L|1\rangle = -\Gamma_{\mathrm{ra}}|1\rangle$. A generalized eigenbasis can be found by including a third vector $|2\rangle$ that fulfills[148,190] $L|2\rangle = -\Gamma_{\mathrm{ra}}|2\rangle + |1\rangle$, i.e., one adds the eigenvector of the degenerate subspace. By repeated multiplication with L follows $L^k|2\rangle = (-\Gamma_{\mathrm{ra}})^k|2\rangle + k(-\Gamma_{\mathrm{ra}})^{k-1}|1\rangle$, which implies

$$f(L)|2\rangle = f(\lambda_2)|2\rangle + f'(\lambda_2)|1\rangle, \tag{C.5}$$

where both the function of a matrix and its derivative are defined as the corresponding Taylor series. This relation together with the usual $f(L)|k\rangle = f(\lambda_k)|k\rangle$ for $k = 0, 1$, allows us to evaluate any $f(L)$. In particular, we find the propagator

$$e^{Lt} = \begin{pmatrix} e^{-\Gamma_{\mathrm{ra}}t} & \Gamma_{\mathrm{ra}}te^{-\Gamma_{\mathrm{ra}}t} & 0 \\ 0 & e^{-\Gamma_{\mathrm{ra}}t} & 0 \\ 1 - e^{-\Gamma_{\mathrm{ra}}t} & 1 - (1 + \Gamma_{\mathrm{ra}}t)e^{-\Gamma_{\mathrm{ra}}t} & 1 \end{pmatrix}, \tag{C.6}$$

and the resolvent

$$(z - L)^{-1} = \begin{pmatrix} \frac{1}{z+\Gamma_{\mathrm{ra}}} & \frac{\Gamma_{\mathrm{ra}}}{(z+\Gamma_{\mathrm{ra}})^2} & 0 \\ 0 & \frac{1}{z+\Gamma_{\mathrm{ra}}} & 0 \\ \frac{\Gamma_{\mathrm{ra}}}{z(z+\Gamma_{\mathrm{ra}})} & \frac{\Gamma_{\mathrm{ra}}^2}{z(z+\Gamma_{\mathrm{ra}})^2} & \frac{1}{z} \end{pmatrix}. \tag{C.7}$$

One also may apply this rule directly on the correlation function of the occupation imbalance $C(z - \mathcal{L}_{ra})$ as done in Eq. (4.13).

A poor man's approach to this procedure[148] is to introduce a small perturbation that lifts the degeneracy of L. After evaluating $f(L)$, one considers the limit of vanishing perturbation.

C.2. Stationary state of the drive circuit

The effective ratchet Liouvillian derived in Sec. 4.2 contains correlations stemming from the drive circuit. To determine this correlations, we notice that the Liouvillian of the drive, $\mathcal{L}_{\mathrm{dr}}$, is described by the master equation (2.20) in the high bias limit, where $H_{S,\mathrm{dr}} = -T_{\mathrm{dr}}\left(c_3^\dagger c_4 + c_4^\dagger c_3\right)$ is the system Hamiltonian of the drive. Solving $\mathcal{L}_{\mathrm{dr}}\rho_{\mathrm{dr}} = \mathbf{0}$ yields for the Fock basis the stationary state

$$\rho_{\mathrm{dr}}^{\mathrm{stat}} = \frac{1}{\Gamma_{\mathrm{dr}}^2 + 12|T_{\mathrm{dr}}|^2} \begin{pmatrix} 4|T_{\mathrm{dr}}|^2 & 0 & 0 \\ 0 & \Gamma_{\mathrm{dr}}^2 + 4|T_{\mathrm{dr}}|^2 & -2i\Gamma_{\mathrm{dr}}T_{\mathrm{dr}}^* \\ 0 & 2i\Gamma_{\mathrm{dr}}T_{\mathrm{dr}} & 4|T_{\mathrm{dr}}|^2 \end{pmatrix}. \tag{C.8}$$

Therewith, the auto correlation function of the population imbalance $\Delta N_{\rm dr} = N_4 - N_3$ can be obtained which in Laplace space is defined as

$$\begin{aligned} C(z) &= \int_0^\infty dt\; e^{-zt}\Big[\langle \Delta\tilde{N}_{\rm dr}(t)\Delta N_{\rm dr}\rangle - \langle \Delta N_{\rm dr}\rangle^2\Big] \\ &= \langle \Delta\tilde{N}_{\rm dr}(z)\Delta N_{\rm dr}\rangle - \frac{1}{z}\langle \Delta N_{\rm dr}\rangle^2. \end{aligned} \tag{C.9}$$

The stationary occupation is given by $\langle \Delta N_{\rm dr}\rangle = -\Gamma_{\rm dr}^2/(\Gamma_{\rm dr}^2 + 12|T_{\rm dr}|^2)$, and the corresponding correlation function reads

$$\langle \Delta\tilde{N}_{\rm dr}(z)\Delta N_{\rm dr}\rangle = \frac{1}{z}\frac{2z+\Gamma_{\rm dr}}{\Gamma_{\rm dr}^2 + 12|T_{\rm dr}|^2}\frac{\Gamma_{\rm dr}^2(z+\Gamma_{\rm dr})^2 + 4z(2z+3\Gamma_{\rm dr})|T_{\rm dr}|^2}{(z+\Gamma_{\rm dr})^2(2z+\Gamma_{\rm dr}) + 4(2z+3\Gamma_{\rm dr})|T_{\rm dr}|^2}. \tag{C.10}$$

D Computation of frequency dependent correlation functions

Frequency dependent correlation functions are usually obtained from Bayes' theorem.[127,153] They may either be expressed in terms of conditional probabilities or may be directly computed from frequency dependent counting statistics, see Sec. 2.2. Here, we provide the correlation functions for the double quantum dot model in the classical limit, see Sec. 5.2, which are required to compute Eqs. (5.2) and (5.8) according the former scheme. This work was done in collaboration with Jorge Gómez-García.[156]

In order to obtain the correlation of the detector current with the DQD currents, we use Eq. (5.8) to write the detector current in terms of the DQD occupations and obtain $\langle N_1(t) I_R(t')\rangle$, as well as similar expressions with other combination of the indices 1, 2 and L, R. Following Refs. 127,153 we define the differential $dN_R(t) = I_R(t)dt$ which describes the change of the charge state in the right dot by a current flow to the leads. Then we express the probabilities of all trajectories that contribute to $\langle N_1(t) I_R(t')\rangle dt = \langle N_1(t) dN_R(t')\rangle$ by the conditional probability (5.7).

For $t' < t$, the only contribution to the mentioned term stems from a trajectory starting at time t' with an electron on the right dot which leaves during the infinitesimal time dt to the right lead, such that the DQD will be in state 0. At a later time t, the left dot must be occupied. For the opposite time ordering, the DQD starts at time t' in state 1, propagates to state 2 at time t, while subsequently an electron leaves to the right dot during dt. The joint probability for these events reads

$$\langle dN_R(t) N_1(t')\rangle = \begin{cases} P(0, t+dt|2,t) P(2,t|1,t') P_1^{\mathrm{st}}, & t > t' \\ P(1,t'|0,t) P(0,t+dt|2,t) P_2^{\mathrm{st}}, & t < t' \end{cases}. \tag{D.1}$$

The auto-correlation function of the DQD current at the right barrier requires an initial occupation of state 2 at t', tunneling to the right lead during dt, propagation from 0 to 2 during $t - t'$, and finally electron tunneling to the right lead. This happens with probability

$$\langle dN_R(t) dN_R(t')\rangle = P(0,t+dt|2,t) P(2,t|0,t') P(0,t'+dt|2,t') P_2^{\mathrm{st}}, \tag{D.2}$$

valid for $t' < t$ while the opposite time ordering again follows by relabeling. At equal times, we have to add the shot noise contribution to obtain $C_{I_R I_R}(t-t') = \langle dN_R(t) dN_R(t')\rangle/dt^2 + \langle I_R\rangle \delta(t-t')$. A derivation of the shot noise in the spirit of the present calculation can be found in Ref. 127.

The correlation functions for all other possible combinations of the indices L and R can be obtained in the same way. As discussed above, correlations between DQD occupations and DQD current from lead $\alpha = L, R$ can be expressed by the differential

$dN_\alpha = I_\alpha dt$ and joint probabilities. For the currents through the left and the right contact, we thus obtain

$$\langle I_L\rangle dt = \langle dN_L(t)\rangle = P(1,t+dt|0,t)P_0^{\mathrm{st}}, \tag{D.3}$$
$$\langle I_R\rangle dt = \langle dN_R(t)\rangle = P(0,t+dt|2,t)P_2^{\mathrm{st}}, \tag{D.4}$$

where we find in consistency with charge conservation $\langle I_L\rangle = \langle I_R\rangle$. The two-time correlations follow from the conditional probability (5.7) and Bayes' theorem which yields

$$\langle N_1(t)dN_L(t')\rangle = \begin{cases} P(1,t'+dt|0,t')P(0,t'|1,t)P_1^{\mathrm{st}}, & t<t' \\ P(1,t|1,t'+dt)P(1,t'+dt|0,t')P_0^{\mathrm{st}}, & t>t' \end{cases}, \tag{D.5}$$

$$\langle N_2(t)dN_L(t')\rangle = \begin{cases} P(1,t'+dt|0,t')P(0,t'|2,t)P_2^{\mathrm{st}}, & t<t' \\ P(2,t|1,t'+dt)P(1,t'+dt|0,t')P_0^{\mathrm{st}}, & t>t' \end{cases}, \tag{D.6}$$

$$\langle N_2(t)dN_R(t')\rangle = \begin{cases} P(0,t'+dt|2,t')P(2,t'|2,t)P_2^{\mathrm{st}}, & t<t' \\ P(2,t|0,t'+dt)P(0,t'+dt|2,t')P_2^{\mathrm{st}}, & t>t' \end{cases}. \tag{D.7}$$

Subtracting $\langle N_\ell\rangle\langle dN_{\ell'}\rangle$ and dividing by dt yields the desired occupation-current correlations.

Accordingly, the correlation function of the left DQD current can be expressed in terms of

$$\langle dN_L(t)dN_L(t')\rangle = P(1,t+dt|0,t)P(0,t|1,t'+dt)P(1,t'+dt|0,t')P_0^{\mathrm{st}}. \tag{D.8}$$

Notice that this expression provides the auto-correlation function $C_{I_LI_L}(t-t')$ only for $t \neq t'$, while for equal times, the shot noise contribution $\langle I_L\rangle\delta(t-t')$ must be added.[127]

E Exchange fluctuation theorem and generalized Onsager relations

The scaling of the fluctuation theorem violations is quantified in chapter 6by the Taylor coefficients $R^{\alpha_1\cdots\alpha_m}_{\beta_1\cdots\beta_n}$, see Eq. (6.15). They vanish when the fluctuation theorem is fulfilled stated by the symmetry relation in Eq. (2.12). This definition contains coefficients which are linearly dependent or even zero when the cumulants cancel out. In the following, we list a minimal set of these relations. To this end, we take advantage of the fact that only cumulants of the same order in the derivatives occur. This can be seen from

$$R^{\boldsymbol{m}}_{\boldsymbol{n}} = \kappa^{\boldsymbol{m},\boldsymbol{n}} - (-1)^{|\boldsymbol{m}|}\sum_{\boldsymbol{k}=\boldsymbol{0}}^{\boldsymbol{n}}\binom{\boldsymbol{n}}{\boldsymbol{k}}\beta^{|\boldsymbol{k}|}\kappa^{\boldsymbol{m}+\boldsymbol{k},\boldsymbol{n}-\boldsymbol{k}}, \tag{E.1}$$

by using an equivalent definition of the Taylor coefficients,

$$R^{\boldsymbol{m}}_{\boldsymbol{n}} = \frac{\partial^{\boldsymbol{m}+\boldsymbol{n}}}{(\partial i\boldsymbol{\chi})^{\boldsymbol{m}}(\partial\boldsymbol{\mu})^{\boldsymbol{n}}}\Big[Z(\boldsymbol{\chi}) - Z(-\boldsymbol{\chi} - i\beta\boldsymbol{\mu})\Big]\Big|_{\boldsymbol{\chi}=\boldsymbol{\mu}=\boldsymbol{0}}, \tag{E.2}$$

suitable for the multi-index notation.

The idea is to regard all possible Taylor coefficients, Eq. (E.1), to an order, $|\boldsymbol{m}|+|\boldsymbol{n}|$, and express them as linear equations in the occurring cumulants $\kappa^{\boldsymbol{m}+\boldsymbol{k},\boldsymbol{n}-\boldsymbol{k}}$. The resulting linear system of equations then can be reduced by Gaussian elimination to obtain a set of linearly independent equations.[191] The results for the two-terminal case are listed in table E.1.

Order	Transport coefficients, $R^{\boldsymbol{m}}_{\boldsymbol{n}}$	Remarks
1	$\kappa^{10,00}$	(a)
	$\kappa^{01,00}$	(a)
2	$2\kappa^{10,10} - \beta\kappa^{20,00}$	(b)
	$2\kappa^{10,01} - \beta\kappa^{11,00}$	(c)
	$2\kappa^{01,10} - \beta\kappa^{11,00}$	(c)
	$2\kappa^{01,01} - \beta\kappa^{02,00}$	(b)
3	$\kappa^{30,00}$	
	$\kappa^{21,00}$	
	$\kappa^{12,00}$	
	$\kappa^{10,20} - \beta\kappa^{20,10}$	
	$2\kappa^{10,11} - \beta\kappa^{11,10} - \beta\kappa^{20,01}$	

continuation ...

	... continuation
	$\kappa^{10,02} - \beta\kappa^{11,01}$
	$\kappa^{03,00}$
	$\kappa^{01,20} - \beta\kappa^{11,10}$
	$2\kappa^{01,11} - \beta\kappa^{02,10} - \beta\kappa^{11,01}$
	$\kappa^{01,02} - \beta\kappa^{02,01}$
4	$2\kappa^{30,10} - \beta\kappa^{40,00}$
	$2\kappa^{30,01} - \beta\kappa^{31,00}$
	$2\kappa^{21,10} - \beta\kappa^{31,00}$
	$2\kappa^{21,01} - \beta\kappa^{22,00}$
	$2\kappa^{12,10} - \beta\kappa^{22,00}$
	$2\kappa^{12,01} - \beta\kappa^{13,00}$
	$4\kappa^{10,30} - 6\beta\kappa^{20,20} + \beta^3\kappa^{40,00}$
	$4\kappa^{10,21} - 2\beta\kappa^{11,20} - 4\beta\kappa^{20,11} + \beta^3\kappa^{31,00}$
	$4\kappa^{10,12} - 4\beta\kappa^{11,11} - 2\beta\kappa^{20,02} + \beta^3\kappa^{22,00}$
	$4\kappa^{10,03} - 6\beta\kappa^{11,02} + \beta^3\kappa^{13,00}$
	$2\kappa^{03,10} - \beta\kappa^{13,00}$
	$2\kappa^{03,01} - \beta\kappa^{04,00}$
	$4\kappa^{01,30} - 6\beta\kappa^{11,20} + \beta^3\kappa^{31,00}$
	$4\kappa^{01,21} - 2\beta\kappa^{02,20} - 4\beta\kappa^{11,11} + \beta^3\kappa^{22,00}$
	$4\kappa^{01,12} - 4\beta\kappa^{02,11} - 2\beta\kappa^{11,02} + \beta^3\kappa^{13,00}$
	$4\kappa^{01,03} - 6\beta\kappa^{02,02} + \beta^3\kappa^{04,00}$

Table E.1.: Minimal set of the transport coefficients, $R^{\boldsymbol{m}}_{\boldsymbol{n}}$, defining the fluctuation relations, $R^{\boldsymbol{m}}_{\boldsymbol{n}} = 0$, up to fourth order. (a) Current vanishes at equilibrium. (b) Johnson-Nyquist relation, $2G^{\mathrm{eq}}_{\alpha,\alpha} = \beta S^{\mathrm{eq}}_{\alpha\alpha}$, where $\beta = 1/k_B T$. (c) Johnson-Nyquist relation for cross terms, $2G^{\mathrm{eq}}_{\alpha,\beta} = \beta S^{\mathrm{eq}}_{\alpha\beta}$, also referred to as Onsager relation.

These cumulants are defined as

$$\kappa^{m_1 m_2, n_1 n_2} = \frac{\partial^{m_1+m_2+n_1+n_2}}{(\partial i\chi_1)^{m_1}(\partial i\chi_2)^{m_2}(\partial\mu_1)^{n_1}(\partial\mu_2)^{n_2}} Z(\boldsymbol{\chi})\Big|_{\boldsymbol{\chi}=\boldsymbol{\mu}=\mathbf{0}}, \tag{E.3}$$

similar to Eqs. (2.5) and (3.2).

References

[1] G. Moore, Proc. IEEE **86**, 82 (1998).

[2] D. J. Frank, R. H. Dennard, E. Nowak, P. M. Solomon, Y. Taur, and H.-S. P. Wong, Proc. IEEE **89**, 259 (2001).

[3] H. Grabert, Z. Phys. B **85**, 319 (1991).

[4] Y. Blanter and M. Büttiker, Phys. Rep. **336**, 1 (2000).

[5] W. G. van der Wiel, S. De Franceschi, J. M. Elzerman, T. Fujisawa, S. Tarucha, and L. P. Kouwenhoven, Rev. Mod. Phys. **75**, 1 (2002).

[6] M. Ciorga, A. S. Sachrajda, P. Hawrylak, C. Gould, P. Zawadzki, S. Jullian, Y. Feng, and Z. Wasilewski, Phys. Rev. B **61**, R16315 (2000).

[7] V. S. Khrapai, S. Ludwig, J. P. Kotthaus, H. P. Tranitz, and W. Wegscheider, Phys. Rev. Lett. **97**, 176803 (2006).

[8] K. D. Petersson, C. G. Smith, D. Anderson, P. Atkinson, G. A. C. Jones, and D. A. Ritchie, Phys. Rev. Lett. **103**, 016805 (2009).

[9] C. W. J. Beenakker and H. van Houten, in *Semiconductor Heterostructures and Nanostructures*, Solid State Physics, Vol. 44, edited by H. Ehrenreich and D. Turnbull (Academic Press, 1991) pp. 1 – 228.

[10] Y. Alhassid, Rev. Mod. Phys. **72**, 895 (2000).

[11] M. A. Reed, J. N. Randall, R. J. Aggarwal, R. J. Matyi, T. M. Moore, and A. E. Wetsel, Phys. Rev. Lett. **60**, 535 (1988).

[12] R. C. Ashoori, H. L. Stormer, J. S. Weiner, L. N. Pfeiffer, K. W. Baldwin, and K. W. West, Phys. Rev. Lett. **71**, 613 (1993).

[13] S. Tarucha, D. G. Austing, T. Fujisawa, and L. P. Kouwenhoven, in *Optical and Electronic Process of Nano-Matters*, Advances in Optoelectronics (ADOP), Vol. 8, edited by M. Ohtsu (Springer Netherlands, 2001) pp. 57–93.

[14] L. P. Kouwenhoven, D. G. Austing, and S. Tarucha, Rep. Prog. Phys. **64**, 701 (2001).

[15] G. Schedelbeck, W. Wegscheider, M. Bichler, and G. Abstreiter, Science **278**, 1792 (1997).

[16] T. H. Oosterkamp, T. Fujisawa, W. G. van der Wiel, K. Ishibashi, R. V. Hijman, S. Tarucha, and L. P. Kouwenhoven, Nature **395**, 873 (1998).

[17] L. Gaudreau, S. A. Studenikin, A. S. Sachrajda, P. Zawadzki, A. Kam, J. Lapointe, M. Korkusinski, and P. Hawrylak, Phys. Rev. Lett. **97**, 036807 (2006).

[18] D. Schröer, A. D. Greentree, L. Gaudreau, K. Eberl, L. C. L. Hollenberg, J. P. Kotthaus, and S. Ludwig, Phys. Rev. B **76**, 075306 (2007).

[19] D. Taubert, M. Pioro-Ladrière, D. Schröer, D. Harbusch, A. S. Sachrajda, and S. Ludwig, Phys. Rev. Lett. **100**, 176805 (2008).

[20] G. Granger, L. Gaudreau, A. Kam, M. Pioro-Ladrière, S. A. Studenikin, Z. R. Wasilewski, P. Zawadzki, and A. S. Sachrajda, Phys. Rev. B **82**, 075304 (2010).

[21] S. Gustavsson, M. Studer, R. Leturcq, T. Ihn, K. Ensslin, D. C. Driscoll, and A. C. Gossard, Phys. Rev. Lett. **99**, 206804 (2007).

[22] M. C. Rogge and R. J. Haug, Phys. Rev. B **77**, 193306 (2008).

[23] G. Platero, L. Brey, and C. Tejedor, Phys. Rev. B **40**, 8548 (1989).

[24] L. E. F. Foa Torres, C. H. Lewenkopf, and H. M. Pastawski, Phys. Rev. Lett. **91**, 116801 (2003).

[25] D. Taubert, D. Schuh, W. Wegscheider, and S. Ludwig, Rev. Sci. Instrum. **82**, 123905 (2011).

[26] W. van der Wiel, T. Fujisawa, T. Oosterkamp, and L. Kouwenhoven, Phys. B: Cond. Mat. **272**, 31 (1999).

[27] N. C. van der Vaart, S. F. Godijn, Y. V. Nazarov, C. J. P. M. Harmans, J. E. Mooij, L. W. Molenkamp, and C. T. Foxon, Phys. Rev. Lett. **74**, 4702 (1995).

[28] G. Shinkai, T. Hayashi, T. Ota, and T. Fujisawa, Phys. Rev. Lett. **103**, 056802 (2009).

[29] J. Stehlik, Y. Dovzhenko, J. R. Petta, J. R. Johansson, F. Nori, H. Lu, and A. C. Gossard, Phys. Rev. B **86**, 121303(R) (2012).

[30] J. R. Petta, A. C. Johnson, J. M. Taylor, E. A. Laird, A. Yacoby, M. D. Lukin, C. M. Marcus, M. P. Hanson, and A. C. Gossard, Science **309**, 2180 (2005).

[31] H. Bluhm, S. Foletti, I. Neder, M. Rudner, D. Mahalu, V. Umansky, and A. Yacoby, Nat Phys **7**, 109 (2011).

[32] Y. Nakamura, Y. A. Pashkin, and J. S. Tsai, Nature **398**, 786 (1999).

[33] J. Koch, T. M. Yu, J. Gambetta, A. A. Houck, D. I. Schuster, J. Majer, A. Blais, M. H. Devoret, S. M. Girvin, and R. J. Schoelkopf, Phys. Rev. A **76**, 042319 (2007).

[34] J. A. Schreier, A. A. Houck, J. Koch, D. I. Schuster, B. R. Johnson, J. M. Chow, J. M. Gambetta, J. Majer, L. Frunzio, M. H. Devoret, S. M. Girvin, and R. J. Schoelkopf, Phys. Rev. B **77**, 180502 (2008).

[35] H. Paik, D. I. Schuster, L. S. Bishop, G. Kirchmair, G. Catelani, A. P. Sears, B. R. Johnson, M. J. Reagor, L. Frunzio, L. I. Glazman, S. M. Girvin, M. H. Devoret, and R. J. Schoelkopf, Phys. Rev. Lett. **107**, 240501 (2011).

[36] J. Martinis, Quantum Inf. Process. **8**, 81 (2009).

[37] D. Loss and D. P. DiVincenzo, Phys. Rev. A **57**, 120 (1998).

[38] I. Žutić, J. Fabian, and S. Das Sarma, Rev. Mod. Phys. **76**, 323 (2004).

[39] R. Hanson, L. P. Kouwenhoven, J. R. Petta, S. Tarucha, and L. M. K. Vandersypen, Rev. Mod. Phys. **79**, 1217 (2007).

[40] T. D. Ladd, F. Jelezko, R. Laflamme, Y. Nakamura, C. Monroe, and J. L. O'Brien, Nature **464**, 45 (2010).

[41] L. Buluta, S. Ashhab, and F. Nori, Rep. Prog. Phys. **74**, 104401 (2011).

[42] B. Schumacher, Phys. Rev. A **51**, 2738 (1995).

[43] D. P. Divincenzo, in *Mesoscopic Electron Transport*, NATO ASI Series, Vol. 345, edited by L. L. Sohn, L. P. Kouwenhoven, and G. Schön (Springer Netherlands, 1997) pp. 657–677.

[44] S. Stenholm, J. Mod. Opt. **47**, 311 (2000).

[45] A. N. Jordan, B. Trauzettel, and G. Burkard, Phys. Rev. B **76**, 155324 (2007).

[46] N. Katz, M. Neeley, M. Ansmann, R. C. Bialczak, M. Hofheinz, E. Lucero, A. O'Connell, H. Wang, A. N. Cleland, J. M. Martinis, and A. N. Korotkov, Phys. Rev. Lett. **101**, 200401 (2008).

[47] A. P. Lund, New J. Phys. **13**, 053024 (2011).

[48] S. Wu, Sci. Rep. **3**, 1193 (2013).

[49] D. Das and Arvind, Phys. Rev. A **89**, 062121 (2014).

[50] H. M. Wiseman and G. J. Milburn, Phys. Rev. Lett. **70**, 548 (1993).

[51] A. N. Korotkov, Phys. Rev. B **60**, 5737 (1999).

[52] A. A. Clerk, M. H. Devoret, S. M. Girvin, F. Marquardt, and R. J. Schoelkopf, Rev. Mod. Phys. **82**, 1155 (2010).

[53] J. Preskill, Proc. R. Soc. Lond. **454**, 385 (1998).

[54] A. M. Childs, E. Farhi, and J. Preskill, Phys. Rev. A **65**, 012322 (2001).

[55] J. P. Pekola, O.-P. Saira, V. F. Maisi, A. Kemppinen, M. Möttönen, Y. A. Pashkin, and D. V. Averin, Rev. Mod. Phys. **85**, 1421 (2013).

[56] T. Gilad and S. A. Gurvitz, Phys. Rev. Lett. **97**, 116806 (2006).

[57] H. J. Jiao, X.-Q. Li, and J. Y. Luo, Phys. Rev. B **75**, 155333 (2007).

[58] S. Ashhab, J. Q. You, and F. Nori, Phys. Scr. **T137**, 014005 (2009).

[59] C. Kreisbeck, F. J. Kaiser, and S. Kohler, Phys. Rev. B **81**, 125404 (2010).

[60] E. L. Hahn, Phys. Rev. **80**, 580 (1950).

[61] F. H. L. Koppens, K. C. Nowack, and L. M. K. Vandersypen, Phys. Rev. Lett. **100**, 236802 (2008).

[62] Z.-Z. Li, C.-H. Lam, T. Yu, and J. Q. You, Sci. Rep. **3**, (2013).

[63] **Robert Hussein**, J. Gómez-García, and S. Kohler, Phys. Rev. B **90**, 155424 (2014).

[64] B. J. van Wees, H. van Houten, C. W. J. Beenakker, J. G. Williamson, L. P. Kouwenhoven, D. van der Marel, and C. T. Foxon, Phys. Rev. Lett. **60**, 848 (1988).

[65] D. A. Wharam, T. J. Thornton, R. Newbury, M. Pepper, H. Ahmed, J. E. F. Frost, D. G. Hasko, D. C. Peacock, D. A. Ritchie, and G. A. C. Jones, J. Phys. C: Solid State Phys. **21**, L209 (1988).

[66] D. Tobben, D. A. Wharam, G. Abstreiter, J. P. Kolthaus, and F. Schaffler, Semicond. Sci. Technol. **10**, 711 (1995).

[67] H. van Houten and C. Beenakker, Phys. Today **49**, 7 (1996).

[68] M. Field, C. G. Smith, M. Pepper, D. A. Ritchie, J. E. F. Frost, G. A. C. Jones, and D. G. Hasko, Phys. Rev. Lett. **70**, 1311 (1993).

[69] S. Gustavsson, R. Leturcq, B. Simovič, R. Schleser, T. Ihn, P. Studerus, K. Ensslin, D. C. Driscoll, and A. C. Gossard, Phys. Rev. Lett. **96**, 076605 (2006).

[70] T. Fujisawa, T. Hayashi, R. Tomita, and Y. Hirayama, Science **312**, 1634 (2006).

[71] C. Fricke, F. Hohls, W. Wegscheider, and R. J. Haug, Phys. Rev. B **76**, 155307 (2007).

[72] T. Ihn, S. Gustavsson, U. Gasser, B. Küng, T. Müller, R. Schleser, M. Sigrist, I. Shorubalko, R. Leturcq, and K. Ensslin, Solid State Commun. **149**, 1419 (2009), fundamental Phenomena and Applications of Quantum Dots.

[73] J. Güttinger, J. Seif, C. Stampfer, A. Capelli, K. Ensslin, and T. Ihn, Phys. Rev. B **83**, 165445 (2011).

[74] B. J. van Wees, L. P. Kouwenhoven, E. M. M. Willems, C. J. P. M. Harmans, J. E. Mooij, H. van Houten, C. W. J. Beenakker, J. G. Williamson, and C. T. Foxon, Phys. Rev. B **43**, 12431 (1991).

[75] L. S. Levitov, H. W. Lee, and G. B. Lesovik, J. Math. Phys. **37**, 4845 (1996).

[76] C. Flindt, T. Novotný, A. Braggio, M. Sassetti, and A.-P. Jauho, Phys. Rev. Lett. **100**, 150601 (2008).

[77] N. G. Van Kampen, *Stochastic Processes in Physics and Chemistry*, 3rd ed. (Elsevier, 2007).

[78] A. G. Redfield, IBM J. Res. Develop. **1**, 19 (1957).

[79] H. J. Carmichael, *Statistical Methods in Quantum Optics 1* (Springer–Verlag, 2002).

[80] M. Stark and S. Kohler, Europhys. Lett. **91**, 20007 (2010).

[81] **Robert Hussein** and S. Kohler, Phys. Rev. B **86**, 115452 (2012).

[82] R. Aguado and L. P. Kouwenhoven, Phys. Rev. Lett. **84**, 1986 (2000).

[83] E. Onac, F. Balestro, L. H. W. van Beveren, U. Hartmann, Y. V. Nazarov, and L. P. Kouwenhoven, Phys. Rev. Lett. **96**, 176601 (2006).

[84] **Robert Hussein** and S. Kohler, Phys. Rev. B **89**, 205424 (2014).

[85] G. B. Lesovik and L. S. Levitov, Phys. Rev. Lett. **72**, 538 (1994).

[86] D. A. Bagrets and Yu. V. Nazarov, Phys. Rev. B **67**, 085316 (2003).

[87] A. O. Gogolin and A. Komnik, Phys. Rev. B **73**, 195301 (2006).

[88] D. K. C. MacDonald, Rep. Prog. Phys. **12**, 56 (1949).

[89] C. Flindt, T. Novotný, A. Braggio, and A.-P. Jauho, Phys. Rev. B **82**, 155407 (2010).

[90] J. Tobiska and Y. V. Nazarov, Phys. Rev. B **72**, 235328 (2005).

[91] D. Andrieux and P. Gaspard, J. Stat. Mech. **2006**, P01011 (2006).

[92] K. Saito and A. Dhar, Phys. Rev. Lett. **99**, 180601 (2007).

[93] K. Saito and Y. Utsumi, Phys. Rev. B **78**, 115429 (2008).

[94] S. Nakamura, Y. Yamauchi, M. Hashisaka, K. Chida, K. Kobayashi, T. Ono, R. Leturcq, K. Ensslin, K. Saito, Y. Utsumi, and A. C. Gossard, Phys. Rev. Lett. **104**, 080602 (2010).

[95] R. Kubo, J. Phys. Soc. Jpn. **12**, 570 (1957).

[96] M.-T. Tran, Z. Phys. B **95**, 515 (1994).

[97] E. Lukacs, Amer. Math. Monthly **62**, pp. 340 (1955).

[98] W. P. Johnson, Amer. Math. Monthly **109**, 217 (2002).

[99] C. Emary, C. Pöltl, A. Carmele, J. Kabuss, A. Knorr, and T. Brandes, Phys. Rev. B **85**, 165417 (2012).

[100] R. Landauer, Nature **392**, 658 (1998).

[101] C. Beenakker and C. Schönenberger, Phys. Today **56**, 37 (2003).

[102] M. V. Berry, Proc. R. Soc. A **461**, 1735 (2005).

[103] C. Flindt, C. Fricke, F. Hohls, T. Novotný, K. Netočný, T. Brandes, and R. J. Haug, Proc. Natl. Acad. Sci. USA **106**, 10116 (2009).

[104] K. Blum, *Density Matrix Theory and Applications*, 2nd ed. (Springer, New York, 1996).

[105] H.-P. Breuer and F. Petruccione, *Theory of open quantum systems* (Oxford University Press, Oxford, 2003).

[106] P. Zedler, C. Emary, T. Brandes, and T. Novotný, Phys. Rev. B **84**, 233303 (2011).

[107] G. Schaller, G. Kießlich, and T. Brandes, Phys. Rev. B **80**, 245107 (2009).

[108] F. J. Kaiser and S. Kohler, Ann. Phys. (Leipzig) **16**, 702 (2007).

[109] J. J. Sakurai, *Modern Quantum Mechanics*, 2nd ed. (Addison-Wesley, Reading, 1995).

[110] L. Mandel and E. Wolf, *Optical Coherence and Quantum Optics* (Cambridge University Press, 2008).

[111] D. Kambly, C. Flindt, and M. Büttiker, Phys. Rev. B **83**, 075432 (2011).

[112] R. Sánchez and M. Büttiker, Europhys. Lett. **100**, 47008 (2012).

[113] R. Sánchez and M. Büttiker, Europhys. Lett. **104**, 49901 (2013).

[114] F. Haupt, M. Leijnse, H. L. Calvo, L. Classen, J. Splettstoesser, and M. R. Wegewijs, Phys. Status Solidi B **250**, 2315 (2013).

[115] M. Esposito, U. Harbola, and S. Mukamel, Rev. Mod. Phys. **81**, 1665 (2009).

[116] M. Campisi, P. Hänggi, and P. Talkner, Rev. Mod. Phys. **83**, 771 (2011).

[117] Y. Utsumi, D. S. Golubev, M. Marthaler, K. Saito, T. Fujisawa, and G. Schön, Phys. Rev. B **81**, 125331 (2010).

[118] O.-P. Saira, Y. Yoon, T. Tanttu, M. Möttönen, D. V. Averin, and J. P. Pekola, Phys. Rev. Lett. **109**, 180601 (2012).

[119] T. H. Stoof and Y. V. Nazarov, Phys. Rev. B **53**, 1050 (1996).

[120] S. A. Gurvitz and Y. S. Prager, Phys. Rev. B **53**, 15932 (1996).

[121] B. Elattari and S. Gurvitz, Phys. Lett. A **292**, 289 (2002).

[122] G. Kießlich, P. Samuelsson, A. Wacker, and E. Schöll, Phys. Rev. B **73**, 033312 (2006).

[123] C. Emary, Phys. Rev. A **78**, 032105 (2008).

[124] P. C. Martin and J. Schwinger, Phys. Rev. **115**, 1342 (1959).

[125] T. Brandes, Phys. Rep. **408**, 315 (2005).

[126] D. F. Walls and G. J. Milburn, eds., *Quantum Optics* (Springer Berlin Heidelberg, 2008).

[127] A. N. Korotkov, Phys. Rev. B **49**, 10381 (1994).

[128] C. Flindt, T. Novotný, and A.-P. Jauho, Phys. E **29**, 411 (2005).

[129] C. Emary, D. Marcos, R. Aguado, and T. Brandes, Phys. Rev. B **76**, 161404 (2007).

[130] D. Marcos, C. Emary, T. Brandes, and R. Aguado, New J. Phys. **12**, 123009 (2010).

[131] I. M. Gradshteyn and I. S. Ryzhik, *Table of Integrals, Series, and Products*, 5th ed. (Academic Press, San Diego, 1994).

[132] W. H. Press, S. A. Teukolsky, W. T. Vetterling, and B. P. Flannery, *Numerical recipes: the art of scientific computing*, 3rd ed. (Cambridge University Press, 2007).

[133] Y. V. Nazarov and M. Kindermann, Eur. Phys. J. B **35**, 413 (2003).

[134] W. Belzig, "CFN lectures on functional nanostructures vol. 1," (Springer Berlin Heidelberg, 2005) Chap. Full Counting Statistics in Quantum Contacts, pp. 123–143.

[135] H. Haug and A.-P. Jauho, *Quantum Kinetics in Transport and Optics of Semiconductors* (Springer Berlin Heidelberg, 2008).

[136] **Robert Hussein**, A. Metelmann, P. Zedler, and T. Brandes, Phys. Rev. B **82**, 165406 (2010).

[137] S. Bachmann, G. Graf, and G. Lesovik, J. Stat. Phys. **138**, 333 (2010).

[138] R. M. Wilcox, J. Math. Phys. **8**, 962 (1967).

[139] T. Brandes, Ann. Phys. **17**, 477 (2008).

[140] N. A. Mortensen, K. Flensberg, and A.-P. Jauho, Phys. Rev. Lett. **86**, 1841 (2001).

[141] R. Sánchez, R. López, D. Sánchez, and M. Büttiker, Phys. Rev. Lett. **104**, 076801 (2010).

[142] M. Gattobigio, G. Iannaccone, and M. Macucci, Phys. Rev. B **65**, 115337 (2002).

[143] P. Barthold, F. Hohls, N. Maire, K. Pierz, and R. J. Haug, Phys. Rev. Lett. **96**, 246804 (2006).

[144] R. Sánchez, S. Kohler, P. Hänggi, and G. Platero, Phys. Rev. B **77**, 035409 (2008).

[145] G. Granger, D. Taubert, C. E. Young, L. Gaudreau, A. Kam, S. A. Studenikin, P. Zawadzki, D. Harbusch, D. Schuh, W.Wegscheider, Z. R.Wasilewski, A. A. Clerk, S. Ludwig, and A. S. Sachrajda, Nature Phys. **8**, 522 (2012).

[146] C. Nietner, G. Schaller, C. Pöltl, and T. Brandes, Phys. Rev. B **85**, 245431 (2012).

[147] H. J. Carmichael, *Statistical Methods in Quantum Optics 2* (Springer–Verlag, 2008).

[148] C. Moler and C. V. Loan, SIAM Rev. **20**, 801 (1978).

[149] M. Strass, P. Hänggi, and S. Kohler, Phys. Rev. Lett. **95**, 130601 (2005).

[150] L. S. Levitov and M. Reznikov, Phys. Rev. B **70**, 115305 (2004).

[151] J. Basset, D.-D. Jarausch, A. Stockklauser, T. Frey, C. Reichl, W. Wegscheider, T. M. Ihn, K. Ensslin, and A. Wallraff, Phys. Rev. B **88**, 125312 (2013).

[152] H. M. Wiseman, D. W. Utami, H. B. Sun, G. J. Milburn, B. E. Kane, A. Dzurak, and R. G. Clark, Phys. Rev. B **63**, 235308 (2001).

[153] S. Kohler, Eur. Phys. J. B **86**, 285 (2013).

[154] S. Ashhab, J. Q. You, and F. Nori, Phys. Rev. A **79**, 032317 (2009).

[155] J. Rech and S. Kehrein, Phys. Rev. Lett. **106**, 136808 (2011).

[156] J. Gómez-García, "Bachelor thesis at the Universidad Complutense de Madrid," (2014).

[157] W. Shockley, J. Appl. Phys. **9**, 635 (1938).

[158] D. Mozyrsky, L. Fedichkin, S. A. Gurvitz, and G. P. Berman, Phys. Rev. B **66**, 161313 (2002).

[159] D. Mozyrsky, S. Kogan, V. N. Gorshkov, and G. P. Berman, Phys. Rev. B **65**, 245213 (2002).

[160] S. A. Gurvitz, Phys. Rev. B **56**, 15215 (1997).

[161] A. Braggio, C. Flindt, and T. Novotný, J. Stat. Mech. **2009**, P01048 (2009).

[162] D. S. Golubev, Y. Utsumi, M. Marthaler, and G. Schön, Phys. Rev. B **84**, 075323 (2011).

[163] G.-L. Ingold and Yu. V. Nazarov, "Charge tunneling rates in ultrasmall junctions," in *Single Charge Tunneling*, NATO ASI Series B, Vol. 294, edited by H. Grabert and M. H. Devoret (Plenum, New York, 1992) pp. 21–107.

[164] P. Bouzas, M. Valderrama, and A. Aguilera, App. Math. Modell. **30**, 1021 (2006).

[165] H. Risken, *The Fokker-Planck Equation*, 2nd ed., Springer Series in Synergetics, Vol. 18 (Springer, Berlin, 1989).

[166] N. Ubbelohde, C. Fricke, C. Flindt, F. Hohls, and R. J. Haug, Nat. Comm. **3**, 612 (2012).

[167] P. G. Kirton, A. D. Armour, M. Houzet, and F. Pistolesi, Phys. Rev. B **86**, 081305 (2012).

[168] M. Lax, Phys. Rev. **129**, 2342 (1963).

[169] M. Lax, Phys. Rev. **157**, 213 (1967).

[170] G. Bulnes Cuetara, M. Esposito, G. Schaller, and P. Gaspard, Phys. Rev. B **88**, 115134 (2013).

[171] D. A. Ruiz-Tijerina, E. Vernek, and S. E. Ulloa, Phys. Rev. B **90**, 035119 (2014).

[172] J. Jin, M. Marthaler, P.-Q. Jin, D. Golubev, and G. Schön, New J. Phys. **15**, 025044 (2013).

[173] T. Novotný, Europhys. Lett. **59**, 648 (2002).

[174] G. Bulnes Cuetara, M. Esposito, and P. Gaspard, Phys. Rev. B **84**, 165114 (2011).

[175] R. López, J. S. Lim, and D. Sánchez, Phys. Rev. Lett. **108**, 246603 (2012).

[176] M. Esposito, U. Harbola, and S. Mukamel, Phys. Rev. B **75**, 155316 (2007).

[177] J. Ren, P. Hänggi, and B. Li, Phys. Rev. Lett. **104**, 170601 (2010).

[178] L. Nicolin and D. Segal, J. Chem. Phys. **135**, 164106 (2011).

[179] G. Lindblad, Commun. Math. Phys. **48**, 119 (1976).

[180] V. Gorini, A. Kossakowski, and E. C. G. Sudarshan, J. Math. Phys. **17**, 821 (1976).

[181] P. Pechukas, Phys. Rev. Lett. **73**, 1060 (1994).

[182] F. J. Kaiser, M. Strass, S. Kohler, and P. Hänggi, Chem. Phys. **322**, 193 (2006).

[183] J. Thingna, J.-S. Wang, and P. Hänggi, J. Chem. Phys. **136**, 194110 (2012).

[184] T. Krause, G. Schaller, and T. Brandes, Phys. Rev. B **84**, 195113 (2011).

[185] M. Rey, M. Strass, S. Kohler, P. Hänggi, and F. Sols, Phys. Rev. B **76**, 085337 (2007).

[186] M. Büttiker, Phys. Rev. Lett. **57**, 1761 (1986).

[187] R. Sánchez, S. Kohler, and G. Platero, New J. Phys. **10**, 115013 (2008).

[188] P. Jordan and E. Wigner, Z. Phys. **47**, 631 (1928).

[189] E. H. Lieb, J. Comb. Theo. **5**, 313 (1968).

[190] G. H. Golub and J. H. Wilkinson, SIAM Rev. **18**, 578 (1976).

[191] D. Cox, J. Little, and D. O'Shea, *Ideals, Varieties, and Algorithms* (Springer New York, 2007).

Publications

During the PhD studies the following articles originated forming the basis of this thesis:

[63] **Robert Hussein**, J. Gómez-García, and S. Kohler,
Monitoring quantum transport: Backaction and measurement correlations,
Phys. Rev. B **90**, 155424 (2014).

[84] **Robert Hussein** and S. Kohler,
Quantum transport, master equations, and exchange fluctuations,
Phys. Rev. B **89**, 205424 (2014).

[81] **Robert Hussein** and S. Kohler,
Coherent quantum ratchets driven by tunnel oscillations: Fluctuations and correlations,
Phys. Rev. B **86**, 115452 (2012).

Further publication of the author:

[136] **Robert Hussein**, A. Metelmann, P. Zedler, and T. Brandes,
Semiclassical dynamics of nanoelectromechanical systems,
Phys. Rev. B **82**, 165406 (2010).

Acknowledgment

I would like to take the opportunity to acknowledge all my colleagues and friends who have accompanied me during the past years—both on a professional and personal level.

First and foremost, I would like to express my gratitude to my supervisor Sigmund Kohler for his guidance and continuous support throughout my doctoral studies. In particular, I want to thank him for this exciting and challenging assignment and for sharing his professional experience with me. I appreciated always our thought-provoking and inspiring discussions during coffee breaks. Moreover, I am grateful for the opportunity to participate in several conferences: The ICTP Workshop in Triest, the Nonlinear transport conference in Madrid, the Spring meeting of the DPG in Berlin, and the CFN Summer School in Karlsruhe.

My tutor Juan-Carlos Cuevas always lend me an open ear for discussions, motivated me, and helped me with administrative matters. I enjoyed the friendly atmosphere at my institute (ICMM) and the vivid scientific discourse during weekly seminars of our theory department. Especially, I would like to thank Gloria Platero for many enjoyable discussions, her advice, and support.

I would like to thank Jorge Gómez for collaboration on Ref. 63. For many helpful discussions on various topics of this thesis, such as full counting statistics and fluctuation relations I am obliged to Fernando Domínguez and Rafael Sánchez. Fernando Gallego has helped me with the Spanish translation for which I am grateful. Furthermore, I appreciated the company and friendship of Mónica Benito, Jose Carlos, Jorge Cayao, as well as Álvaro Gómez, Ángel Gutiérrez, Michael Niklas, Roberto Moreno, and Laura Fanfarillo with whom I shared an office.

I am indebted to Christin David who accompanied me during all the different stages of my PhD, for her advice, and for proof-reading this thesis. Moreover, I thank my parents and my brother Lenard for their encouragement and continuous support.

This work was made possible through financial support of the Spanish Ministry of Economy and Competitiveness which granted me an FPU scholarship.

Robert Hussein

Noise–induced quantum transport

In this thesis we study the electronic and thermal properties of few electron quantum dot circuits such as two capacitively coupled double quantum dots. We like to understand the transport mechanisms and the complex interplay between measurement, decoherence, and non-equilibrium dynamics. In particular, we investigate transport properties of a driven quantum ratchet, fluctuation relations in the framework of master equations, and the suitability of a quantum point contact as charge and current detector. As main quantity to acquire information about the transport characteristics serves the tunnel probability of the electrons traversing the circuitry. We analyze it by means of full-counting statistics.

Cover illustration: Scheme of a Poissonian tunnel probability $P(N,t)$ as function of the number of electrons N that is passing an electronic circuit after time t. The tunnel process is fully characterized by its moments, such as the mean value $m = \langle N \rangle$ and the variance $\sigma^2 = \langle \Delta N^2 \rangle$.